INVESTIGATION OF THE INHIBITORY EFFECT OF SOME SECONDARY METABOLITES TO HIV-1 CAPSID PROTEIN OLIGOMERIZATION

A Thesis Submitted to
the Graduate School of
İzmir Institute of Technology
in Partial Fulfillment of the Requirements for the Degree of

MASTER OF SCIENCE

in Bioengineering

by
Selin Gül TURGUT

June 2025
İZMİR

We approve the thesis of **Selin Gül TURGUT**

Asst. Prof. Dr. Hümeyra TAŞKENT SEZGİN
Department of Bioengineering, İzmir Institute of Technology

Prof. Dr. Erdal BEDİR
Department of Bioengineering, İzmir Institute of Technology

Assoc. Prof. Dr. Burcu KAPLAN TÜRKÖZ
Department of Food Engineering, Ege University

12 June 2025

Asst. Prof. Dr. Hümeyra TAŞKENT SEZGİN
Supervisor, Department of Bioengineering
İzmir Institute of Technology

Assoc. Prof. Dr. Ceyda Öksel Karakuş
Head of the Department of Bioengineering

Prof. Dr. Mehtap EANES
Head of the Graduate School

ACKNOWLEDMENTS

I would like to express my sincere gratitude to my thesis advisor Dr. Hümeyra Taşkent Sezgin, who contributed to my scientific development with her knowledge, experience and guidance during my master's education and thesis study.

I would like to thank Prof. Dr. Erdal Bedir and his research group for providing the compounds and making the natural product library available.

My thesis is funded through TÜSEB A Group A4-03 Emergency R&D Project, (Project number: 34359). I would like to thank Health Institutes of Türkiye (TÜSEB).

I am grateful to Gamze TERLEMEZ for her sincere help and companionship, who supported me during the experimental processes and increased my determination to work. I would also like to sincerely thank my dear laboratory mates Ezgisu AYDIN and İpek ARKCA who always made me feel their moral support in this process. The laboratory was not only a workspace but also an environment of friendship with you.

I would like to thank Kutay Emre DOĞRU, Büşra UZUN and Doğa KÖKSALAR for their moral support and inspiration. Your presence made this challenging process more meaningful.

I would like to thank my cats Fiona and Bambi, who have been my source of morale throughout my master's program. Lastly, I would like to thank my dear family, who have always been with me in this process and have given me strength with their support and love.

ABSTRACT

INVESTIGATION OF THE INHIBITORY EFFECT OF SOME SECONDARY METABOLITES TO HIV-1 CAPSID PROTEIN OLIGOMERIZATION

HIV-1 infection remains a major global public health concern, and the search for new antiviral agents continues alongside existing therapies. The capsid (CA) protein plays crucial roles in HIV-1 replication including nuclear entry, reverse transcription, and integration making it an attractive target for drug development.

In this thesis, 279 secondary metabolites isolated from microorganisms or plants in Türkiye by Prof. Dr. Erdal Bedir's group were screened for HIV-1 CA binding potential using molecular docking. Simulations were performed on the CA monomer, and compounds with high binding scores were experimentally tested.

Two biophysical assays were employed: the capsid assembly assay to evaluate effects on oligomerization kinetics, and Differential Scanning Fluorimetry (DSF) to assess changes in CA thermal stability.

Among tested compounds, ATB-01 and ATB-05 were found to increase CA oligomerization rate, while MD-MG-03 and MD-MG-04 decreased CA melting temperature in DSF. Since HIV-1 CA also exists as a multimer, additional docking studies were conducted on a multimeric CA model encompassing all capsid-capsid interaction sites. Notably, most compounds showed their best binding at the tri-hexamer interface. MD-MG-03 and MD-MG-04 exhibited similar docking scores for monomer and multimer, while ATB-01 and ATB-05 had improved scores at the tri-hexamer interface.

These results suggest that selected natural compounds may interact with HIV-1 CA in distinct modes. Further computational and experimental studies are needed to better understand their mechanisms of action and evaluate their relevance for CA-targeted antiviral research.

ÖZET

BAZI SEKONDER METABOLİTLERİN HIV-1 KAPSİT PROTEİNİ OLİGOMERİZASYONUNA ETKİSİNİN ARAŞTIRILMASI

HIV-1 enfeksiyonu dünya çapında küresel bir sağlık sorunu olmaya ve mevcut tedavilerin yanında yeni antiviral ajanlara olan ihtiyaç artmaya devam etmektedir. HIV-1'in yaşam döngüsünde önemli bir rol oynayan kapsid proteini, virüsün yapısal bütünlüğünü sağlamanın yanı sıra ters transkripsiyon ve viral genomun konakçı hücre genomuna entegrasyonu gibi kritik adımları da düzenlemektedir. Bu nedenle kapsid proteini, ilaç geliştirme aşamalarında giderek daha fazla öne çıkan bir hedef haline gelmiştir. Bu tez çalışmasında, Türkiye'deki mikroorganizma ve bitkilerden ve izole edilen Bedir Grup sekonder metabolitlerin HIV-1 kapsid ile etkileşim potansiyeli araştırılmıştır.

Tez kapsamında 279 sekonder metabolit HIV-1 kapsid monomeri ile moleküler yanaştırma yapılmış ve en yüksek bağlanma skoruna sahip moleküller seçilerek deneysel çalışmalarda incelenmiştir. Deneysel aşamada iki farklı biyofiziksel yöntem kullanılmıştır. Protein stabilitesi üzerindeki etkileri değerlendirmek için Diferansiyel Taramalı Florimetre (DSF) ve oligomerleşme kinetiği üzerindeki etkileri incelemek için oligomerizasyon deneyi kullanılmıştır. DSF analizinde, MD-MG-03 ve MD-MG-04 molekülleri proteinin erime sıcaklığını azaltırken, kapsid oligomerizasyon deneyinde ATB-01 ve ATB-05 molekülleri oligomerizasyonu önemli ölçüde hızlandırmıştır.

HİV-1 kapsid doğada monomer ve multimer formda bulunabilir. Moleküllerin HİV-1 kapsid multimeri ile etkileşimini incelemek için dört monomerden oluşan bir kapsid multimeri oluşturulmuştur. Bu multimer yapı üzerine, MD-MG ve ATB grubu molekülleriyle moleküler yanaştırma uygulanmıştır. En iyi moleküler yanaştırma sonuçlarında moleküller kapsid monomerinde C-terminal bölgeye, kapsid multimerde üç farklı hekzamerin etkileştiği bölgeye bağlanmış görünmektedir. Moleküllerin HİV-1 kapsid proteini ile etkileşimini anlayabilmek için daha fazla deneysel ve hesaplamalı çalışma yapılması gerekmektedir.

TABLE OF CONTENTS

LIST OF FIGURES

Figure **Page**

LIST OF TABLES

CHAPTER 1

INTRODUCTION

1.1. Human Immunodeficiency Virus Type 1 (HIV-1)

Human immunodeficiency virus (HIV) is a pathogen that compromises the immune system by attacking white blood cells. If left untreated, the infection can progress to its most severe stage, known as acquired immunodeficiency syndrome (AIDS). HIV weakens the immune system and reduces an individual's ability to defend itself against infections. The virus is transmitted through bodily fluids such as blood, breast milk, semen, and vaginal secretions. Additionally, HIV can be passed from mother to child during childbirth or breastfeeding (World Health Organization 2024).

The transmission of HIV can be prevented by pre-exposure prophylaxis and HIV infection can be managed with antiretroviral therapy (ART). Without treatment, the virus may gradually advance to AIDS over several years. In 2023, an estimated 39.9 million (36.1 million- 44.6 million) people worldwide were living with HIV. During the same year, approximately 1.3 million (1 million–1.7 million) new HIV infections occurred, while 630,000 (500,000–820,000) individuals lost their lives due to AIDS-related illnesses. Access to antiretroviral therapy (ART) has significantly improved, with 30.7 million (27–31.9 million) people receiving treatment in 2023. Since the beginning of the HIV epidemic, a total of 88.4 million (71.3 million–112.8 million) individuals have been infected with the virus, and 42.3 million (35.7 million–51.1 million]) people have died from AIDS-related complications (UNAIDS 2025).

1.2. Structure and Function of the HIV-1 Capsid Protein

The human immunodeficiency virus type 1 (HIV-1) capsid protein (CA) is a pivotal component of the viral life cycle, acting as both a structural component and a key modulator of infection. The CA protein forms the conical core of the virus (Figure 1), enclosing the viral RNA genome and essential enzymes for reverse transcription and integration into the host genome (Ganser-Pornillos, Yeager, and Sundquist 2008). The CA protein plays a crucial role in both the early and late phases of the HIV-1 life cycle, interacting with various host cell factors that have been identified as direct binding partners (Rossi et al. 2021).

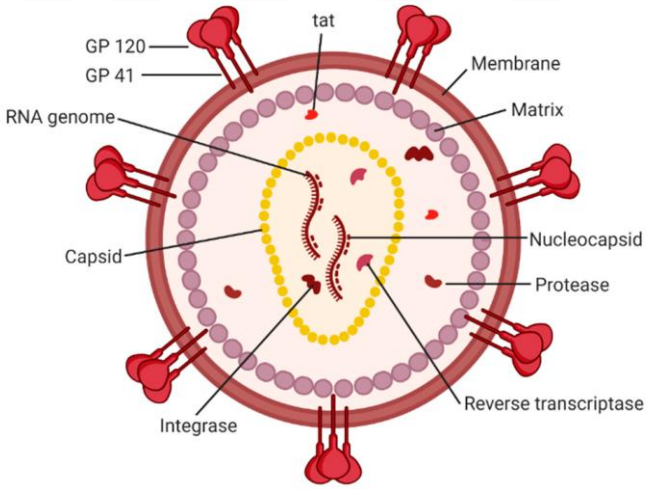

Figure 1. A schematic of the HIV-1 virion (Source: Rossi et al. 2021).

Structurally, CA is divided into two distinct domains: the N-terminal domain (NTD) and the C-terminal domain (CTD), connected by a flexible linker region. The NTD comprises seven α-helices (α1–α7), a β-hairpin, and an extended cyclophilin A (CypA)-binding loop, while the CTD consists of four α-helices (α8–α11), a short 3_{10}-helix, and the major homology region (Figure 2). The stability and assembly of the capsid are governed by multiple CA-CA interactions. NTD-NTD contacts between CA monomers reinforce the formation of hexamers and pentamers, creating a central pore with the β-

hairpin at the gate. Additionally, NTD-CTD interactions between adjacent monomers further stabilize these structures. CTD-CTD interactions contribute to dimeric and trimeric interfaces, facilitating the organization of hexamers and pentamers into a stable lattice. These structural features establish at least three distinct binding interfaces for host factors, which influence capsid function and viral replication. This protective shell is composed of approximately 1,500 CA monomers that self-assemble into a fullerene-like lattice consisting of 250 hexamers and 12 pentamers, which determine the stability and morphology of capsid (Ganser-Pornillos, Yeager, and Pornillos 2012; Pornillos et al. 2009; Yu et al. 2020; Dwivedi et al. 2024).

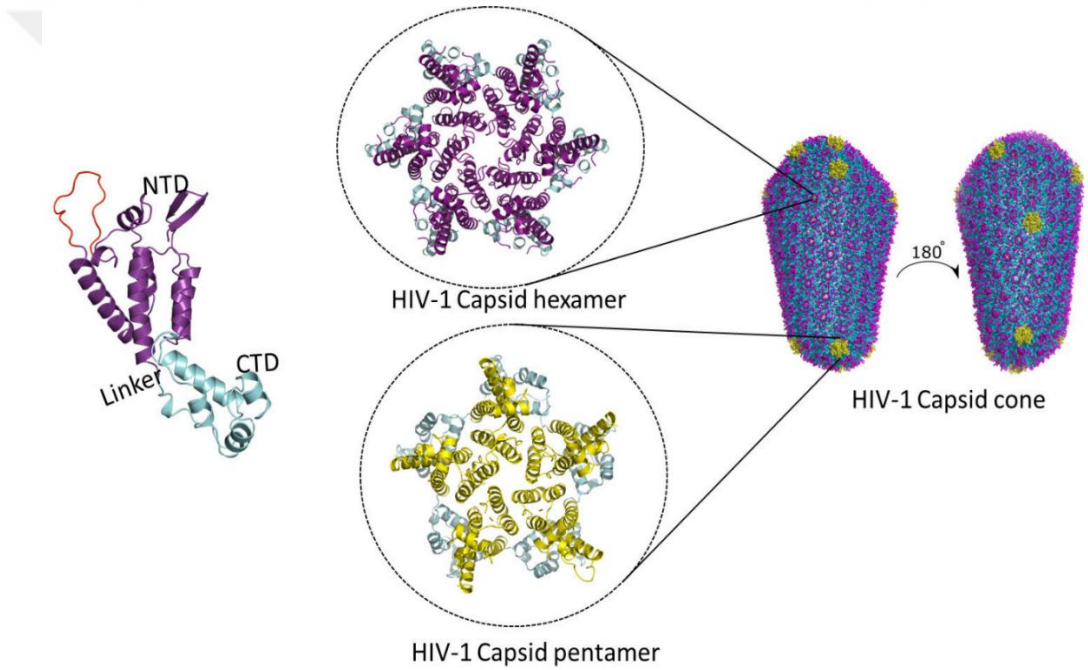

Figure 2. Structural assembly of the HIV-1 CA from monomeric to conical CA core (Source: Dwivedi et al. 2024).

Functionally, HIV-1 capsid plays a critical role in multiple stages of viral infection (Figure 3). Following viral entry, it protects the viral genome from host immune recognition while enabling efficient reverse transcription within the host cytoplasm (Jacques et al. 2016) Capsid also interacts with cellular proteins such as cyclophilin A (CypA) and nucleoporins, which facilitate nuclear import and determine the preferred

sites of viral integration (Matreyek and Engelman 2011; Di Nunzio 2013). The capsid core traffics towards the nucleus while the viral RNA genome is reverse transcribed into DNA within an intact capsid shell, a process influenced by host factors such as IP6, which stabilizes the capsid structure to promote efficient reverse transcription (Mallery et al. 2018). Capsid protein further mediates nuclear entry by directly engaging with nucleoporins like Nup153 and CPSF6, guiding the pre-integration complex (PIC) through the nuclear pore complex (NPC) (Matreyek and Engelman 2011; Burdick et al. 2017). This interaction is essential for HIV-1 to traverse the nuclear envelope, allowing the viral genome to integrate into transcriptionally active regions of the host genome (Hulme, Perez, and Hope 2011). Mutations affecting capsid stability or its interactions with host factors can significantly impair viral replication, highlighting the capsid's critical role in coordinating HIV-1 infection (Bester et al. 2020).

The capsid not only regulates early infection events but also has a role in later stages of the viral life cycle. During the early phase of replication, CA promotes reverse transcription and nuclear import. Recent findings suggest that CA remains functionally relevant even after nuclear entry, influencing integration site selection and subsequent transcriptional activity of the viral genome (Gifford and Melikyan 2024). In the late stages of infection, CA regulates the formation of a hexameric lattice essential for assembling immature virions. It also plays a crucial role in the maturation process, ensuring the correct assembly of the capsid core that encapsulates the viral genome and associated proteins within infectious virions (Campbell and Hope 2015).

Due to its multifunctional nature, HIV-1 capsid protein is a prime target for antiviral drug development. Disrupting its assembly, stability, or host interactions could provide new therapeutic strategies to inhibit viral replication at multiple checkpoints.

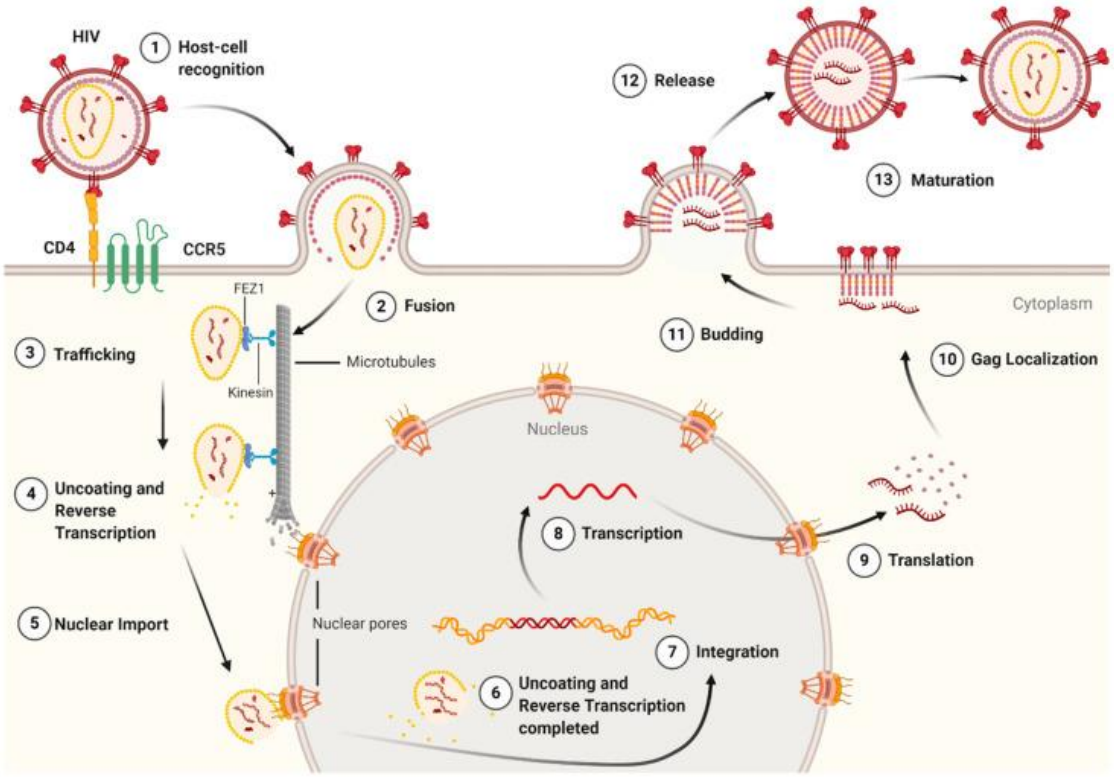

Figure 3. Life Cycle of HIV-1 virus (Source: Rossi et al. 2021).

1.3. Anti-Viral HIV-1 Drugs

Combination antiretroviral therapy (cART) has significantly reduced AIDS-related deaths, enabling HIV infected individuals to achieve a near normal life expectancy. However, while cART effectively suppresses viral replication, a functional cure remains elusive, and lifelong treatment is still necessary. Antiviral therapies for HIV-1 primarily target various stages of the viral life cycle, including reverse transcription, integration, and proteolytic maturation (McGraw et al. 2024). While most cART regimens are taken orally once daily, recent advancements include long-acting injectable treatments like Cabenuva, an INSTI/NNRTI combination approved in 2021 for monthly or bi-monthly use. The HIV-1 capsid has emerged as a highly promising antiviral target due to its essential role in multiple stages of infection, including viral uncoating, reverse transcription, nuclear import, and virion assembly (Campbell and Hope 2015). Targeting

the capsid allows for the disruption of critical interactions between the virus and host cellular factors, thereby hindering viral replication (Zhuang and Torbett 2021).

Lenacapavir (Figure 4), a first-in-class long-acting capsid inhibitor, represents a breakthrough in HIV-1 treatment by directly binding to the capsid protein (Link et al. 2020). Unlike conventional therapies that focus on viral enzymes such as reverse transcriptase, protease, and integrase, Lenacapavir interferes with capsid stability and function, leading to impaired viral replication by targeting multiple stages of the viral lifecycle. Specifically, it binds to the interface of CA monomers, disrupting capsid assembly and disassembly processes essential for viral infectivity (Paik 2022). By targeting a structurally conserved region of the capsid, Lenacapavir exhibits a high barrier to resistance, making it a potent addition to the antiviral arsenal (Jogiraju et al. 2024).

Beyond FDA-approved drugs, several small molecules have been identified as potential HIV-1 capsid inhibitors. These include PF-3450074 (also known as PF74), which binds to the N-terminal domain of the CA protein, interfering with capsid-host interactions crucial for viral replication (Shi et al. 2010). BI-2 is another small molecule that targets the same binding pocket as PF74, demonstrating potent inhibition of capsid function (W. Wang et al. 2017). CAP-1 and CAP-2 are the first small-molecule inhibitors of the HIV-1 capsid, identified through computational screening for binding to the CA-NTD domain. CAP-1 disrupts mature capsid assembly by blocking CA-NTD/CA-CTD interactions. Another inhibitor, CAI, a 12-residue peptide, blocks both immature and mature capsid assembly *in vitro* but cannot penetrate cells. Studies suggest CAI peptide has an allosteric effect on immature assembly and directly binds the CTD pocket during mature assembly (Thenin-Houssier and T. Valente 2016). The continuous exploration of small molecules targeting HIV-1 CA highlights the importance of capsid inhibition as a viable antiviral strategy.

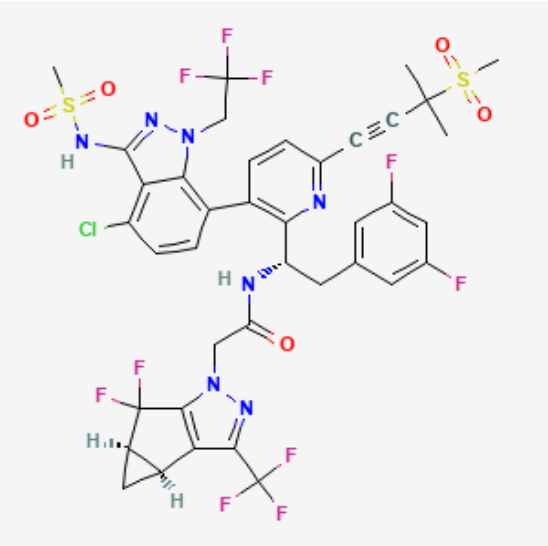

Figure 4. Lenacapavir (GS-6207) | HIV-1 Capsid Inhibitor ("Lenacapavir | C39H32ClF10N7O5S2 | CID 133082658 - PubChem," n.d.).

1.4. Natural Products Antivirals

Natural products, mainly secondary metabolites derived from microorganisms, fungi and plants have been a rich source of bioactive compounds with therapeutic potential. Secondary metabolites are organic compounds that are not directly involved in the growth, development, or reproduction of an organism but play essential roles in interactions, including defense against pathogens and adaptation of environmental stress. Many clinically approved drugs, including antiviral agents, are either directly obtained from natural sources or inspired by their structure (Newman and Cragg 2020). Their complexity, structural diversity and distinct pharmacological activities, shaped by natural selection and evolutionary pressures over millennial make them valuable candidates for developing new treatments, especially against challenging viral infections such as HIV-1 (Serna-Arbeláez et al. 2021; Srivastava et al. 2025).

The antiviral potential of natural products has been extensively explored, leading to the discovery of molecules that interfere with different stages of viral replication. These include entry inhibitors, reverse transcriptase inhibitors, protease inhibitors, and compounds that modulate the host immune response (Jassim and Naji 2003). The ability

of natural compounds to interact with viral proteins or disrupt essential host-virus interactions highlights their significance in drug development (Srivastava et al. 2025).

Several natural products and their derivatives have demonstrated anti-HIV activity by interfering with main viral processes. For instance, betulinic acid, a triterpene derived from plants such as *Quisqualis fructu*s, *Syzygium claviflorum* etc., functions as an HIV-1 maturation inhibitor by disrupting the processing of the viral Gag polyprotein. Bevirimat is derived from betulinic acid compound that targets the capsid-spacer peptide 1 (CA-SP1) cleavage site, thereby preventing the formation of infectious virion (Serna-Arbeláez et al. 2021). Recent studies have also identified other natural compounds with potential anti-HIV activity. For example, griffithsin, a lectin derived from *Griffithsia species*, exhibits potent antiviral activity by binding to HIV-1 envelope glycoprotein gp120 and blocking viral entry. (Lusvarghi and Bewley 2016).

1.5. Known Bioactive Compounds in the Natural Product Library Used in this Thesis

Several compounds included in the natural product library screened in this study are well-documented for their diverse bioactivities related to human health (Table 1). For instance, asiatic acid and asiaticoside, both derived from Centella asiatica, are widely recognized for their anti-inflammatory and wound-healing properties and have demonstrated antiviral activity, particularly against hepatitis B virus (R. Li et al. 2024; Jaisi et al. 2021). Astragaloside IV, a triterpenoid saponin found in Astragalus species, has shown immunomodulatory effects and antiviral activity against influenza and hepatitis B viruses (S. Wang et al. 2009). Quercetin, rutin, and fisetin, common dietary flavonoids, have been reported to possess broad-spectrum antiviral activities, including inhibition of dengue and chikungunya virus replication (Di Petrillo et al. 2021). In addition, chlorogenic acid and ferulic acid have shown inhibitory effects against influenza and enterovirus 71, respectively (X. Li et al. 2013; DIng et al. 2017), while ellagic acid has been studied for its potential to suppress viral replication and modulate cytokine production (Sharifi-Rad et al. 2022). Notably, glycyrrhetinic acid, a compound used in traditional medicine, has demonstrated antiviral activity against hepatitis B virus and

Kaposi's sarcoma-associated herpesvirus (Zuo et al. 2023). In addition, oleandrin, a cardiac glycoside, has been reported to exhibit *in vitro* antiviral effects, including HIV (Prassas and Diamandis 2008).

These findings underscore the functional and structural diversity of the natural compound library used in this study and provide further rationale for their evaluation as potential inhibitors of the HIV-1 capsid protein.

Table 1. Known natural compounds with reported activity.

Compound Name	Known Use/Industry	Reported Antiviral Activity	References
Asiatic acid	Wound healing, cosmetics	Yes (anti-HBV)	(R. Li et al. 2024; Jaisi et al. 2021)
Asiaticoside	Skin care, wound healing	Limited	(Jaisi et al. 2021)
Astragaloside IV	Immunomodulatory, herbal medicine	Yes (anti-influenza, HBV)	(S. Wang et al. 2009)
Betulin	Anti-tumor, anti-inflammatory	Yes (anti-HIV)	(Alakurtti et al. 2006; Aiken and Chen 2005)
Catechin	Antioxidant, nutraceutical	Yes (anti-DENV, CHIKV)	(Yi et al. 2023)
Chlorogenic acid	Food additive, antioxidant	Yes (enterovirus 71, anti-influenza)	(X. Li et al. 2013; DIng et al. 2017)
Ellagic acid	Antioxidant, anti-inflammatory	Yes (anti-hepatitis B and hepatitis C virus)	(Sharifi-Rad et al. 2022)
Escin	Anti-inflammatory, venotonics	Yes (anti-HIV-1, anti-SARS)	(Yang et al. 1999; Wu et al. 2004)
Ferulic acid	Antioxidant, skincare	Yes (anti-RSV, HSV-1, EV71)	(Antonopoulou et al. 2022; Mancuso and Santangelo 2014)

(cont. on next page)

Table 1. (cont.)

Fisetin	Neuroprotective, antioxidant	Yes (anti-DENV, anti-CHIKV)	(Keivan et al. 2014; Martins et al. 2020)
Glycyrrhetinic acid	Anti-inflammatory, herbal medicine	Yes (anti-HBV, anti-KSHV)	(Zuo et al. 2023)
Oleandrin	Cardiac glycoside, traditional medicine	Yes (in vitro antiviral)	(Prassas and Diamandis 2008)
Quercetin	Antioxidant, nutraceutical	Yes (broad-spectrum)	(Di Petrillo et al. 2021)
Rutin	Antioxidant, food additive	Yes (anti-DENV)	(Keivan et al. 2014)

1.6. Microorganism and Endemic Plant Diversity of Türkiye

Türkiye is recognized as a biodiversity hotspot, hosting a vast array of endemic plant species and diverse microbial populations due to its unique geographical location, varied climate conditions, and rich ecosystems. The country spans multiple phytogeographical regions, including the Mediterranean, Irano-Turanian, and Euro-Siberian zones, each contributing to its exceptional floristic diversity. Approximately 32% of Türkiye's plant species are endemic, making it a significant reservoir for bioactive secondary metabolites with potential pharmaceutical applications (Türe and Böcük 2010; Noroozi et al. 2019; Tekman et al. 2024).

The high endemism in Türkiye has drawn scientific interest, particularly in the field of natural product chemistry. Many endemic plants have been studied for their secondary metabolite content, which plays a crucial role in plant defense mechanisms and possesses therapeutic potential. Species from genera such as Astragalus have been extensively investigated for their bioactive compounds, including alkaloids, flavonoids, terpenoids, and saponins, which have demonstrated antiviral, antimicrobial, and anti-inflammatory properties (Aslanipour et al. 2017; Gülcemal, Aslanipour, and Bedir 2019; Yesilada et al. 2005; Gezer et al. 2022).

The rich biodiversity of Türkiye continues to be an invaluable source for the discovery of novel secondary metabolites. Further research into endemic plant and microbial species has the potential to uncover new bioactive compounds that could serve as lead candidates in drug development, particularly for antiviral and antimicrobial therapies (Şener and Orhan 2005; Heydari, Gözcelioğlu, and Konuklugil 2019; Sener and Orhan 2011).

1.7. Molecular Docking Approaches Using Natural Molecule Libraries

Molecular docking is a widely used computational technique in drug discovery that predicts the interaction between small molecules and target proteins. This method plays a crucial role in identifying potential antiviral agents by screening large libraries of natural compounds and evaluating their binding affinities to viral proteins. Given the structural diversity and bioactive potential of natural products, molecular docking offers a powerful approach for exploring their therapeutic potential against HIV-1 (Zubair et al. 2020; Terefe and Ghosh 2022).

Natural molecule libraries, composed of secondary metabolites from plants, fungi, and microorganisms, provide a vast chemical space for identifying novel inhibitors targeting HIV-1 proteins. Many docking studies have successfully identified natural compounds with high binding affinities for essential viral targets, including reverse transcriptase, protease, integrase, and capsid proteins (Atanasov et al. 2021; Terefe and Ghosh 2022). For instance, virtual screening of flavonoids, alkaloids, and terpenoids has led to the discovery of molecules that exhibit inhibitory activity against HIV-1 enzymes, thereby disrupting key steps in the viral replication cycle (Newman and Cragg 2020).

Recent studies have increasingly focused on targeting the HIV-1 capsid, an essential structural component involved in multiple stages of the viral life cycle. Computational docking has been instrumental in identifying natural compounds capable of interfering with capsid assembly and stability. Therefore, docking studies have facilitated the selection of promising candidates for experimental validation (Kobayakawa et al. 2024; Lamorte et al. 2013). A recent study identified novel HIV-1 capsid inhibitors targeting the PF74 binding site using structure-based virtual screening.

Screening 1.6 million compounds from the ZINC database, researchers refined the top candidates with binding free energy calculations. Two compounds, ZINC520357473 and ZINC4119064, targeting the capsid hexamer, suggesting their potential as new inhibitors by binding to an unexplored sub-pocket of the capsid dimer interface. This study indicates the effectiveness of computational screening in discovering novel HIV-1 capsid inhibitors (Sun et al. 2022).

Several molecular docking tools are widely used for screening small molecules, including AutoDock Vina, DOCK, and Glide. AutoDock Vina, an open-source docking program, is particularly popular due to its efficiency in predicting ligand-protein interactions and its improved scoring function compared to its predecessor, AutoDock (Agu et al. 2023).In molecular docking simulations, different software tools handle the flexibility of proteins and ligands in varying ways. AutoDock Vina, for instance, typically treats the protein as rigid while allowing the ligand to be flexible, optimizing its binding pose within the active site (Trott and Olson 2010).

1.8. Differential Scanning Fluorometry (DSF) in Drug Screening

Differential scanning fluorimetry (DSF) is a rapid, affordable, and widely accessible biophysical technique commonly employed in drug discovery to evaluate protein stability and identify potential ligands that bind to specific target proteins. DSF (Figure 5) works by monitoring fluorescence signal intensity changes of a dye that binds to exposed hydrophobic regions of the protein as it unfolds with heat, enabling the measurement of the melting temperature (Tm) of the protein, which reflects protein's thermal stability (Niesen, Berglund, and Vedadi 2007). This technique has become increasingly important in early-stage drug development, particularly in high-throughput screening, as it allows for the rapid identification of small molecules that can bind to and modulate protein function (Gao, Oerlemans, and Groves 2020).

DSF has been shown to be particularly useful for screening large chemical libraries to discover potential inhibitors or stabilizers of therapeutic targets. By observing shifts in Tm, researchers can identify compounds that bind to proteins, offering a valuable tool for drug development. The ability to conduct protein-ligand interaction studies in a

highly sensitive, cost-effective manner, and high-throughput format has made DSF a preferred method in the pharmaceutical industry (Pantoliano et al. 2001). Furthermore, DSF provides a straightforward and efficient way to assess the effects of various ligands on protein stability, making it an indispensable tool in modern drug discovery workflows.

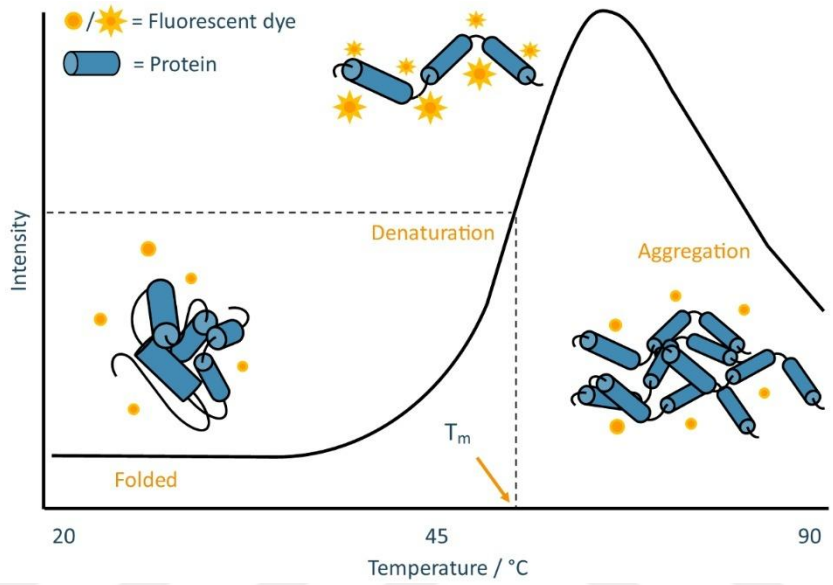

Figure 5. Differential Scanning Fluorometry Assay. (Source: Link et al. 2020)

1.9. Aim of the Thesis

The aim of this study was to investigate the antiretroviral drug potential of natural products derived from microorganisms and plants from Türkiye on the HIV-1 capsid (CA) protein. To achieve this, molecular docking analyses were conducted to evaluate the potential interactions between HIV-1 CA and 279 natural molecules previously isolated in Bedir Group. Based on the docking results, selected molecules with high binding affinity were further analyzed to assess their effects on CA oligomerization kinetics and thermal stability. This research contributes to the discovery of novel anti-HIV-1 agents from rich biodiversity of Türkiye and provides valuable insights into their potential mechanisms of action.

CHAPTER 2

MATERIALS AND METHODS

2.1. Molecular Docking Procedure

2.1.1. Protein Input Preparation Process for Molecular Docking

The Protein Data Bank (PDB) is the only global repository of biological macromolecule structural data. The structures are determined by methods including X-ray crystallography, cryogenic electron microscopy (cryo-EM), and nuclear magnetic resonance (NMR). The data in the PDB is derived from sources such as three-dimensional coordinates, crystal structure information, macromolecular sequences, and organismal origins. (Berman 2000). The structure of the HIV-1 capsid protein has been determined many times by X-ray crystallography, NMR and cryo-EM methods (Pornillos et al. 2009; Gres et al. 2015; Byeon et al. 2009). For docking studies, the HIV-1 capsid structure with PDB code 6VKV (Bester et al. 2020) was selected as the most suitable structure in the protein database.

To prepare HIV-1 capsid protein (PDB ID: 6VKV) for docking studies, the following steps were carried out using Chimera software. The 6VKV structure represents a multimeric complex. Since this study specifically focuses on the HIV-1 capsid monomer, a single monomer was selected for the docking analysis. The monomer of interest was saved using Chimera's selection tools. The other remaining models and ligands were also removed to avoid interference with the docking process. After completing these steps, the prepared monomeric protein was saved as a separate .pdb file (Figure 6). A test docking setup was initiated in Chimera's AutoDock plugin with default parameters to prepare and save the monomeric protein in pdbqt format. During the test

setup, polar hydrogens were automatically added to the protein, non-polar hydrogens were merged and Kollman charges were assigned to the protein. The final pdbqt file containing the structure of the monomer was ready for molecular docking studies.

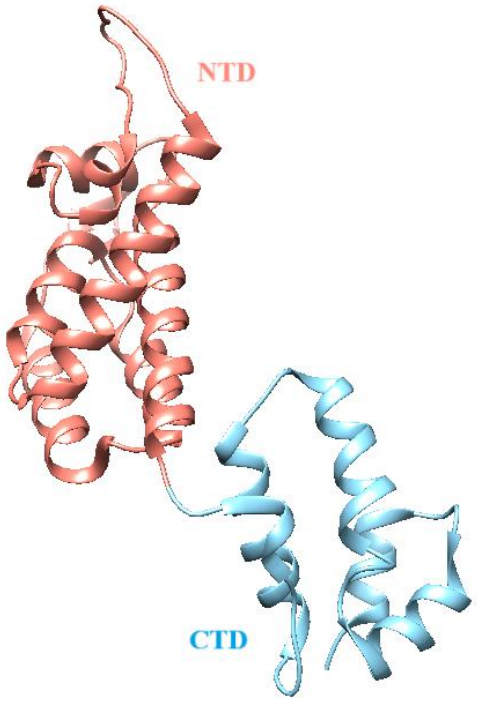

Figure 6. 3D structure of HIV-1 CA monomer. PDB id: 6VKV, visualized using UCSF Chimera.

2.1.2. Ligand Input Preparation Process for Molecular Docking

The library of 279 secondary metabolites isolated from plants and microorganisms provided by Bedir Group has not been previously investigated for interactions with the HIV-1 capsid protein. As part of this study, the interactions between these molecules and the HIV-1 capsid protein were examined using molecular docking methods.

The natural product library was initially provided in SMILES (Simplified Molecular Input Line Entry System) format, which represents the molecular structure in a compact, text-based form. Each SMILES string was converted into a 3D molecular

structure using the Chimera software. The generated 3D structures were saved in .pdb format, compatible with molecular docking workflows. The ligands in .pdb format were imported into Chimera's AutoDock Vina plugin. A test docking setup was performed, during the test setup, addition of polar hydrogens, calculation of charges, conversion of the structure into the .pdbqt format was applied. The processed.pdbqt files were then used for molecular docking simulations with HIV-1 capsid protein.

2.1.3. Molecular Docking Environment Setup

The molecular docking studies were conducted using AutoDock Vina, executed within the Google Colab environment. To perform docking simulations Google Colab, which is a cloud-based platform, was utilized. Python scripts was used to install the required tools, including AutoDock Vina. The scripts contained instructions for managing and uploading ligand and protein files. Define the docking settings, including exhaustiveness and grid dimensions.

2.1.4. Grid Box Setup

The grid box for docking was defined using the Chimera software. HIV-1 capsid protein is known to have five potential binding sites, but the exact binding site for the ligands in this study is unknown (McFadden et al. 2021). Therefore, a blind docking was employed in this study. Blind docking approach evaluates ligand interactions across the entire protein surface rather than focusing on predefined binding sites.

The grid was defined to encompass the entire protein structure that ensures all potential binding regions were included in docking simulations. Grid box dimensions and center were set as X 71 Y 71 Z 71 and X 7 Y -67 Z 2, respectively (Figure 7).

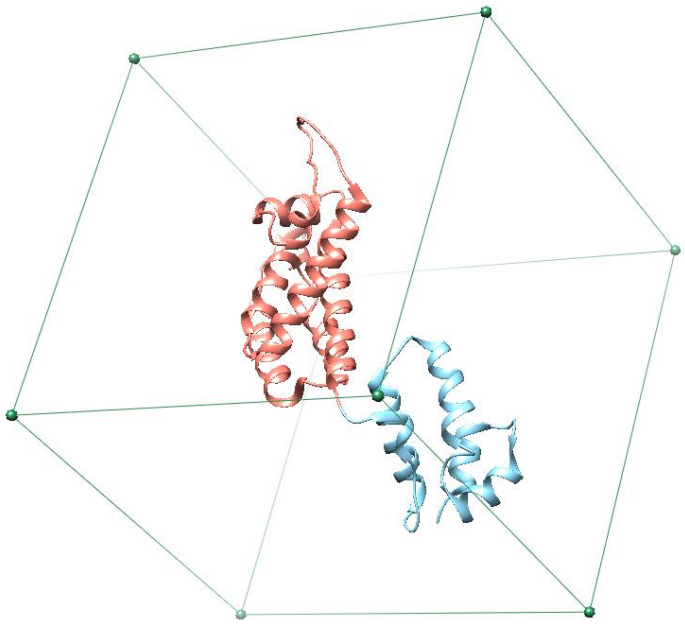

Figure 7. Grid Box of HIV-1 Capsid Monomer. PDB id: 6VKV, visualized using UCSF Chimera.

2.1.5. Execution of Docking Process

Molecular docking was performed using AutoDock Vina (version 1.2.3) to evaluate the binding interactions between the HIV-1 CA protein and a set of 290 ligands. AutoDock Vina is a widely used molecular docking software that predicts ligand binding affinities by searching for optimal conformations within a defined grid space (Trott and Olson 2010).

To efficiently execute the docking process, computations were carried out in the Google Colab environment. Google Colab is a cloud-based platform that provides free access to GPUs and allows users to run Python scripts and command-line tools without requiring local installations. This platform simplifies the execution of computationally intensive tasks such as molecular docking while ensuring reproducibility and ease of access.

AutoDock Vina (v1.2.3) was downloaded and set up in Google Colab by obtaining the executable file from the official GitHub repository. The file was configured for ease

of use, with necessary execution permissions adjusted and an alias created to simplify command usage.

Docking simulations were conducted by specifying the receptor file, ligand file, and grid box dimensions. The process generated output files containing predicted binding poses and binding affinities for each ligand. These results were analyzed to identify compounds with strong binding potential to the HIV-1 CA protein.

2.1.6. Visualization of Docking Results Using Chimera

After performing molecular docking with AutoDock Vina, the docking results were analyzed and visualized using Chimera. The output file generated from the docking process (ligand.pdbqt) was loaded into Chimera alongside the receptor structure to assess ligand binding positions and interactions.

The docking results were visualized using the following steps. The HIV-1 capsid protein (6vkvmodified.receptor.pdbqt) was opened in Chimera using, File → Open → Select receptor. The docked ligand (ligand.pdbqt) was opened in Chimera using, Tools → Stucture/Binding Analysis → ViewDock.

2.1.7. PDBsum Analysis

The interaction profiles of protein-ligand complexes were analyzed using the PDBsum web server (Wallace, Laskowski, and Thornton 1995). Two-dimensional interaction maps were obtained by uploading the PDB format files of the protein-ligand complexes obtained as a result of docking studies via LIGPLOT tool of PDBsum. Within the scope of this analysis, hydrogen bonds and hydrophobic interactions were detected and the binding modes of the ligands to the target protein were evaluated. Visualizations, interaction distances and possible amino acids contacted were automatically reported, and the interaction intensity and diversity were interpreted.

2.2. Production and Purification of HIV-1 Capsid Protein

2.2.1. Transformation of pet11a to BL21(DE3) Competent Cells

The wild-type HIV-1 CA gene sequence was cloned into the pET-11a expression plasmid. The plasmids carrying the HIV-1 CA gene were introduced into *E. coli* BL21(DE3) competent cells through transformation. First, the competent cells were thawed on ice for 2 to 20 minutes, while the plasmid stocks were retrieved from -20°C and placed on ice for equilibration. For each transformation, 1 µl of plasmid DNA was added to 50 µl of competent cells, and the mixture was incubated on ice for 5 to 20 minutes to facilitate DNA uptake. Following incubation, the cells underwent a heat shock treatment at 42°C for 45 seconds in a water bath, immediately followed by rapid cooling on ice for 2 minutes. To aid recovery, 950 µl of LB medium was added to each transformation mixture, and the cultures were incubated at 37°C for 1 hour with shaking at 220 RPM. For selection, the transformed cultures were spread onto LB agar plates supplemented with 0.1 mg/ml ampicillin, then incubated overnight at 30°C. The remaining cultures were centrifuged at 7000 RPM for 1 minute to concentrate the cells. After discarding 800 µl of the supernatant, the cell pellets were resuspended by pipetting. Then, 70 µl of the resuspended cells was spread onto a separate LB agar plate containing 0.1 mg/ml ampicillin and incubated overnight at 30°C.

2.2.2. Production of HIV-1 Capsid Monomer

HIV-1 capsid protein was produced and purified by following the production and purification method (Figure 8) in the article by (Pornillos et al. 2010). For production of HIV-1 capsid protein, tranformed colonies were used. The next day, a single colony from the overnight-grown plates was picked and inoculated into a 50 ml falcon tube containing 5 ml of TB medium supplemented with 0.1 mg/ml ampicillin. The cultures were incubated overnight at 37°C with shaking at 220 RPM to allow bacterial growth. To preserve the

transformed bacterial strains for future protein expression experiments, glycerol stocks were prepared by mixing 500 µl of overnight culture with 500 µl of sterile 50% glycerol. These stocks were then stored at -80°C for long-term preservation. A 5 ml overnight culture (corresponding to 2% of the total media volume) was inoculated into 250 ml of fresh TB medium (in a 2 L Erlenmeyer flask) supplemented with 0.1 mg/ml ampicillin and 0.025 mg/ml chloramphenicol. The culture was incubated at 37°C with shaking at 220 RPM until the optical density at 600 nm (OD_{600nm}) reached approximately 0.8. Once the OD value reached ~0.8, 0.5 mM IPTG was added to induce protein expression. Following induction, the culture was incubated overnight at 25°C with shaking at 220 RPM under cooling conditions. The next morning, the entire culture was centrifuged at 3200 RPM and 4°C for 40 minutes to collect the cells. The resulting cell pellet was stored at -20°C for further processing.

2.2.3. Purification of HIV-1 Capsid Monomer

All purification procedures were conducted at +4°C to ensure protein stability. The cell pellet, previously stored at -20°C, was resuspended in Lysis Buffer containing 50 mM Tris (pH 8.0), 50 mM NaCl, 0.2% Deoxycholate, and 20 mM β-mercaptoethanol (βME).

To inhibit bacterial protease activity, 1 mM PMSF (prepared in 100% ethanol) was freshly added to the solution before use. The cell lysis was performed via sonication, and the lysate was then centrifuged at 8000–9000 RPM, 4°C for 90 minutes to remove cell debris. As HIV-1 CA is soluble in the supernatant, the supernatant was collected and filtered using a 0.45 µm syringe filter. A sample was also taken for SDS-PAGE analysis. The collected supernatant was subjected to 25% ammonium sulfate precipitation to initiate protein fractionation. The appropriate amount of ammonium sulfate was slowly added to the supernatant while continuously stirring on ice. Once the solution was thoroughly mixed, the precipitated protein was separated by centrifugation at 7500–9000 RPM, 4°C for 40 minutes, forming a protein pellet. The pellet was resuspended in SP-Binding Buffer (Buffer A: 25 mM MOPS, pH 6.8, and 20 mM βME) and stirred overnight at 4°C to allow complete solubilization. The next morning, the resuspended protein

solution was centrifuged again at 4000 RPM, 4°C for 40 minutes. The resulting supernatant was collected and filtered through a 0.45 µm membrane filter. To remove residual ammonium sulfate, the solution was dialyzed overnight at 4°C against the same SP-Binding Buffer using a 3.5 kDa MWCO dialysis membrane. On the following day, the dialyzed solution was filtered again using a 0.45 µm syringe filter, completing the pre-purification process.

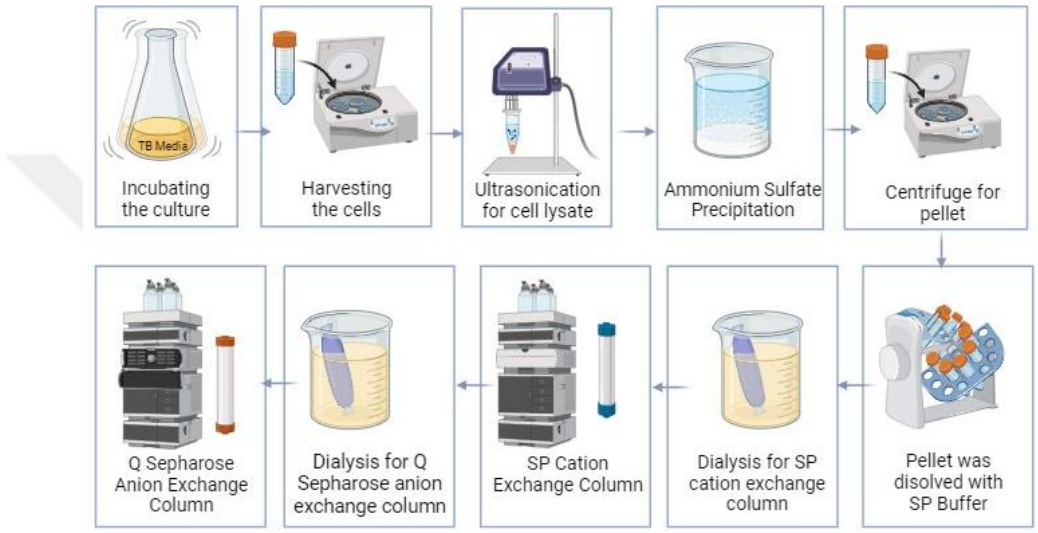

Figure 8. Illustration of production and purification process of HIV-1 capsid protein.

The purification of the wild-type HIV-1 CA protein was carried out using an SP (Sulphopropyl) Sepharose cation exchange column (GE Healthcare). The filtered protein sample was introduced into the SP cation exchange column via the GE Healthcare AKTA Pure FPLC (Fast Protein Liquid Chromatography) system. Throughout the purification process, fractions were collected in two stages. Prior to loading the sample, the system was prepared by flushing it with SP-Binding Buffer (25 mM MOPS, pH 6.8, 20 mM βME). The SP cation exchange column was then integrated into the system. The filtered protein solution was injected and washed with the binding buffer, allowing the target protein to adhere to the column while unbound molecules were removed. The unbound fractions, referred to as flowthrough samples, were collected to verify whether any of the target protein had failed to bind to the column. Subsequently, elution was performed using

SP-Elution Buffer (25 mM MOPS, pH 6.8, 20 mM βME, 1M NaCl) with a gradually increasing salt concentration. The elevated salt concentration facilitated the detachment of the bound protein from the column. The second set of fractions, known as gradient samples, was collected at an elution gradient of 18%–22%.

As a second purification step for the HIV-1 CA protein, a Q (Quaternary Ammonium) Sepharose anion exchange column (GE Healthcare) was utilized. For this step, the gradient fractions obtained from the initial chromatography were pooled together and subjected to overnight dialysis at 4°C using a 3.5 kDa MWCO dialysis membrane against Q-Binding Buffer (20 mM Tris, pH 8.0, 40 mM NaCl, 10 mM βME) to facilitate buffer exchange. The following day, the dialyzed solution was filtered once again using a 0.45 μm membrane filter before being loaded onto the Q anion exchange column in the GE Healthcare AKTA Pure FPLC system. The purification procedure mirrored that of the SP cation exchange column, employing Q-Binding Buffer (20 mM Tris, pH 8.0, 40 mM NaCl, 10 mM βME) for binding and Q-Elution Buffer (20 mM Tris, pH 8.0, 1 M NaCl, 10 mM βME) for elution. Flowthrough fractions containing the purified protein were combined and concentrated using a Pall Macrosep Advance Centrifugal Device (10 kDa MWCO), then stored at -80°C. The absorbance of the concentrated sample was measured at 280 nm, and protein concentration was determined based on its extinction coefficient. Samples collected at various stages of the purification process were analyzed using SDS-PAGE to assess protein presence and purity.

2.2.4. Production and Purification of HIV-1 Capsid Hexamer

HIV-1 capsid hexamer (A14C/E45C/W184A/M185A mutant) was produced and purified by following the production and purification method in the literature (Pornillos et al. 2010). Same protocol as for HIV-1 capsid monomer production was used. HIV-1 capsid hexamer protein was purified using Q (Quaternary Ammonium) Sepharose anion exchange column, SP (Sulphopropyl) Sepharose cation exchange column and Size exclusion chromatography (SEC).

2.2.5. SDS-PAGE Analysis

The production and purification of HIV-1 CA was validated with SDS-PAGE analysis. The samples of before and after IPTG induction, before and after SP cation exchange column and before and after Q Sepharose anion exchange column were collected to run on a 12% SDS-PAGE gel. Following induction, a protein band corresponding to the expected molecular weight was anticipated, which is 25.6 kDa. For sample preparation, cell pellets were resuspended in 1X SDS Running Buffer (25 mM Tris Base, 192 mM Glycine, 0.1% w/v SDS) and diluted according to their OD values. The soluble protein samples were prepared by mixing 40 µL of protein solution with 10 µL of 5X SDS Loading Dye, which contains 100 mM DTT, 1% w/v Bromophenol Blue, 50% v/v Glycerol, 8% w/v SDS, and 250 mM Tris-HCl (pH 6.8). For resuspended cell pelets, A 5X SDS Loading Dye solution was added to each sample at a final concentration of 1X. The samples, along with a protein ladder, were then heated at 95°C for 10 minutes using a block heater. After heating, the samples and ladder were loaded into the gel wells and electrophoresed at 60V in 1X SDS Running Buffer. Upon completion, the gel was carefully removed, rinsed with distilled water, and transferred to a staining box containing Solution 1 (50% Ethanol, 10% Acetic Acid). The gel was heated in a microwave for 30 seconds and subsequently cooled for 5 minutes on a shaker at 25°C. Solution 1 was then discarded, and Solution 2 (5% Ethanol, 7.5% Acetic Acid) was added along with 350 µL of Staining Dye (0.25% Coomassie Brilliant Blue R-250 in 95% Ethanol). The gel was microwaved again for 30 seconds and incubated at 25°C on a shaker for 1 hour. After incubation, Solution 2 was removed, and the gel was washed with distilled water for destaining.

2.3. HIV-1 CA Oligomerization Assay

For the HIV-1 capsid protein oligomerization assay, the method in the article was followed with the aim of screening compounds for their potential effects on oligomerization kinetics (Tsiang et al. 2012). Oligomerization was monitored

spectrophotometrically at 350 nm by measuring light scattering due to polymerized tubular structures formed in high-salt conditions. To prepare the required buffers, two solutions were filtered using a 0.45 μm syringe filter. Buffer 1 contained 50 mM sodium phosphate (pH 7.4), while Buffer 2 was composed of 50 mM sodium phosphate (pH 7.4) and 4 M NaCl. In the first step, HIV-1 CA protein was prepared at a final concentration of 60 μM in Buffer 1, containing 1% DMSO, in a total volume of 24.5 μL (Table 2). Additionally, a blank sample (without protein) was prepared as a negative control. These samples were loaded into a 384-well plate. The compound solution, consisting of 0.5 μL of 5 mM stock in 100% DMSO, was added to each well. The plate was incubated at 25°C for 10 minutes. To initiate the oligomerization reaction, 25 μL of Buffer 2 was added to each well, bringing the final protein concentration to 30 μM and the final buffer composition to 50 mM sodium phosphate (pH 7.6) with 2 M NaCl. The total reaction volume was 50 μL. The plate was sealed with a transparent film to prevent evaporation and placed into a Thermo Scientific™ Multiskan™ GO Microplate Spectrophotometer. Absorbance measurements at 350 nm were recorded every minute for 14 hours at 25°C.

The blank sample was used to account for background signals, while the control sample provided a baseline oligomerization rate. The impact of test compounds on HIV-1 CA oligomerization kinetics was assessed by comparing their effects on the rate and saturation point of the absorbance signal. The oligomerization time was determined by the time required to reach signal saturation, while the oligomerization rate was calculated from the slope of the linear phase of absorbance increase.

Table 2. HIV-1 Capsid Oligomerization Reaction Components and Quantities.

	Amounts in 50 ul reaction (ul)		
Reagents	**30 uM Protein**	**30 uM Protein with compounds**	**Blank**
60 uM Protein (in Buffer 1)	24.5	24.5	-
Buffer 1	-	-	24.5
DMSO	0.5	-	0.5
Buffer 2	25	25	25
Compound in DMSO	24.5	24.5	-

2.4. Differential Scanning Fluorometry Assay

The impact of tested compounds on the melting temperature (Tm) of the HIV-1 CA protein was evaluated using the differential scanning fluorimetry (DSF) method, following established protocols (Miyazaki et al. 2017). During the optimization phase, various protein concentrations (5 μM and 10 μM) and reaction volumes (20 μL and 50 μL) were assessed. The most distinct fluorescence signal was observed at a protein concentration of 5 μM and a reaction volume of 50 μL, which were subsequently used for further analyses. Additionally, SYPRO Orange dye concentrations of 1X and 2X were tested, with 1X providing the optimal signal.

The total reaction volume was set to 50 μL. The buffer was prepared at a final concentration of 50 mM Tris-HCl, pH 8.0 in a total volume of 10 mL. The SYPRO Orange fluorescent dye was diluted with dH2O from its original 5000X stock to a working concentration of 20X. Each reaction mixture contained 10 μM HIV-1 CA protein in a buffer composed of 50 mM Tris-HCl (pH 8.0) and 1 mM 2-mercaptoethanol, with SYPRO Orange dye (Invitrogen) added at a final concentration of 1X (Table 3).

The samples prepared were transferred to a 96-well plate. Three different sample conditions were used: (i) a blank sample containing only buffer and DMSO (no protein, no compounds), (ii) a control sample containing protein, buffer, and 1% DMSO (without test compounds), and (iii) experimental samples containing protein, buffer, and test compounds in 1% DMSO. The amounts of reagents needed for the samples are provided in Table 3.

The calculated amounts of buffer and protein for each sample were added to the respective wells in a 96-well plate. Lastly, SYPRO Orange fluorescent dye was added to each well. The plate was sealed and placed in a qPCR instrument (Roche LightCycler® 480 Real-Time PCR). In the analysis mode, "Melting Curve" was chosen. In the "Temperature Targets Section," the following conditions were set: Target: 20˚C, Acquisition Mode: none, Hold: 00:00:15, Ramp rate: 4.4. For the next set of conditions, the Target was set to 90˚C, Acquisition Mode: continuous, Acquisition (per ˚C): 10, and Ramp rate: 0.03. The final set of conditions was Target: 20˚C, Acquisition Mode: none, Hold: 00:00:15, and Ramp rate: 2.2. Excitation and emission wavelengths were set to 465 nm and 580 nm, respectively.

Table 3. DSF Reaction Components and Quantities.

	Negative Control	Blank Sample	Positive Control	Experimental
Sodium Phosphate	47 uL	47 uL	44.5 uL	44.5 uL
100 uM HIV-1 CA	-	-	2.5 uL	2.5 uL
20X SYPRO Orange	2.5 uL	2.5 uL	2.5 uL	2.5 uL
Compound (in 100% DMSO)	-	0.5 uL	0.5 uL	0.5 uL
100% DMSO	0.5 uL	-	-	-

The Tm of the protein was determined from the midpoint of the fluorescence signal transition in the melting curve or from the peak in the first derivative (dFI/dT) graph. Changes in Tm values in the presence of different compounds were analyzed to determine their influence on the thermal stability of the HIV-1 CA protein. All experiments were conducted in triplicate for reproducibility, and standard deviations of Tm values were calculated.

CHAPTER 3

RESULTS AND DISCUSSION

3.1. Molecular Docking Results

In this study, 279 natural molecules derived from plants and microorganisms were screened for their potential to bind the HIV-1 capsid (CA) monomer using molecular docking. These compounds were selected from the natural product library of Bedir group, representing a structurally diverse collection of secondary metabolites isolated from Turkish flora and microbial sources. To predict the interactions between these molecules and the capsid protein, AutoDock Vina (version 1.2.3.) was employed as the docking software due to its high accuracy and efficiency in binding affinity estimation. The primary aim of this screening was to identify candidate molecules capable of targeting key functional regions of the HIV-1 capsid, which plays a central role in viral assembly and replication.

The docking grid box was defined to encompass the entire capsid monomer structure, allowing for blind docking to explore all potential binding sites, as the exact interaction region of the test compounds was unknown. The center coordinates (X = 7, Y = –67, Z = 2) and dimensions (71 Å × 71 Å × 71 Å) were selected based on protein's structural boundaries. An exhaustiveness value of 32 was set to increase sampling thoroughness and ensure reliable binding predictions. During docking simulations, all ligands were treated as flexible while the protein was kept rigid, following AutoDock Vina's default protocol.

3.1.1. Molecular Docking Validation

To ensure the reliability of our molecular docking approach, a validation step was performed using the HIV-1 capsid protein and its known ligands, Lenacapavir and PF74. These compounds have been extensively studied and are known to bind a specific site on the capsid protein, making them ideal references for assessing docking accuracy.

Lenacapavir, an FDA-approved HIV-1 capsid inhibitor, binds at a pocket between the N-terminal and C-terminal domains of an adjacent capsid hexamer, stabilizing the capsid structure and interfering with viral replication (Link et al. 2020). Similarly, PF74 targets the same binding region and disrupts capsid function (Price et al. 2014). To validate our docking protocol, we re-docked these ligands into their native binding sites using AutoDock Vina, ensuring that the predicted binding poses closely matched their reference structures.

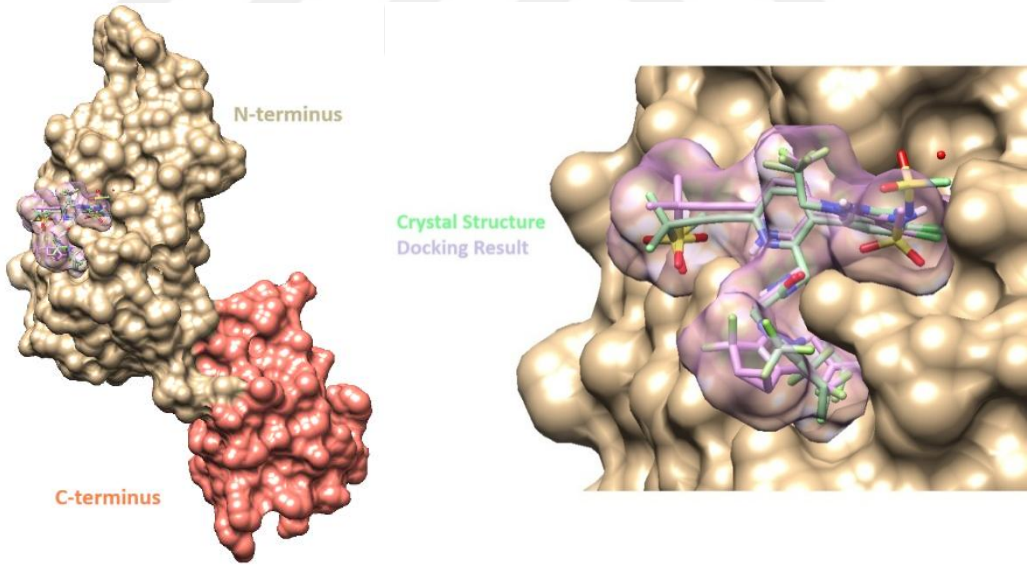

Figure 9. Docking result of Lenacapavir (purple) bound to the HIV-1 capsid was superimposed on HIV-1 CA and Lenacapavir complex crystal structure (green) (PDB id: 7RJ4), visualized using UCSF Chimera.

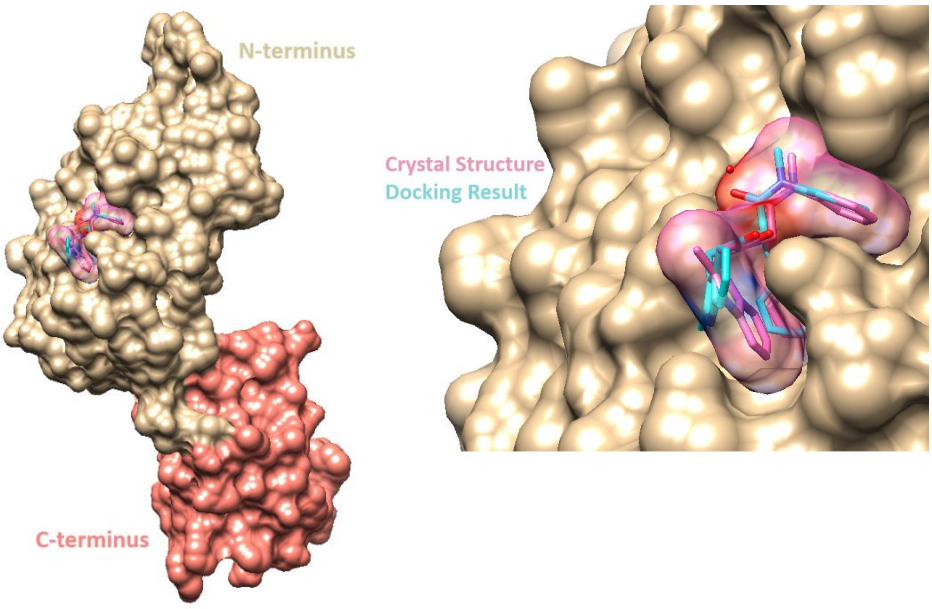

Figure 10. Docking result of PF74 (blue) bound to the HIV-1 capsid was superimposed on HIV-1 CA PF74 complex crystal structure (pink) (PDB id: 4XFZ), visualized using UCSF Chimera.

The accuracy of the docking process was evaluated by comparing the docked ligand conformations to their crystallographic structures. The binding energies of Lenacapavir and PF74 were determined as -9.31 and -8.07 kcal/mol (Table 4), respectively. In line with this data, molecules from our natural molecule library with binding scores of approximately -7 kcal/mol or lower were evaluated as candidates for experimental tests (Figures 9 and 10).

Table 4. AutoDock Vina scores of Lenacapavir and PF74.

	2D Structure	AutoDock Vina Score kcal/mol
Lenacapavir	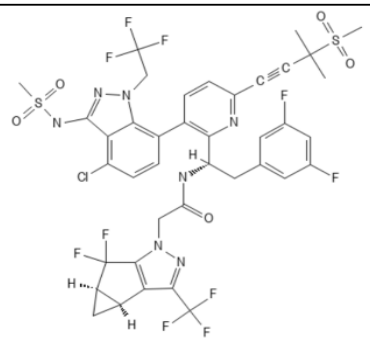	-9.31
PF-74	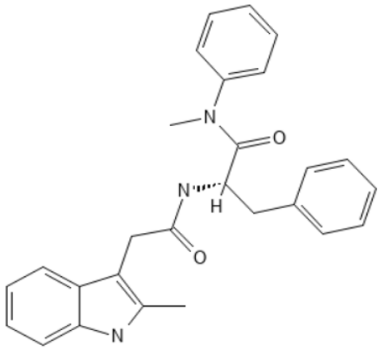	-8.07

3.1.2. Structural Classification of Docked Molecules

In this study, we classified the 279 natural compounds subjected to molecular docking analysis according to their structural features using NPClassifier (Kim et al. 2021) and evaluated their distribution. Triterpenoids constituted the most common structural group, representing 62.7% (n = 175) of the library. Other significant classes included steroidal compounds (6.8%, n = 19), flavonoids (4.3%, n = 12), and polyethers (3.6%, n = 10). Compound classes with fewer than 10 molecules were grouped as 'Others' (Figure 11).

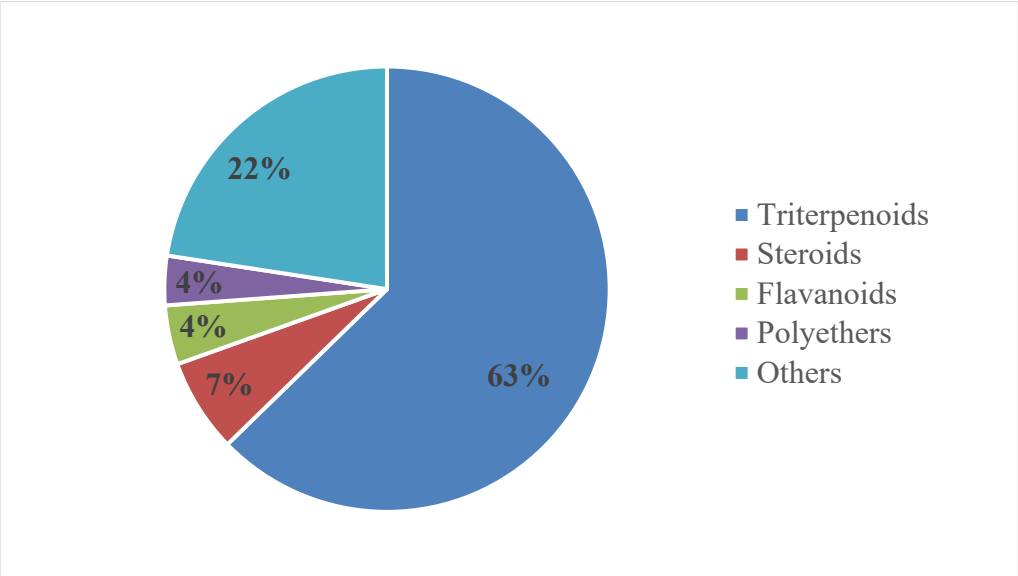

Figure 11. Classification of 279 secondary metabolites.

3.1.3. Molecules Tested Experimentally

In the selection process, not only the binding energies but also the binding sites of the compounds to the capsid protein were considered. In the literature, five main binding sites (Figure 12) have been identified on HIV-1 capsid protein (McFadden et al. 2021). Molecules such as Lenacapavir and PF74 are known to bind to the so-called Site 1.

The C-terminal domain (CTD) of the HIV-1 capsid protein contains a highly conserved hydrophobic groove (designated as site 3) that plays a critical role in viral maturation and assembly processes. In literature, this region was first identified as the binding site of capsid assembly inhibitor (CAI) peptide. Structural studies revealed that the CAI peptide binds to this hydrophobic groove between residues 169-191 on the capsid CTD and that this binding exerts an allosteric effect on capsid dimerization (Curreli et al. 2011).

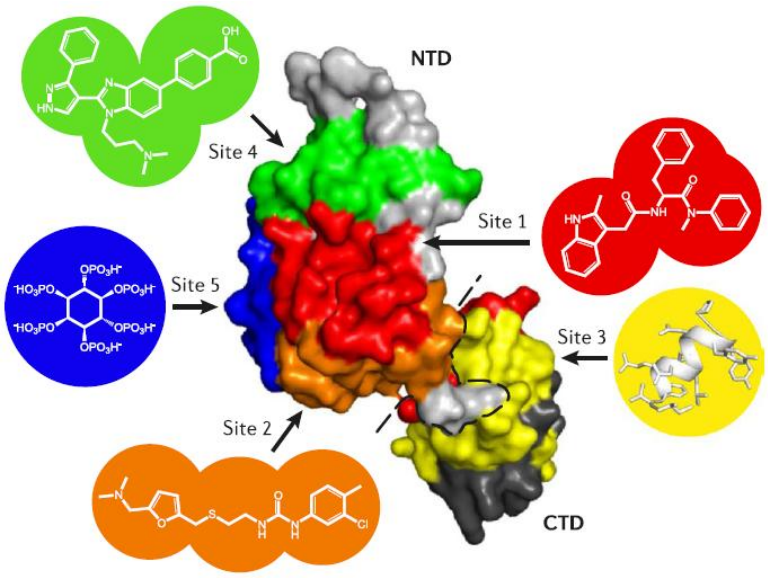

Figure 12. Five binding sites of HIV-1 CA protein. Adapted from (Source: McFadden et al. 2021).

In this study, 175 of the 279 natural compounds were classified as triterpenoids using NPClassifier classification (Table 5) (Kim et al. 2021). Based on docking scores and their potential interactions with Site 3 on CA-CTD, 19 of these 175 triterpenoid compounds were selected for experimental testing. The structural similarities and hydrophobic characteristics of our molecules strengthen their potential to show CAI-like binding behaviors. In this study, we aimed to evaluate the compounds from different subclasses. The experimentally tested triterpenoids belong to subgroups representing various structural skeletons such as cycloartane, cucurbitane, oleanane, lanostane-tirucallane-euphane, polypodane, dammarane-protostane and lupane. This structural diversity allowed us to compare the interaction of the molecules with HIV-1 capsid protein and enabled a more in-depth study of structure-activity relationships. Thus, not only the binding scores but also the differences in the biological effects of triterpenoids depending on their basic structural skeleton were investigated. Previously mentioned HIV-1 CA site 3 is a hydrophobic region and most of the triterpenoid molecules we tested bind to site 3 (Zhang et al. 2020).

Bevirimat, a triterpenoid molecule, was one of the first molecules to disrupt viral assembly by inhibiting the maturation process of Gag-Pol polyproteins of HIV-1 virus. Betulinic acid and its derivatives not only act on the capsid protein, but also interact with

the gp41 glycoprotein of HIV, preventing the viral fusion step (Aiken and Chen 2005). These triterpene compounds are important candidates for anti-HIV-1 therapies due to their low toxicity and broad biological effects (Blundell et al. 2020).

Table 5. AutoDock Vina results of experimentally tested triterpenoid compounds.

Molecule	2D Structure	AutoDock Vina Score kcal/mol	Molecule	2D Structure	AutoDock Vina Score kcal/mol
ATB-01	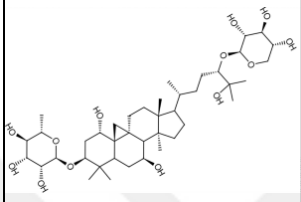	-6.96	**Betulin**	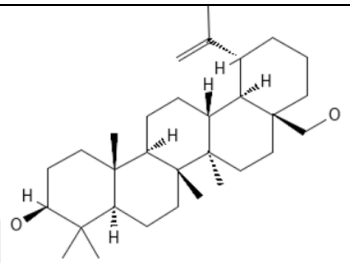	-6.52
ATB-05	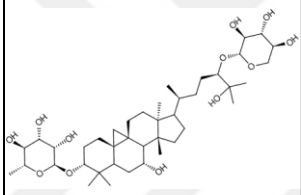	-7.41	**B-SCG-12**	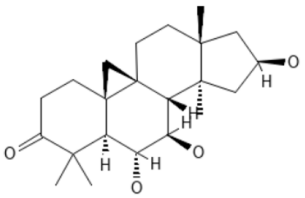	-6.66
B-AG-02	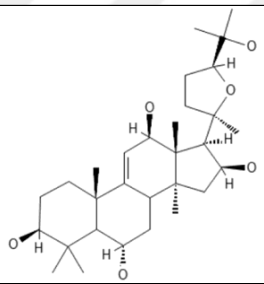	-7.5	**B-SKG-04**	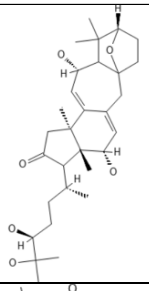	-7.58
B-AG-04	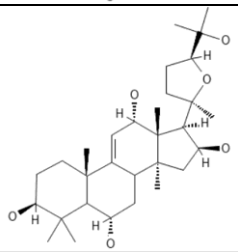	-7.08	**CCPG-24**	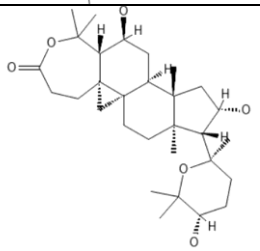	-8.27
B-AG-06	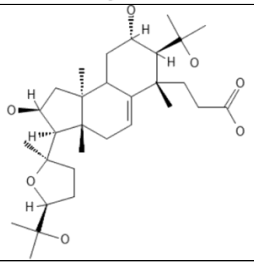	-7.72	**MD-MG-01**	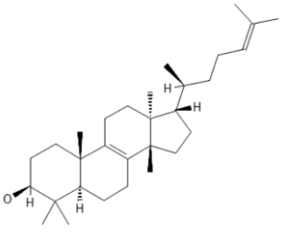	-7.2

(cont. on next page)

Table 5. (cont.)

B-AG-07	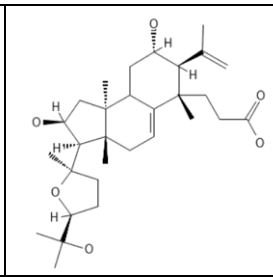	-7.31	**MD-MG-03**	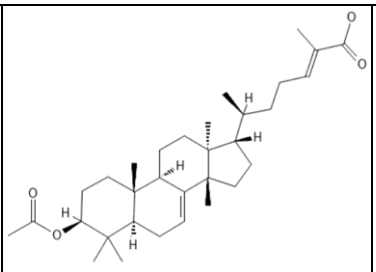	-8.58
B-CG-03	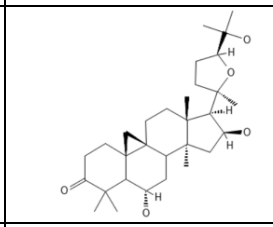	-6.91	**MD-MG-04**	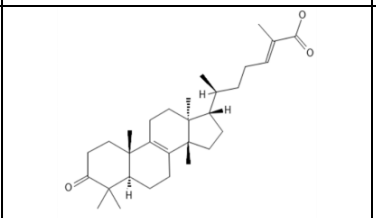	-7.83
B-CG-04	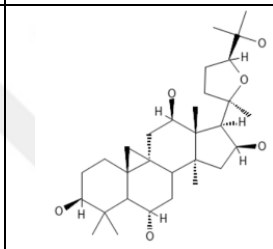	-6.94	**MD-MG-12**	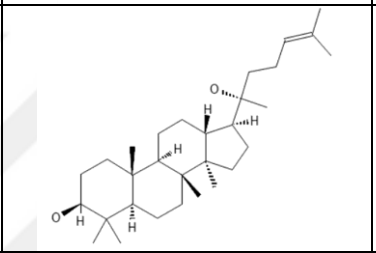	-7.11
B-CG-08	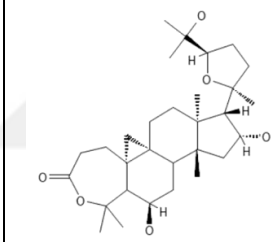	-7.93	**S-SCG-04**	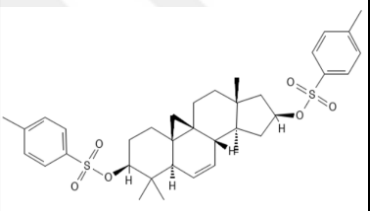	-8.32
B-CG-09	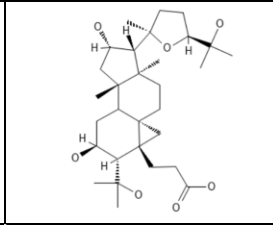	-6.66			

Although most of the compounds tested experimentally in this study were triterpenoids, compounds from structurally different classes were also evaluated. Based on their docking scores and biological activities reported in the literature, we tested flavonoids (n=2), steroids (n=2), polyethers (n=1), oligopeptides (n=1) and macrolides (n=1) (Table 6). These molecules may interact with HIV-1 capsid protein different mechanisms with their different structural properties and polarity levels. Especially flavonoids have the potential to form hydrogen bonds and π-π interactions on the protein surface with their polyphenolic structures (Cushnie and Lamb 2005). Similarly, steroid

derived natural compounds are an important group of secondary metabolites capable of establishing effective interactions with biological targets through their stable four-ring carbon skeletons. Their hydrophobic nature allows them to establish strong interactions with particularly hydrophobic binding pockets of proteins. (Nandu and Jithesh 2024).

Table 6. AutoDock Vina scores of other experimentally tested non-triterpenoid compounds.

Molecule	2D Structure	AutoDock Vina Scores kcal/mol	SuperClass	Origin
ActD	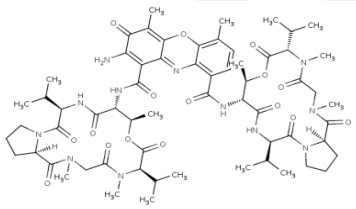	-10.13	Oligopeptides	Microorganism
Chlorogenic Acid	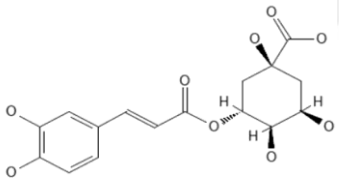	-6.57	Phenylpropanoids (C6-C3)	Plant
Fisetin	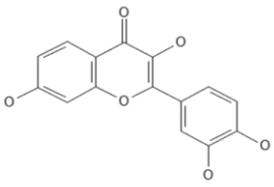	-7.48	Flavonoids	Plant
Pha-Ole-01	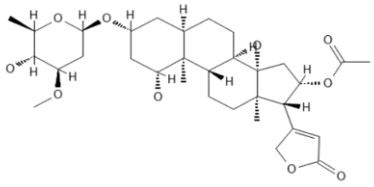	-7.75	Steroids	Plant
Quercetin	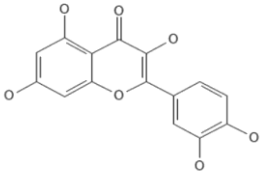	-7.4	Flavonoids	Plant

(cont. on next page)

Table 6. (cont.)

Rapamycin	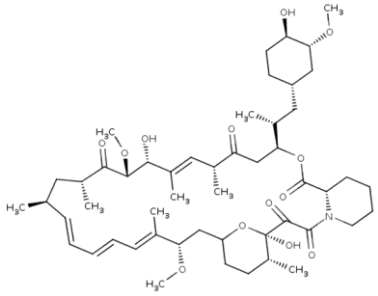	-7.83	Macrolides	Microorganism
Ruscogenin	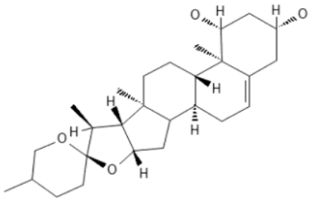	-9.11	Steroids	Plant

3.2. Production and Purification of HIV-1 Capsid Protein

In this study, a total of 1 L culture was prepared to produce HIV-1 capsid (CA) protein for experimental analysis. *E. coli* BL21 (DE3) cells carrying pET-11a/CA plasmid were used for protein expression and cells were grown in Terrific Broth (TB) medium. When the cell density reached $OD_{600} \approx 0.8$, induction was performed with 0.5 mM IPTG, and the culture was incubated overnight at 25°C.

Cell samples taken before (uninduced) and after (induced) induction were analyzed on a 12% SDS-PAGE gel to confirm expression. As seen in Figure 1, lanes 1 and 3 correspond to uninduced samples and lanes 2 and 4 correspond to samples induced overnight with IPTG. The band at approximately 25 kDa observed only in the induced samples indicates that the capsid protein was successfully produced (Figure 13).

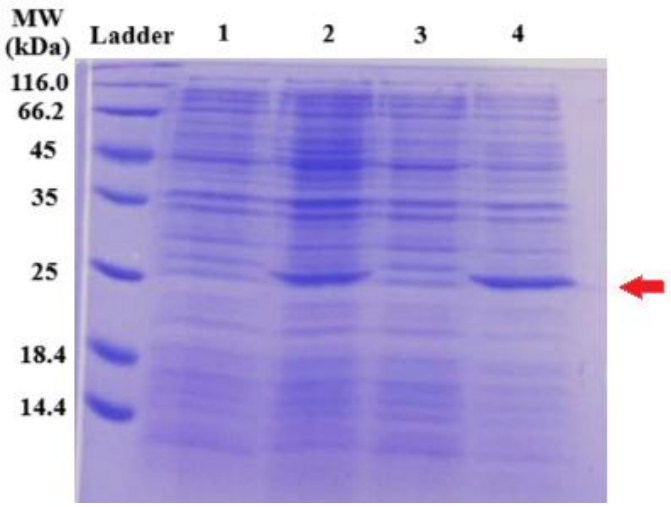

Figure 13. 15% SDS-PAGE gel analysis image of the HIV-1 Capsid protein production. 1: Uninduced sample. 2: Induced sample. 3: Uninduced sample. 4: Induced sample. The red arrow indicates capsid protein observed at approximately 25 kDa.

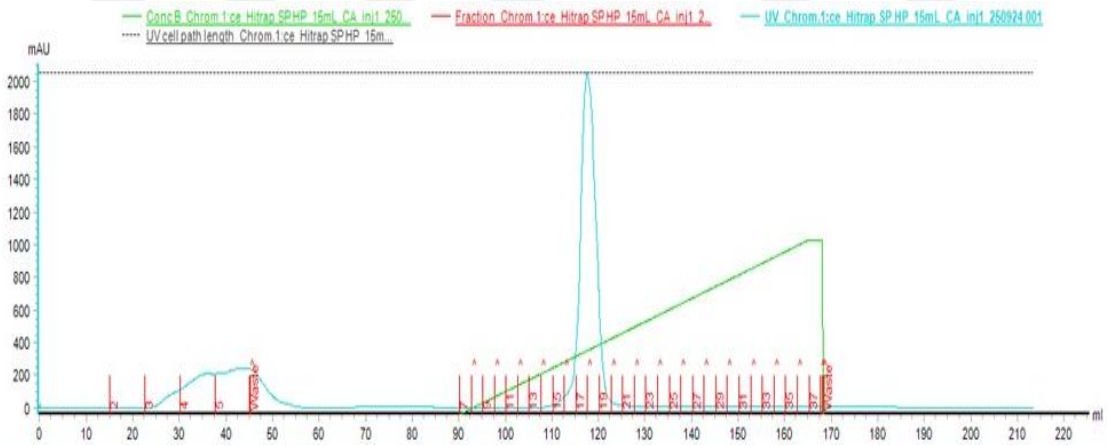

Figure 14. Elution profile of HIV-1 capsid protein purification by SP cation exchange chromatography. The green line indicates NaCl gradient; the cyan line indicates UV absorbance measured at 280 nm. The UV signal peak indicates fractions of HIV-1 CA protein eluted from the column.

Purification of HIV-1 capsid protein was performed by two-step ion exchange chromatography. First, the soluble lysate was loaded onto SP-Sepharose (cation exchange) column and a linear NaCl gradient (green line) was applied to elute the bound proteins. In the chromatogram shown in Figure 14, it was observed that the target protein was eluted in the range of approximately 18-22% NaCl concentration, with a distinct, cyan-colored UV peak in fractions 15, 17 and 19.

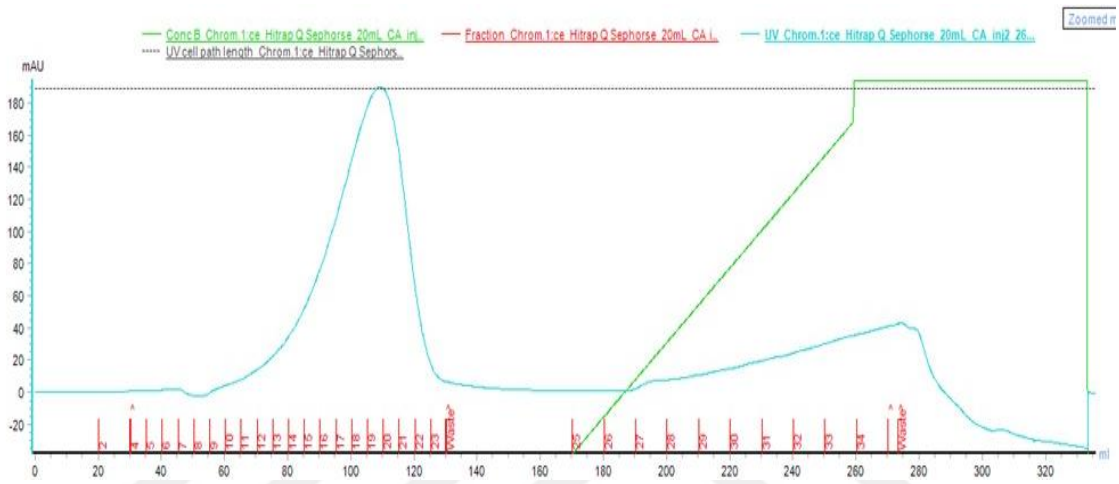

Figure 15. Chromatographic elution profile of the second purification step of HIV-1 capsid protein on a Q-Sepharose anion exchange column. The cyan line represents the UV absorbance measured at 280 nm and the green line represents the NaCl gradient. The sharp peak observed corresponds to fractions of high purity HIV-1 CA protein eluted from the column.

The resulting SP elution fractions were then pooled and applied to a Q-Sepharose (anion exchange) column (Figure 15). In this step, the HIV-1 CA protein failed to bind to the column was collected directly in the flowthrough, corresponding to fractions 11–22 at the peak of the chromatogram shown in Figure 15. This two-step FPLC process yield high-purity CA protein. Final purity and identity were confirmed by SDS-PAGE analysis.

The protein contents of the fractions obtained from SP and Q columns were analyzed by 12% SDS-PAGE gel electrophoresis. As shown in Figure 16, samples from each purification step were loaded into separate wells and the presence of HIV-1 capsid protein was monitored through the band of approximately 25 kDa.

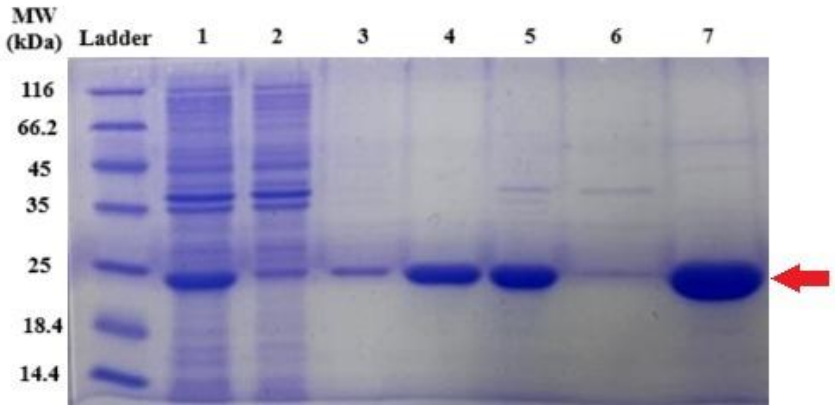

Figure 16. SDS-PAGE analysis of HIV-1 CA protein throughout the purification steps. Wells are in order: 1: SP column injection sample. 2: SP flowthrough. 3: SP wash. 4: SP elution. 5: Q column flowthrough. 6: Q elution. 7: Pure HIV-1 CA protein concentrated after Q column.

Total soluble protein was observed in the SP column loading sample (well 1), while no target protein was observed in the flowthrough (well 2) and wash fractions (well 3). This indicates that the capsid protein is bound to the column. A distinct 25 kDa band was observed in the elution fraction (well 4), which persisted in the Q column flowthrough (well 5) and elution (well 6) samples. Finally, an intense and isolated band was observed in the concentrated fraction (well 7), indicating that high purity HIV-1 CA protein was obtained.

The high purity fractions obtained after Q-Sepharose column were combined and concentrated to increase protein concentration. Concentration was performed using centrifuge filters with a cut-off of 3.5 kDa. After verifying the amount and purity of the concentrated protein solutions, the protein concentration was determined by measuring absorbance at 280 nm.

The equation $A = \varepsilon\text{-}c\text{-}l$ was used for concentration calculation. Here, ε (extinction coefficient) value was taken as 39210 $M^{-1}\text{-}cm^{-1}$ and l (cuvette path length) was taken as 1 cm. As a result of the calculations, the concentrations of the two protein stock solutions were found to be 787 µM and 905.5 µM, respectively. These stock proteins were stored at -80 °C to maintain structural and functional stability.

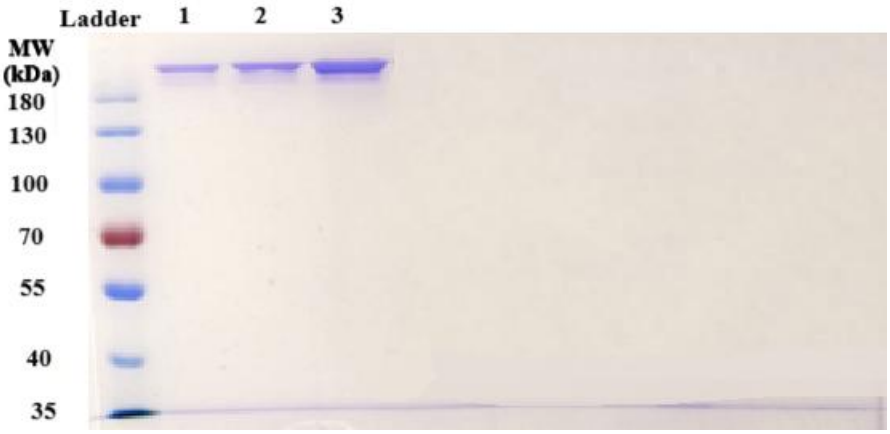

Figure 17. %8 SDS-PAGE analysis of HIV-1 Capsid Hexamer

The protein content of the fractions obtained from SEC column were analyzed by non-reducing 8% SDS-PAGE gel electrophoresis. As shown in Figure 17, samples were loaded into separate well and the presence of HIV-1 capsid hexamer was monitored.

3.3. HIV-1 Capsid Oligomerization Assay

The HIV-1 capsid protein (CA) plays a fundamental structural role in the life cycle of the virus. CA monomers associate in ordered manner by forming hexamer and pentamer rings, resulting in a capsid structure that forms the conical shell in the virus particle. This conical capsid protects the nucleic acid of HIV-1, provides stability in the reverse transcription process, and mediates its transport to the nucleus. Correct assembly of the capsid core is therefore critical for the replication and infectivity of the virus (Kobayakawa et al. 2021).

Under laboratory conditions, this assembly process can be mimicked *in vitro* using a high salt buffer (usually 50 mM sodium phosphate, 2 M NaCl, pH 7.6). In this medium, HIV-1 CA monomers self-assemble to form tubular structures. This tubular assembly process can be monitored spectrophotometrically by an increase in absorbance at 350 nm. This method has been widely used to monitor the kinetics of capsid assembly.

In vitro CA tubular assembly assay has also emerged as a valuable screening tool in drug discovery processes to assess the functional effects of small molecules interacting

with the capsid protein. Molecules can disrupt the correct assembly of CA monomers, prevent assembly or leading to the formation of abnormal structures. Known capsid inhibitors such as PF74, GS-CA1 and GS-6207 (Lenacapavir) have been tested with this method and shown to affect the capsid assembly process. For example, PF74 affects both oligomerization and the infection process by stabilizing or disrupting interactions between capsid monomers (Bhattacharya et al. 2014). Lenacapavir modulates the assembly process by significantly increasing CA hexamer stability and has long-acting antiviral potential (Link et al. 2020).

Furthermore, this method is used to detect molecules that not only inhibit capsid assembly but also stabilize or accelerate CA-CA interactions. In particular, the interactions of small molecules identified during drug development with binding sites on the capsid protein can directly affect the assembly kinetics. Indeed, mutations on capsid can disrupt these interactions, leading to slow or accelerated assembly kinetics. This assay is therefore a valuable tool not only for inhibitor screening but also for understanding molecular mechanisms (Tsiang et al. 2012; Shi et al. 2010).

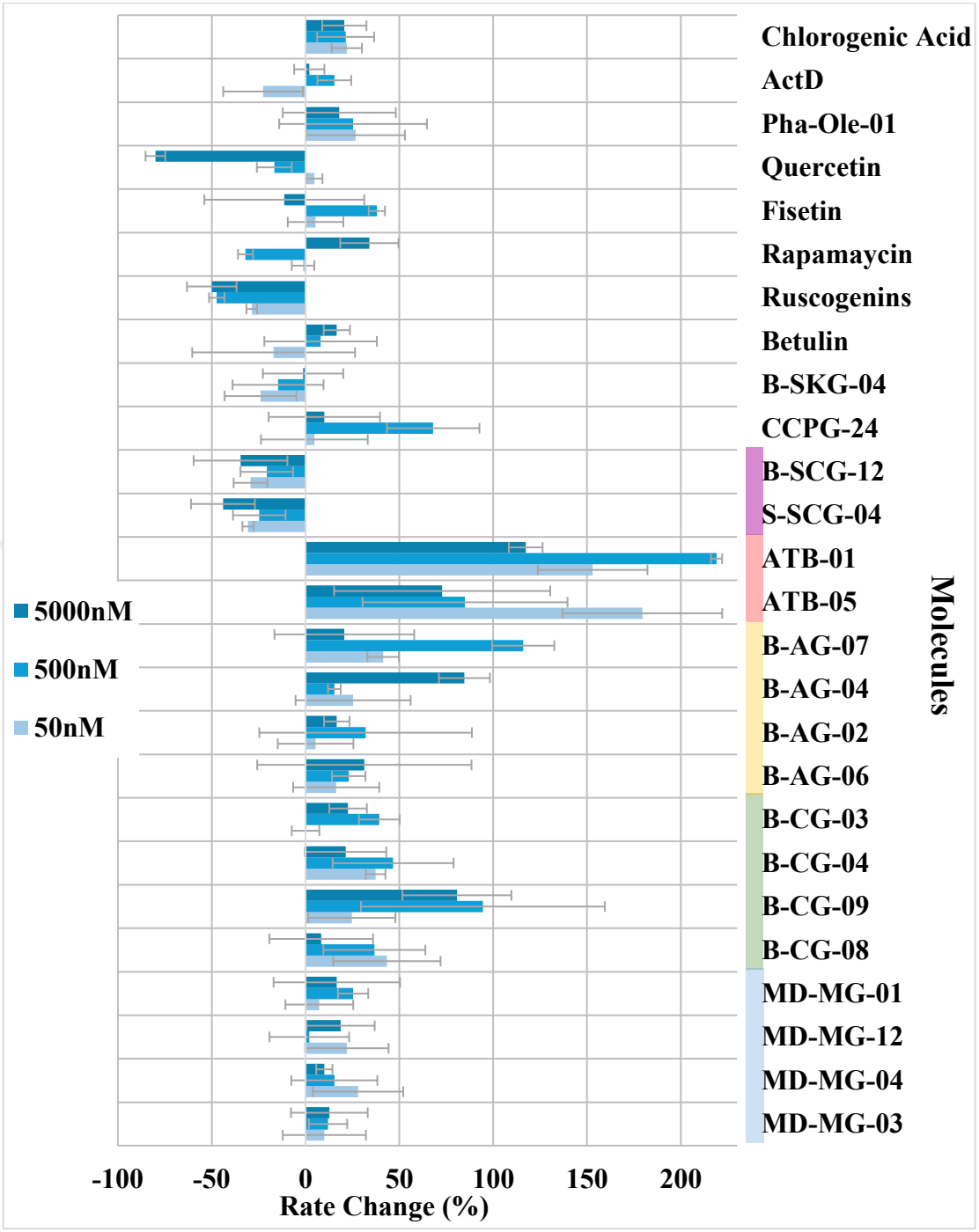

Figure 18. Effect of different concentrations of the tested natural compounds on *in vitro* oligomerization of HIV-1 capsid protein. The graph shows the percentage change in the oligomerization rate of HIV-1 capsid protein at 50 nM, 500 nM and 5000 nM concentrations of 26 selected natural compounds. Molecules are colored according to their groups, standard deviations are indicated at the ends of each bar.

In the oligomerization experiment, the strongest effects were obtained from ATB01 and ATB05 molecules, suggesting that these molecules may have the potential to bind a critical site affecting the formation of tubular capsid structures (Figure 18). Monomeric docking results revealed that both ATB01 and ATB05 molecules bound to site 3 with binding energies of -6.9 and -7.4 kcal/mol, respectively (Figure 18 and 19). In tubular capsid structures formed *in vitro* at high salt concentrations, we focused on molecules showing more than 50% rate change on CA. While examining the effect of the molecules in the oligomerization assay, the similar effect at three concentrations were taken into consideration. Since the ATB group molecules increased the CA tubular assembly rate, we also performed docking on a multimeric structure that represents all possible interaction sites on CA tubes. Multimer contains two adjacent CA monomers in a hexamer and two monomers from two different adjacent hexamers. Tri-hexameric interface is a junction formed by three adjacent capsid hexamers (Figure 21). Where the NTD (N-terminal domain) regions do not participate in the intra-hexamer interface and CTD-CTD interactions dominate the triple junction (Zhao et al. 2013).

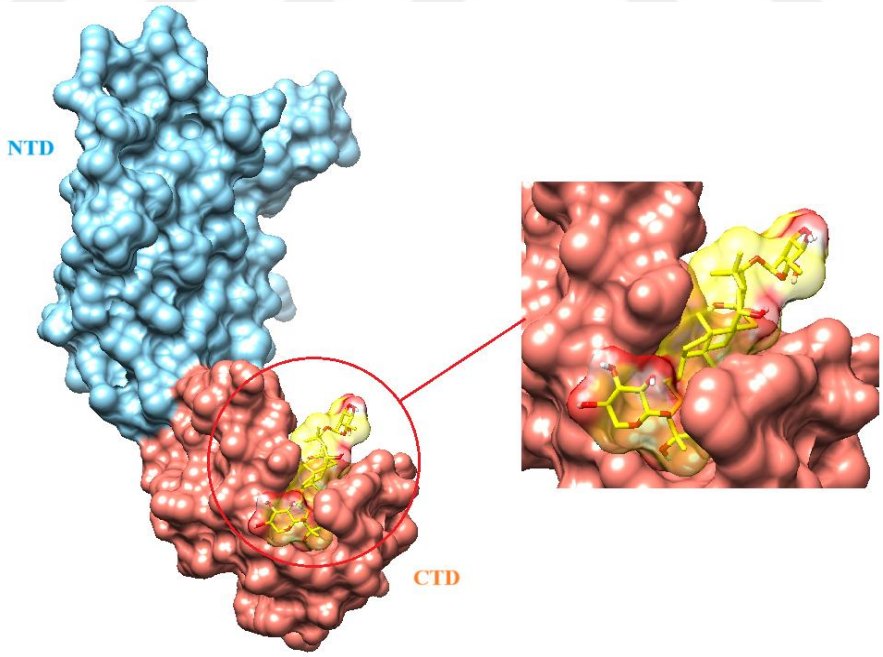

Figure 19. Docking pose of ATB-01 with HIV-1 CA monomer, visualized using UCSF Chimera. AutoDock Vina Score: -6.9 kcal/mol.

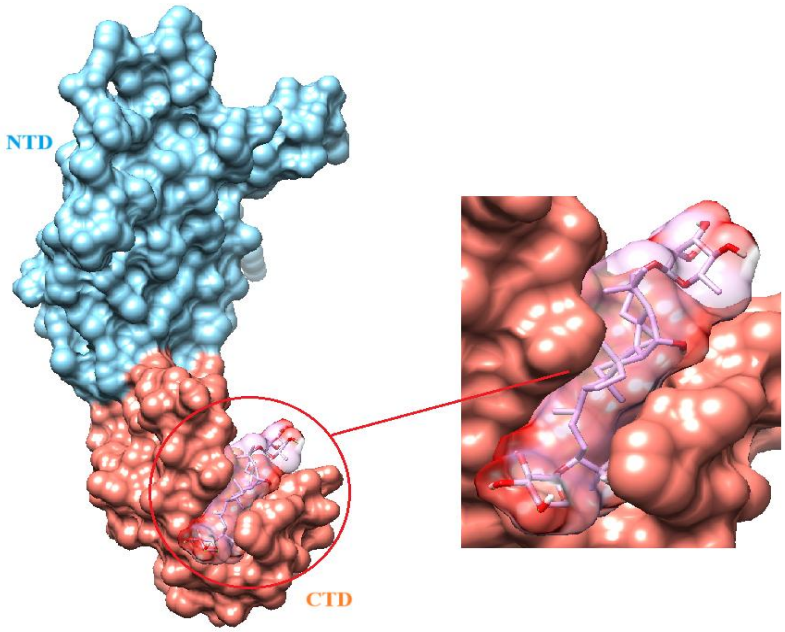

Figure 20. Docking pose of ATB-05 with HIV-1 CA monomer, visualized using UCSF Chimera. AutoDock Vina Score: -7.4 kcal/mol.

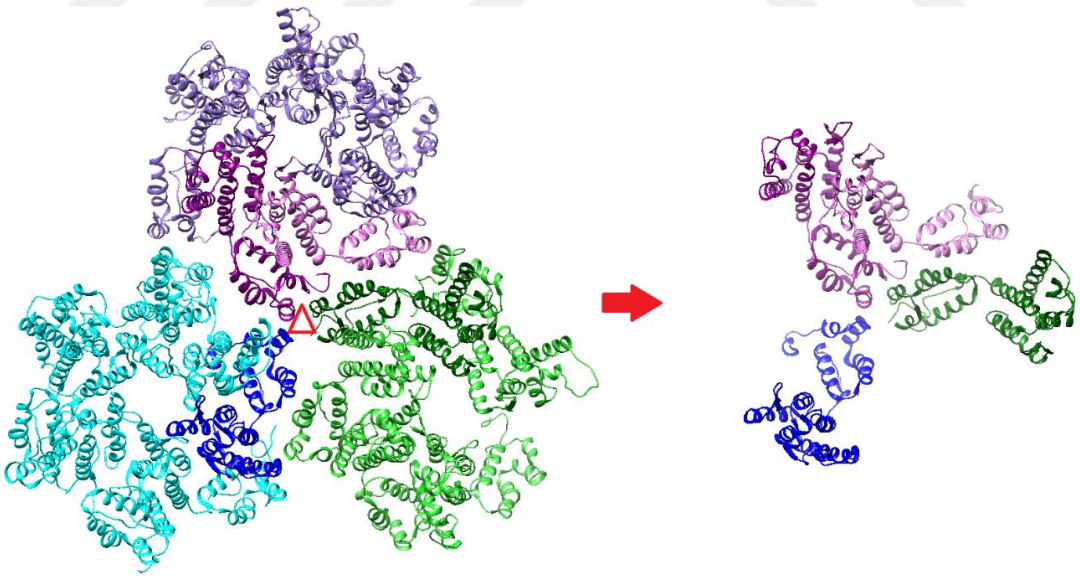

Figure 21. Tri-hexamer center complex was created for docking PDB id: 3J34, visualized using UCSF Chimera. Tri-hexamer interface was indicated with a red triangle (PDB id: 3J34).

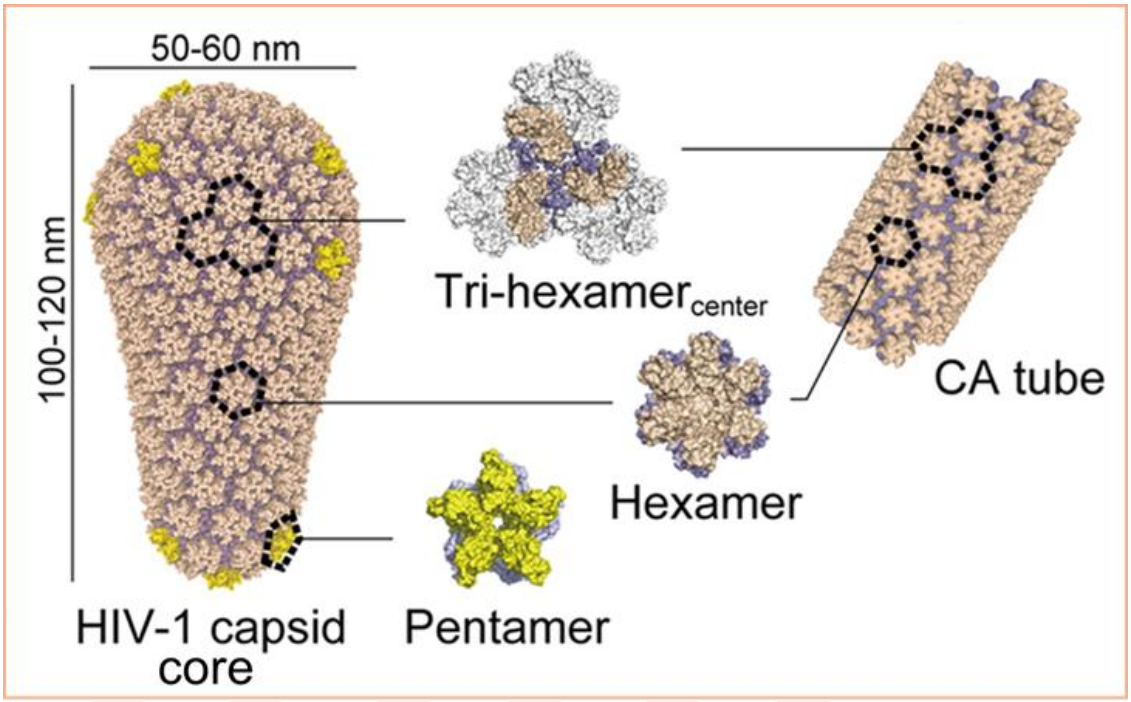

Figure 22. *In vitro* CA assemblies and tri-hexamer center (Source: Shen et al. 2023). The PDB id: 3J34 crystal structure was used to create the structure, a tetrameric structure was obtained by selecting a total of four monomers (subunits shown in dark blue, dark green and dark purple colors) interacting from three different hexamers. This structure was designed to cover the NTD-NTD, NTD-CTD and CTD-CTD interfaces, which are potential binding sites (Figure 21).

ATB01 and ATB05 molecules showed binding energies of -8.89 and -9.08 kcal/mol, respectively, on the tetrameric structure (Figure 23 and 25). These results show that the binding affinity is significantly increased in the multimer model. LigPlot analysis of the best binding pose for ATB01 and the CA multimer revealed 5 hydrogen bonds and numerous hydrophobic interactions at the tri-hexamer interface (Figure 24). Similarly, ATB05 was stabilized by both hydrogen bonds and non-bonded interactions (figure 25). These interactions are on critical amino acids such as LYS203, ALA204, LEU205, GLU213 and ILE201, which have been shown to be important in capsid stabilization in previous studies. It is reported in the literature that the tri-hexamer interface region is very important for drug development and that ligands binding to this region can affect HIV-1 capsid assembly. CTD-CTD interactions are critical for CA proteins to polymerize into

tubular structures (Zhao et al. 2013). In addition, small molecules can bind to the tri-hexamer interface and affect assembly kinetics.

In the light of these findings, ATB-01 and ATB-05 show strong binding potential to the tri-hexamer interface, suggesting that they may directly affect the oligomerization process and thus are potential inhibitor candidates that may disrupt the HIV-1 capsid assembly.

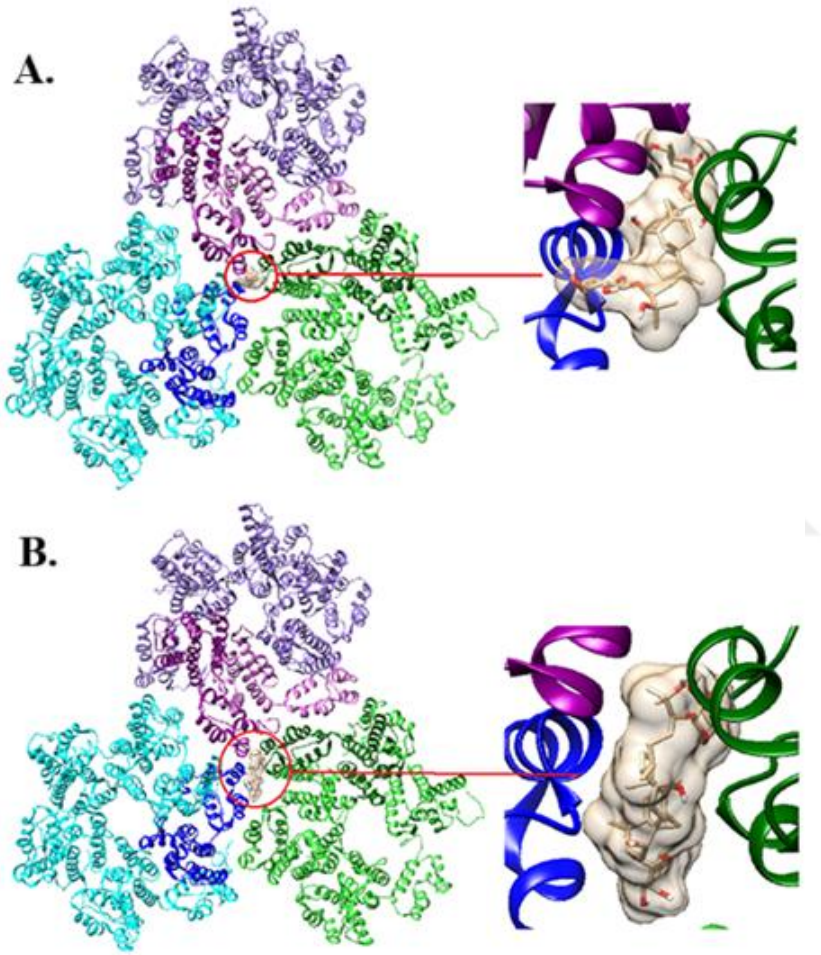

Figure 21. Best (A) and second best (B) Docking poses of ATB-01 with CA tetramer (PDB id: 3J34), visualized using UCSF Chimera. (A) AutoDock Vina score: -8.89 kcal/mol. (B) AutoDock Vina score: -8.88 kcal/mol.

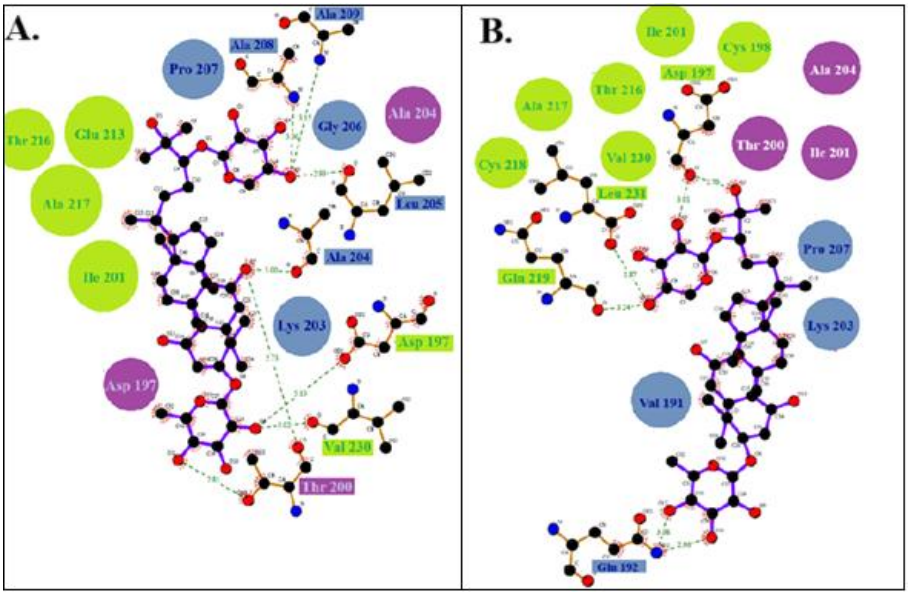

Figure 22. LigPlot analysis of Docking poses of ATB-01 with CA tetramer (PDB id: 3J34). Best (A) and second docking pose (B).

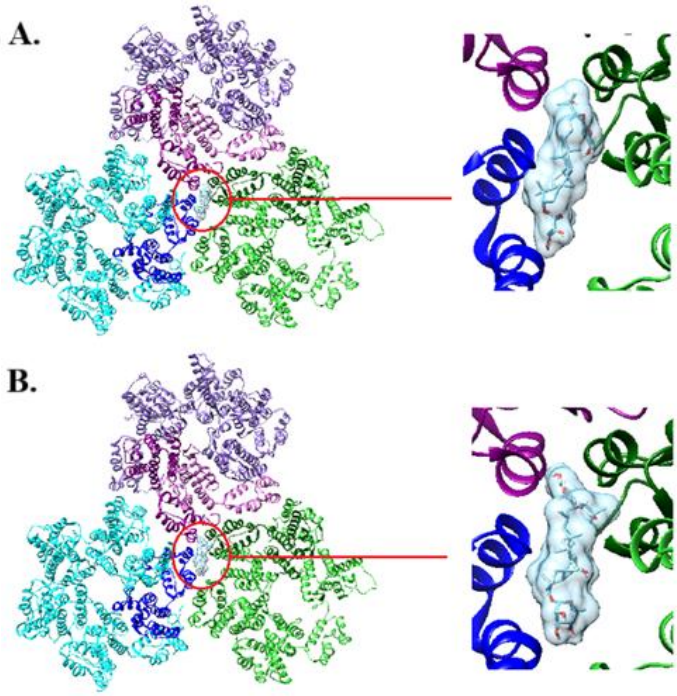

Figure 23. Best (A) and second best (B) Docking poses of ATB-01 with CA tetramer (PDB id: 3J34), visualized using UCSF Chimera. (A) AutoDock Vina score: -9.08 kcal/mol). (B) AutoDock Vina score: -8.79 kcal/mol).

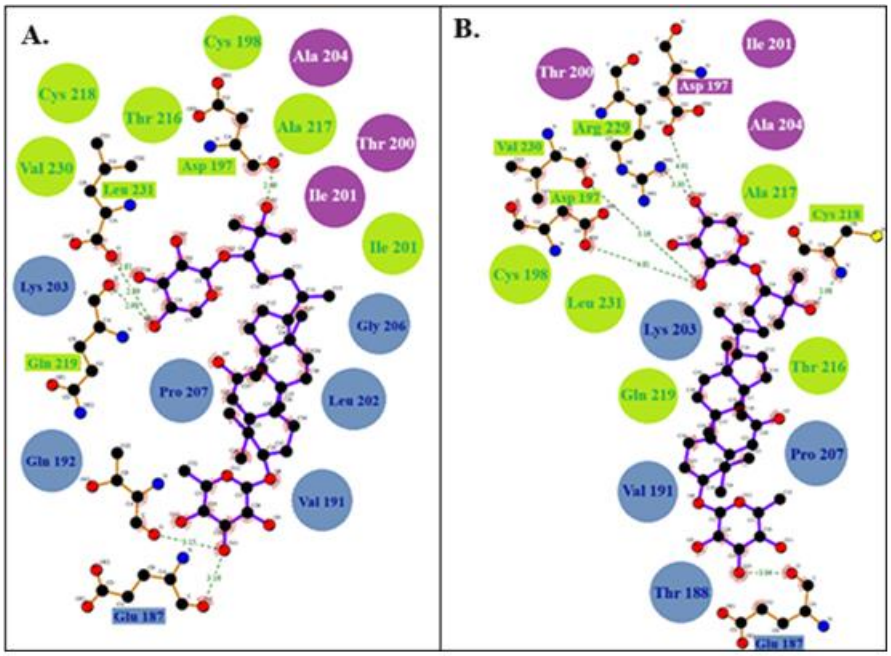

Figure 24. LigPlot analysis of Docking poses of ATB-05 with CA tetramer (PDB id: 3J34). Best (A) and second docking pose (B).

3.4. Differential Scanning Fluorometry (DSF) Assay

Early-stage drug discovery benefits greatly from structural biology since it can help drive, hit compound development by elucidating the binding mechanisms of lead compounds. DSF has been one of the reliable preliminary screening methods in drug discovery for over 20 years. Minimal protein and chemical needed in DSF, together with its straightforward analysis, simplify screening procedures, making it an excellent choice for large library screening (Gao, Oerlemans, and Groves 2020).

In this study, Differential Scanning Fluorimetry (DSF) was used to evaluate the effect of natural compounds on the thermal stability of HIV-1 capsid (CA) protein. DSF is a common and rapid biophysical analysis technique that allows fluorescence-based monitoring of the thermal stability of proteins. In this method, hydrophobic regions of proteins become accessible when proteins begin to melt with increasing temperature and fluorescent dyes (e.g. SYPRO Orange) bind to the hydrophobic regions of proteins generating a fluorescence signal (Vivoli et al. 2014; Huynh and Partch 2015).

DSF is particularly valuable for drug discovery and preliminary screening studies, as it allows rapid assessment of whether small molecules affect the target protein's thermal stability. In this direction, the Tm (melting temperature) changes of HIV-1 CA protein in the presence of the natural compounds were measured; compound binding can increase or decrease the thermal stability of the protein.

In DSF assays with HIV-1 capsid (CA) protein, various parameters were first optimized to increase experimental reliability. Accordingly, factors such as reaction volume (20-50 µL), protein concentration (5-10 µM) were tested (Figure 27). The conditions that give the strongest and most reproducible fluorescence signal were determined by comparing samples prepared as a mixture and individually.

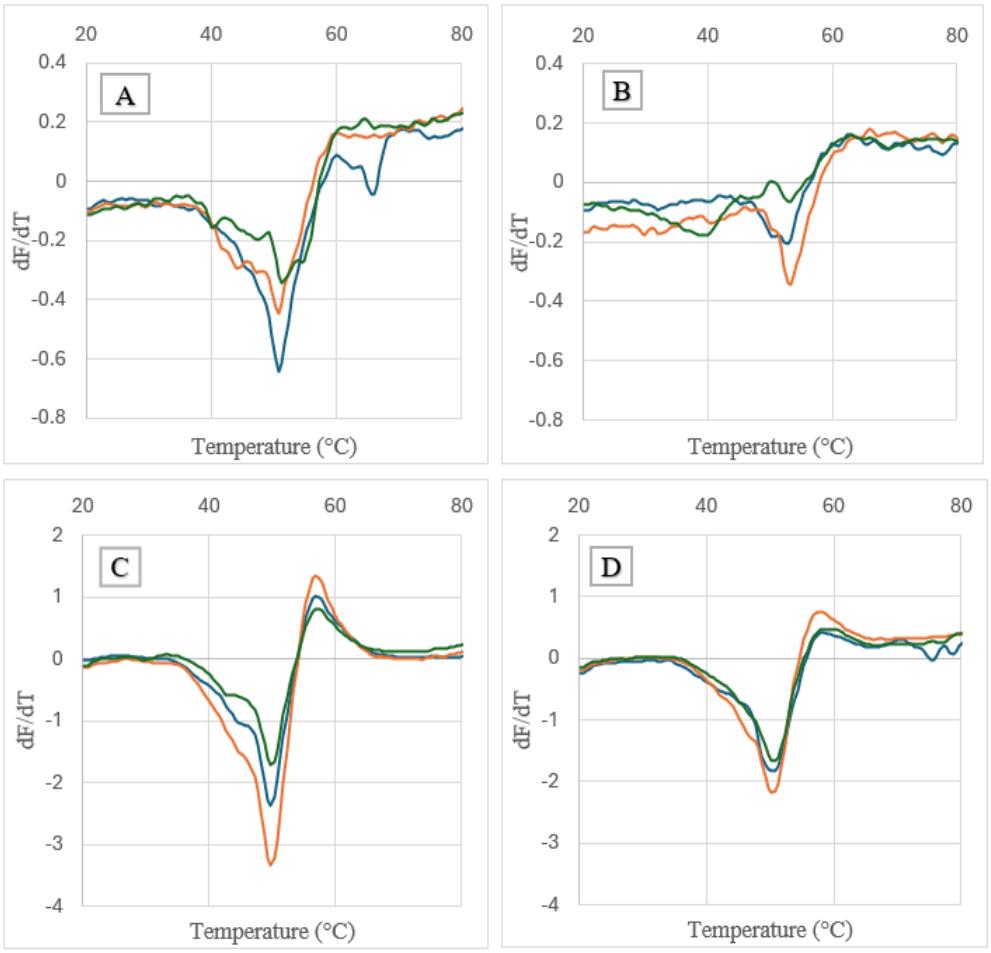

Figure 25. Conditions tested for DSF optimization. A: 10 uM protein in 20 uL final volume, B: 5 uM protein in 20 uL final volume, C: 10 uM protein in 50 uL final volume, D: 5 uM protein in 50 uL final volume.

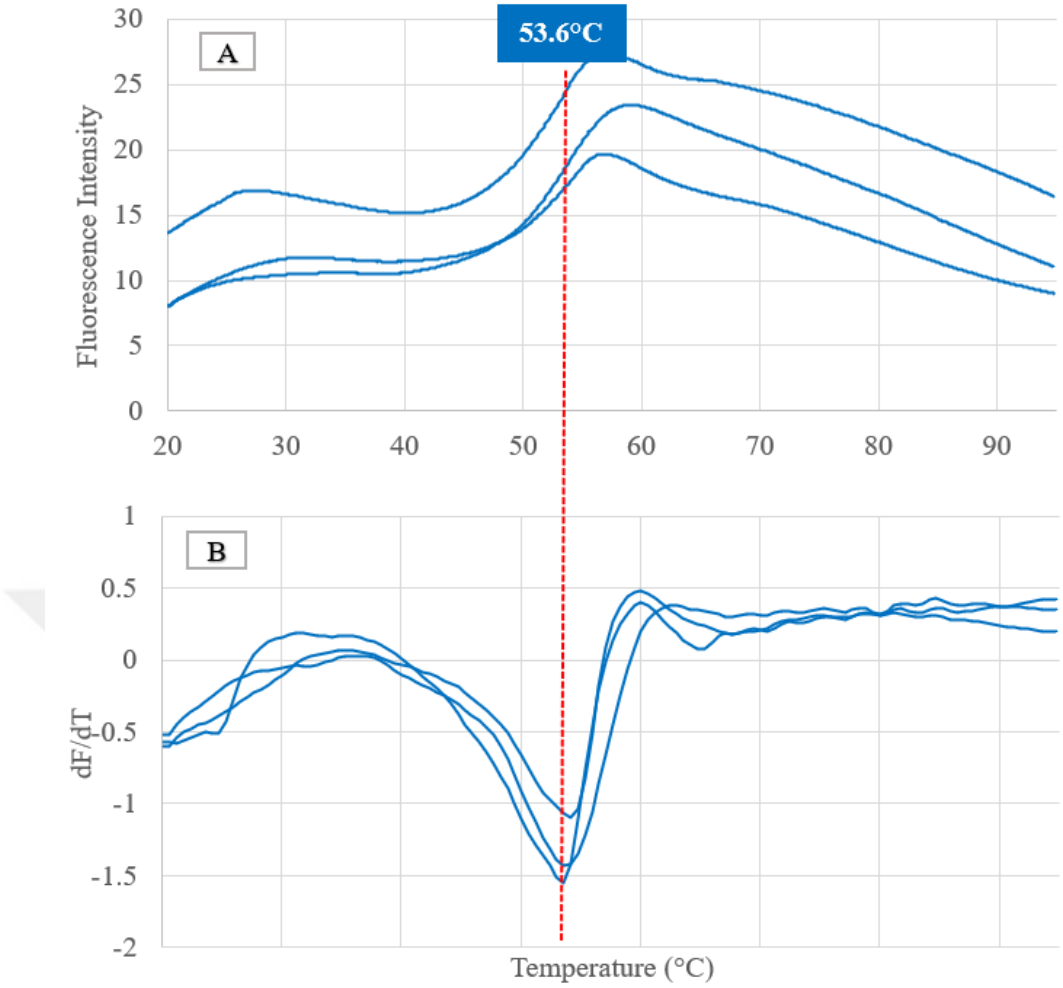

Figure 26. Melting temperature curve (A) and derivative of the melting temperature curve (B) of HIV-1 CA protein (5 uM).

As a result of the optimization studies, mixtures prepared with 5 µM protein concentration, 50 µL reaction volume and 1X SYPRO Orange dye provided the best melting curve and the most accurate Tm (melting temperature) value (Figure 28). These conditions were used as the reference standard for the compound screening experiments.

We tested 26 different natural compounds to determine their effects on the thermal stability of HIV-1 capsid protein by differential scanning fluorimetry (DSF). The experiments were conducted with three replicates for each compound. In the screening phase, all compounds were tested at a concentration of 50 µM as a standard condition (Figure 29).

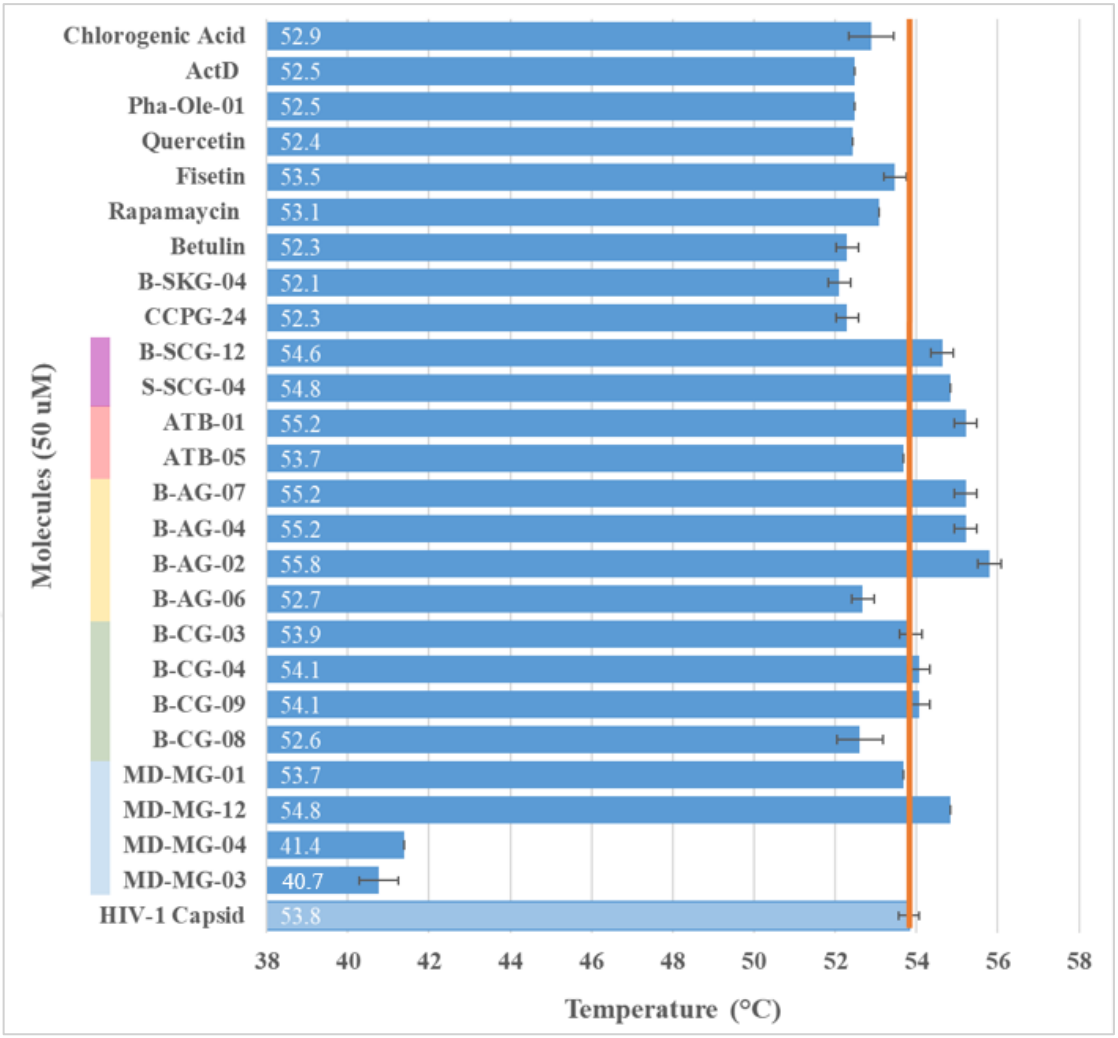

Figure 27. Melting temperature (Tm) of HIV-1 capsid (CA) protein is shown as bar graph in the presence of selected natural compounds (50 μM) in DSF experiment.

Table 7. Melting temperature change of HIV-1 capsid (CA) protein in the presence of selected natural compounds (50 μM).

Molecules	ΔTm (°C)	Molecules	ΔTm (°C)
ActD	1.3	B-AG-04	-1.4
MD-MG-03	13.1	B-AG-07	-1.4
MD-MG-04	12.4	B-SKG-04	1.7

(cont. on next page)

Table 7. (cont.)

MD-MG-12	-1.0	Fisetin	0.3
MD-MG-01	0.1	ATB-05	0.1
CCPG-24	1.5	ATB-01	-1.4
B-CG-08	1.2	Quercetin	1.4
B-CG-09	-0.2	Chlorogenic Acid	0.9
B-CG-04	-0.2	Betulin	1.5
B-CG-03	0.0	Rapamaycin	0.7
Pha-Ole-01	1.3	S-SCG-04	-1.0
B-AG-06	1.1	B-SCG-12	-0.8
B-AG-02	-2.0		

The pure HIV-1 CA protein sample exhibited an average melting temperature (Tm) of 53.8°C. Figure 29 shows the melting temperature of HIV-1 CA protein in the presence of all the compounds at 50 uM concentration. In the presence of two compounds MD-MG-03 and MD-MG-04 the Tm value of HIV-1 capsid protein decreased significantly, with Tm values measured as 40.7°C and 41.4°C, respectively. The change in Tm values reaches -13°C and -12.4°C, respectively (Table 7). The measurements obtained indicate that these compounds significantly destabilize the CA protein structure causing it to melt at a much lower temperature.

In the literature, in the presence of PF74 and Lenacapavir (20 uM), HIV-1 capsid (7.5 uM) shows between +3°C and +8°C higher melting temperature in DSF analysis, respectively (Wang et al. 2020). For instance, the Tm of HIV-1 CA hexamer (15 uM) in the presence of PF74 (20 uM) increases +7.4°C. PF74 does not provide a change in the Tm of monomeric CA because the binding pocket is not fully developed in a monomer (McFadden et al. 2024). This suggests that compounds such as MD-MG-03 and MD-MG-04 have a different mechanism of action than PF74-like binding mechanisms, by destabilizing the capsid monomer structure at the binding site in capsid monomer.

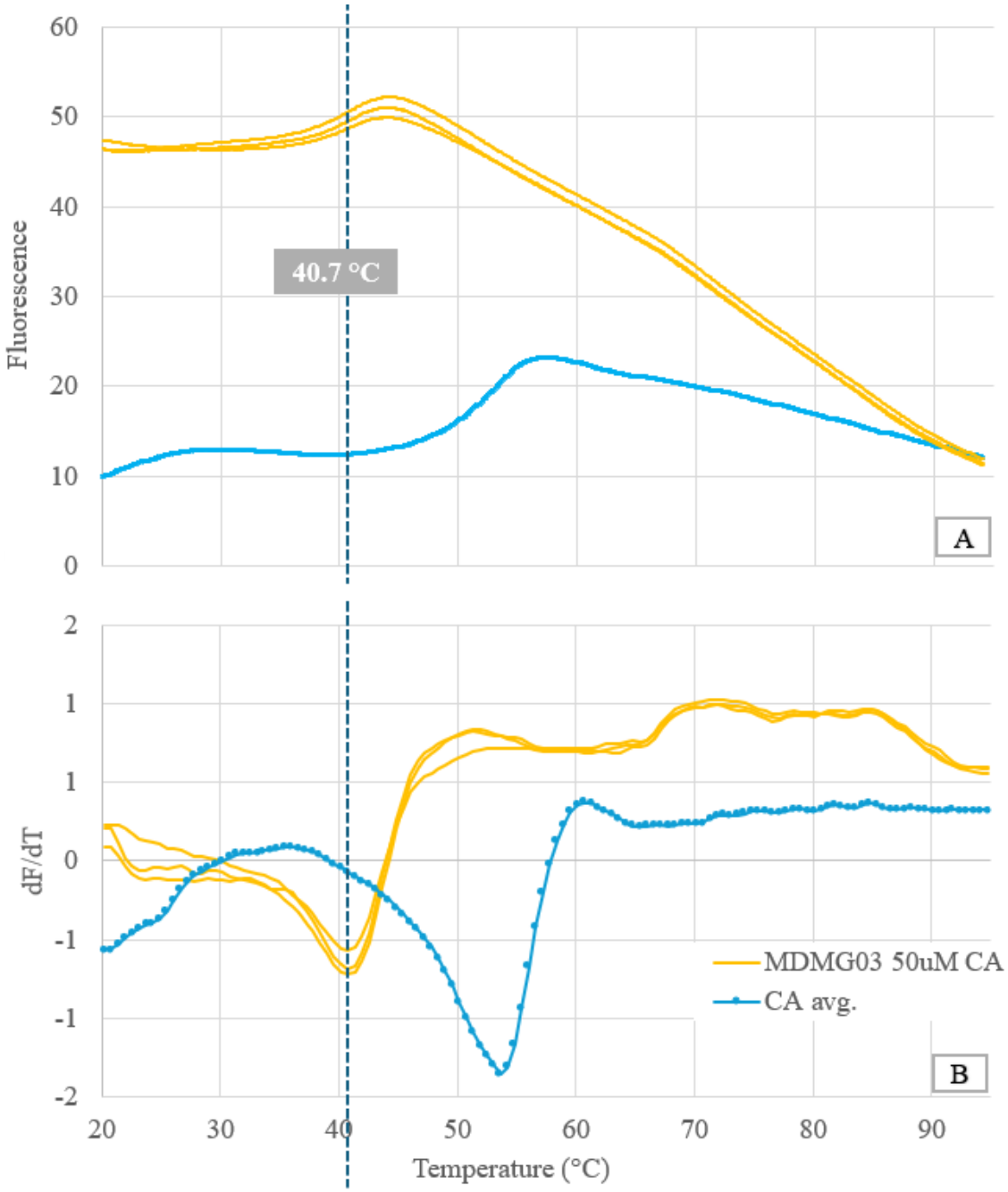

Figure 28. Differential scanning fluorimetry (DSF) data showing the effect of MD-MG-03 molecule on the melting temperature of HIV-1 CA protein at a concentration of 50 µM. (A) Melting curves showing the raw fluorescence signals versus temperature. (B) The minimum on the derivative (dF/dT) plot represents the melting temperature (Tm) of the protein in the presence and absence of MD-MG-03.

MD-MG-03 molecule, drastically destabilized HIV-1 CA monomer. The effect of the molecule on the capsid hexamer was evaluated with the same DSF protocol. However, the results showed that MD-MG-03 changed the melting temperature of CA monomer more than the hexameric form (Table 8.).

Table 8. Change in the melting temperature of CA monomer and Hexamer in the presence of MD-MG-03 molecule at two different concentrations.

Concentration of MD-MG-03	**MD-MG-03 with Monomer (ΔTm)**	**MD-MG-03 with Hexamer (ΔTm)**
5 uM	- 4°C	- 1°C
50 uM	- 12°C	- 8.4°C

The best binding poses from docking study of MD-MG-03 and MD-MG-04 compounds with HIV-1 capsid protein, were analyzed in detail and the ligand-protein interaction profile was visualized through the LIGPLOT program on the PDBsum platform (Wallace, Laskowski, and Thornton 1995). LIGPLOT presents hydrogen bonds, hydrophobic interactions and interacting amino acid residues in two-dimensional detail. Analysis revealed that MD-MG-03 and MD-MG-04 localizes to a hydrophobic pocket known as Site 3 on the C-terminal domain (CTD) of the capsid protein (Figure 30 and 31). According to the docking result, MD-MG-03 and MD-MG-04 molecules were found to form hydrophobic interactions with several key amino acids, including Tyr169, Leu172, Arg173, Glu187 and Met214 and hydrogen bond with Gln179 with AutoDock Vina score of -8.58 kcal/mol and -7.83 kcal/mol, respectively. These residues overlap significantly with the capsid assembly inhibitor (CAI) peptide binding site described in the literature and are critical for the potential antiviral activity of the molecule (Link et al. 2020). In addition, the hydrophobic nature of the chemical structure of MD-MG-03 and MD-MG-04 are highly compatible with the binding site on the protein. This compatibility increases the potential for preferential binding of the molecule to the site and is supported by the low docking score observed.

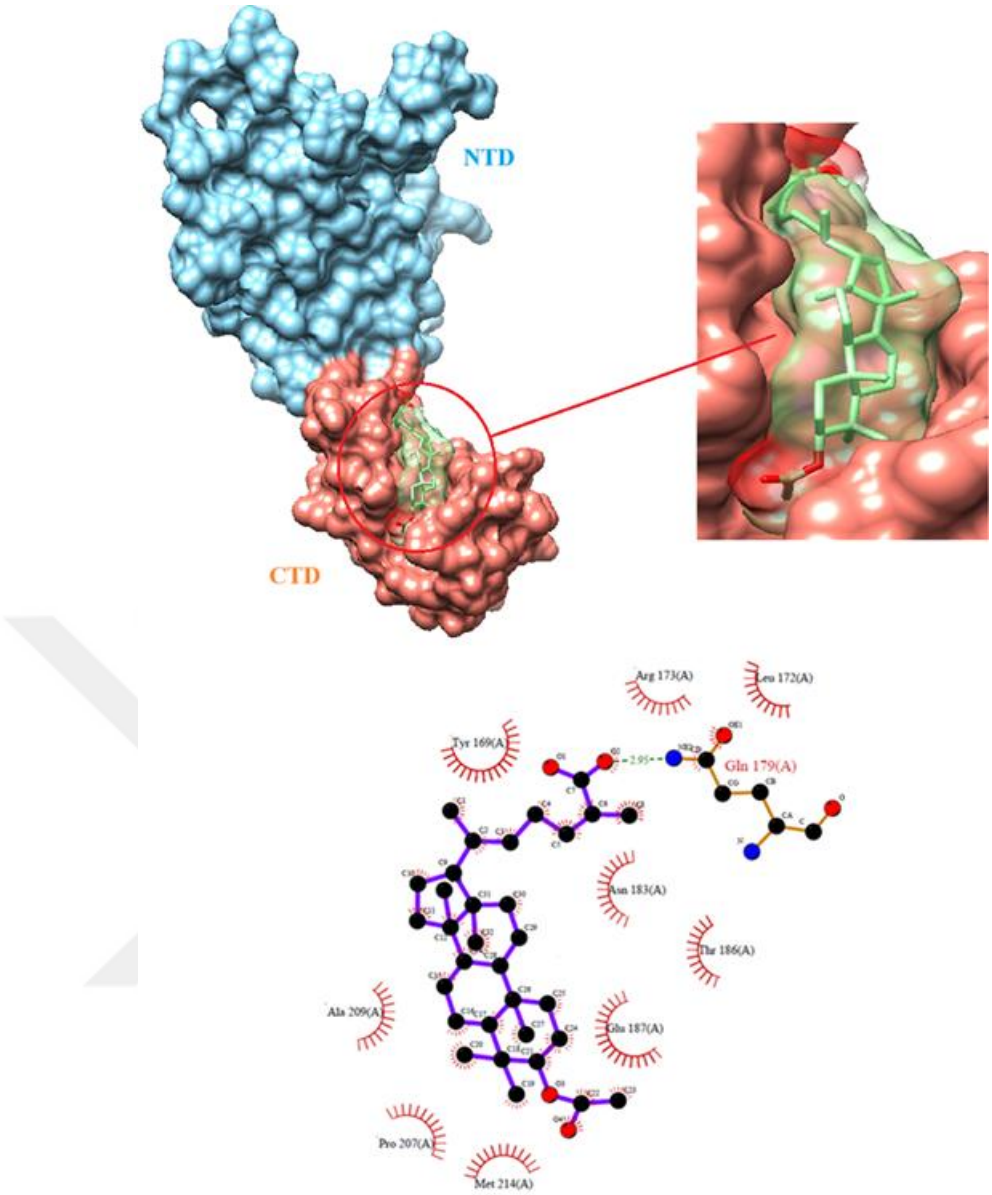

Figure 29. Interaction profile of the highest scoring docking position of the MD-MG-03 molecule (with HIV-1 capsid protein (PDB id: 6VKV, AutoDock Vina Score: -8.57 kcal/mol), visualized using UCSF Chimera. Visualization was created using the LIGPLOT tool on the PDBsum platform. The figure shows interacting amino acid residues.

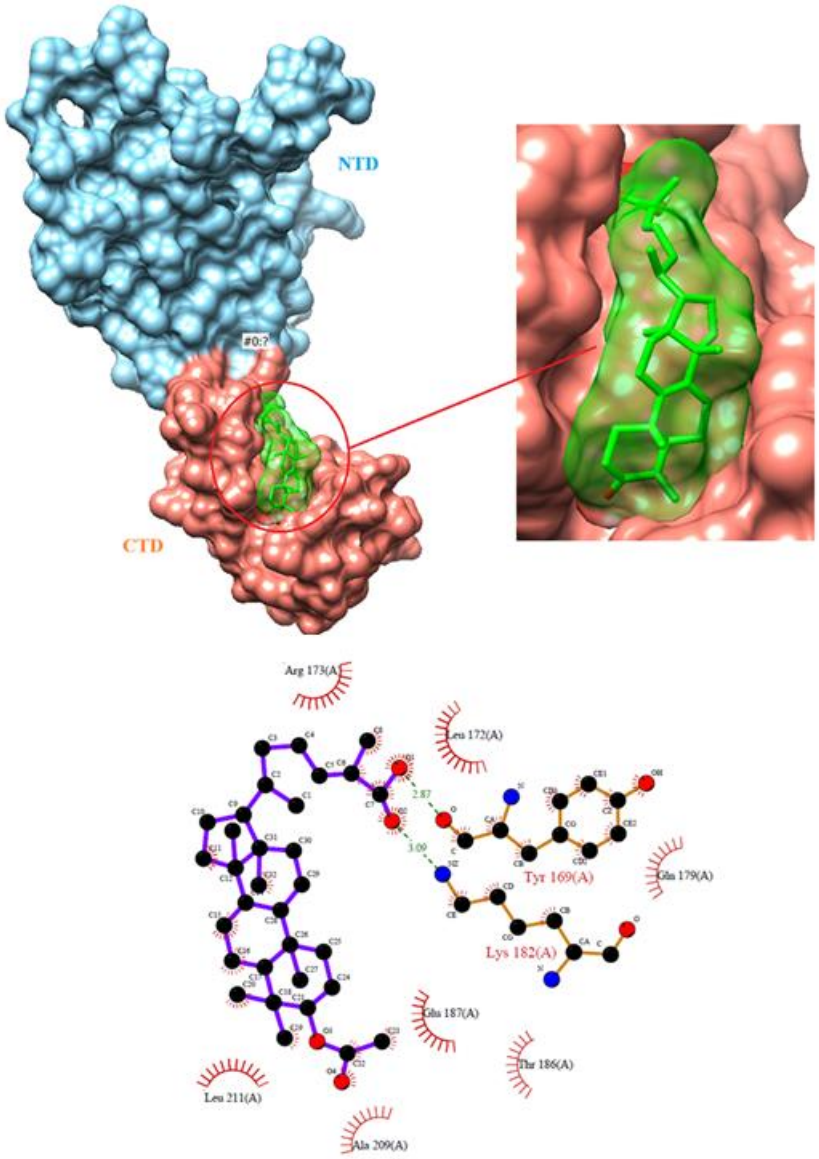

Figure 30. Interaction profile of the highest scoring docking position of the MD-MG-04 molecule with HIV-1 capsid protein (PDB id: 6VKV, AutoDock Vina Score: -7.83 kcal/mol), visualized using UCSF Chimera. Visualization was created using the LIGPLOT tool on the PDBsum platform. The figure shows interacting amino acid residues.

The binding of MD-MG-03 and MD-MG-04 to this site occurs near the protein dimerization surface, indicating the potential to disrupt the oligomerization process. This binding pattern is also consistent with the significant decrease in melting temperature (ΔTm) observed by MD-MG-03 and MD-MG-04 in the DSF analysis. The results support

that MD-MG-03 and MD-MG-04 may disrupt the structural stability of the HIV-1 capsid protein. When evaluated together with the experimental findings in DSF, these interactions may be related to the deterioration of monomer stability rather than a direct effect on capsid oligomerization. In particular, the almost equal binding scores of MD-MG-03 and MD-MG-04 in both monomer and tri-hexamer structures (Figure 31 and 32) support that this molecule has a binding profile that acts directly on the monomer rather than targeting the tubular structure. Therefore, the correlation of DSF data and docking scores suggests that the effects of MD-MG group molecules are mediated through the folding stability of HIV-1 CA monomer and this is consistent with the decreases in protein melting temperature.

In DSF analysis performed to evaluate the dose-dependent effect of MD-MG-03 molecule on HIV-1 capsid protein, it was observed that the effect of the molecule on protein stability was dose-dependent when ΔTm values were plotted against the logarithmic concentration axis (Figure 33). In the 0.001-0.1 µM range, the ΔTm change was minimal, while a significant stabilization effect appeared after 0.25 µM. Increases in ΔTm were observed at concentrations of 5, 25 and 50 µM, respectively, and a maximum ΔTm increase of approximately 12 °C was recorded at 50 µM. The curve obtained shows the change in ΔTm versus dose on the logarithmic axis, and such a dose-response relationship may indicate a specific and high affinity binding profile with the target protein. This finding indicates that the molecule can significantly increase its thermal stability by binding to HIV-1 capsid protein. The R^2 value obtained (0.9256) supports that the data obtained are highly correlated with the dose-dependent trend and that this effect is consistently observed. This suggests that the binding affinity and stabilizing effect of MD-MG-03 is concentration sensitive.

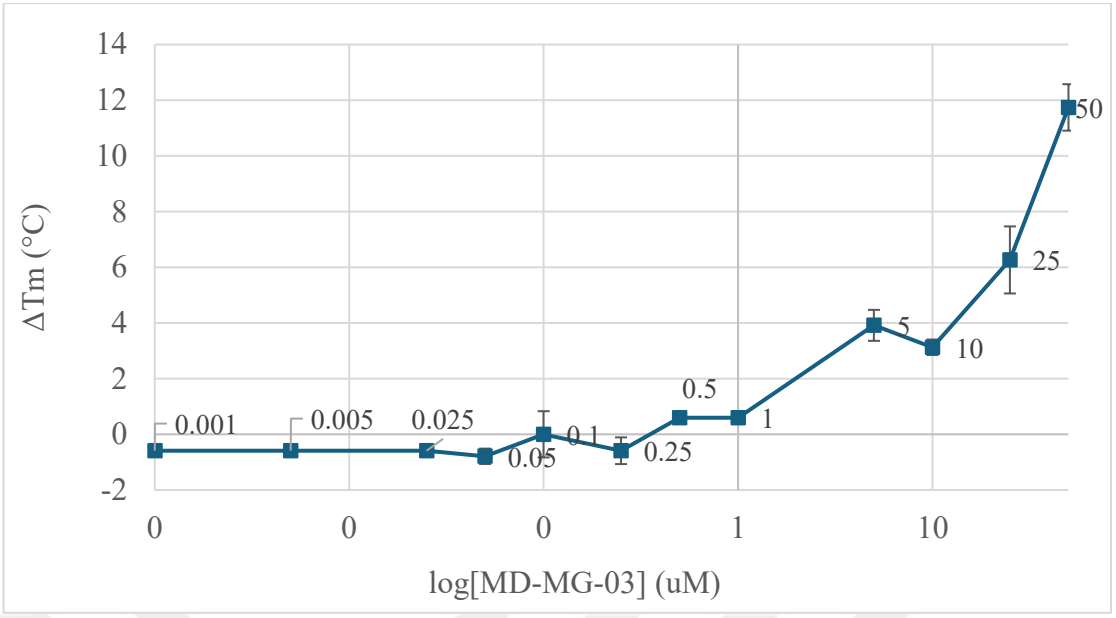

Figure 31. Logarithmic curve examining the dose-dependent effect of MD-MG-03 molecule binding to HIV-1 capsid protein on thermal stability. The molecule was tested in the range 0.001-50 μM.

Since MD-MG-03 and MD-MG-04 molecules affected the melting temperature of HIV-1 CA monomer and multimer in DSF experiments, we investigated and compared the docking of MD-MG-03 and MD-MG-04 molecules to both HIV-1 capsid monomer and multimer. For the MD-MG-03, the monomer docking score was -8.57 kcal/mol, while the multimer docking score was -8.56 kcal/mol (Figure 34). Similarly, for MD-MG-04, the monomer docking score was -7.83 kcal/mol while the multimer docking score was -8.51 kcal/mol (Figure 36). These data reveal that there is no significant difference in docking score between monomer and multimer structure for MD-MG-03 and MD-MG-04 molecules. Small variation in the docking scores might be due to the overall hydrophobic nature of these molecules, i.e. they don't have many functional groups to form strong non-covalent interactions such as hydrogen bonds, electrostatic interactions. Despite showing very similar docking scores, the best docking poses for the monomer and multimer forms are different. Both MD-MG-03 and MD-MG-04 binds to HIV-1 CA CTD, site-3 on the monomer, however, on the multimer, again both molecules bind to tri-hexamer interface (Figure 34 and 36). LigPlot analyses shows the interaction map of the molecules with the CA multimer in the two best docking poses (Figure 35 and 37).

Possible hydrogen bonding interactions between the molecules and HIV-1 CA amino acids are shown in green dashed lines with distances given. Other amino acids from different monomers (representing different hexamers in the multimer structure for docking) are given in different colors (green, purple and blue). From the LigPlot analysis, it is seen that both MD-MG-03 and MD-MG-04 molecules interact with all three monomers from different hexamers, thus best docked poses of both molecules are at the tri-hexamer interface.

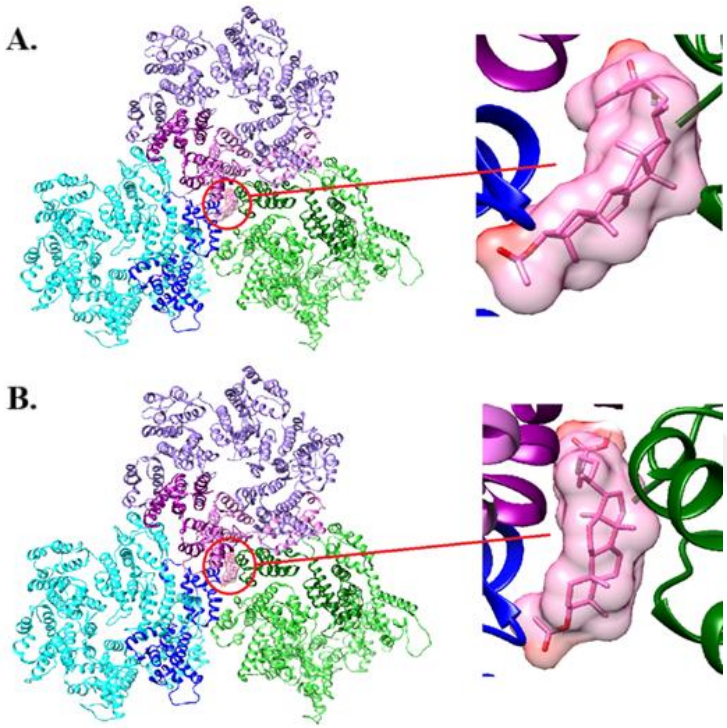

Figure 32. Best (A) and second best (B) Docking poses of MD-MG-03 with CA tetramer superimposed on HIV-1 CA multihexamer structure (PDB id: 3J34), visualized using UCSF Chimera. (A) AutoDock Vina score: -8.56 kcal/mol). (B) AutoDock Vina score: -8.50 kcal/mol).

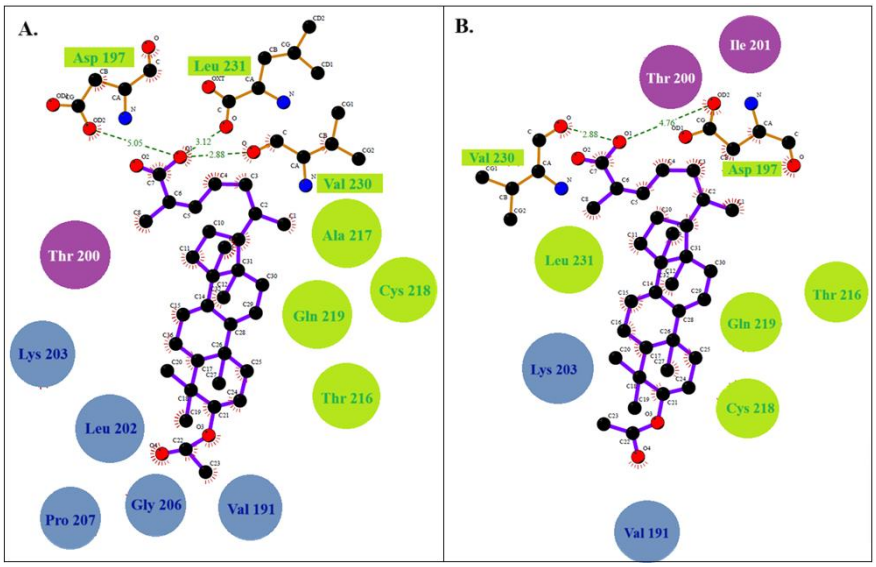

Figure 33. LigPlot analysis of Docking poses of MD-MG-03 with CA tetramer (PDB id: 3J34). Best (A) and second docking pose (B).

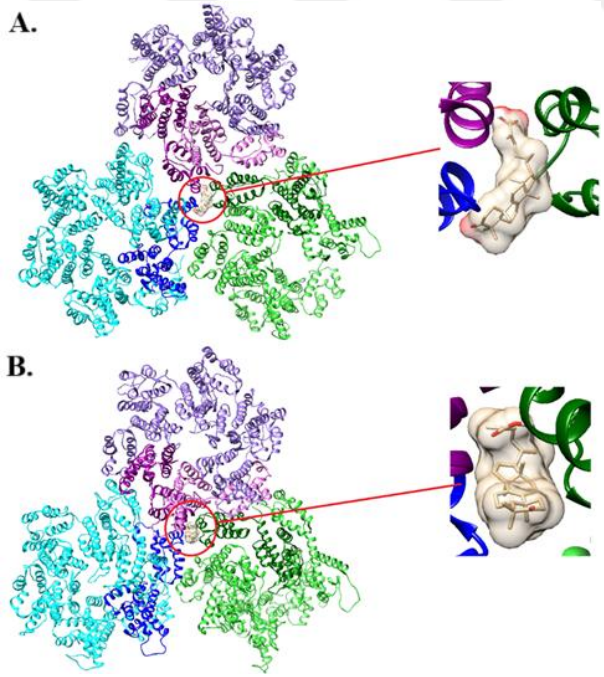

Figure 34. Docking poses of MD-MG-04 with CA tetramer (PDB id: 3J34), visualized using UCSF Chimera. The first docking pose is in 1. (AutoDock Vina score: -8.51 kcal/mol). Second docking pose is in 2. (AutoDock Vina score: -8.17 kcal/mol).

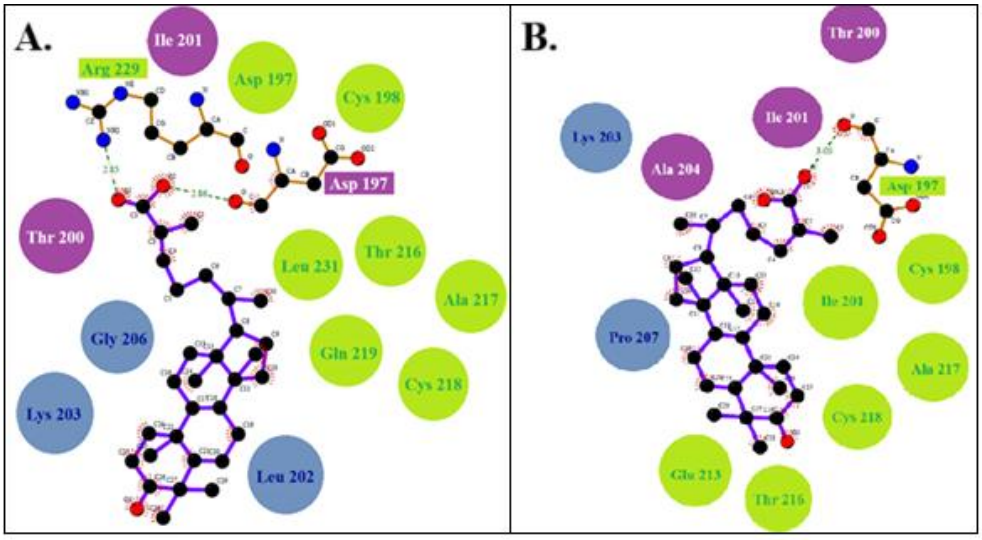

Figure 35. LigPlot analysis of Docking poses of MD-MG-04 with CA tetramer (PDB id: 3J34). Best (A) and second docking pose (B).

CHAPTER 4

CONCLUSION

HIV is a global pandemic that currently threatens public health worldwide. By 2023, approximately 39 million people are living with HIV and millions of new cases are reported each year (UNIAIDS 2025). Although current antiretroviral therapy (ART) options slow disease progression by suppressing viral replication, there are serious limitations including drug resistance, toxicity, the burden of daily drug use and latent reservoirs of HIV. For these reasons, efforts to develop new targeted drugs against HIV-1 are still ongoing.

The CA protein of HIV-1 plays a critical role at various stages of the virus life cycle. The CA protein is the main component of the conical capsid that surrounds viral RNA and is functionally involved in many steps such as viral entry, reverse transcription, nuclear transport and integration. This functional diversity has made the CA protein a highly attractive target for drug development. In particular, the conical capsid structure formed by hexameric and pentameric units derived from the monomeric structure of CA can be disrupted by drugs and the replication process of the virus can be inhibited.

In this study, the inhibitory potential of naturally derived secondary metabolites derived from plants and microorganisms on HIV-1 CA protein was evaluated. In the first stage of the study, 279 molecules obtained from Bedir Group were subjected to molecular docking against the capsid monomer via AutoDock Vina in Google Colab environment and 26 molecules showing good binding score were selected for experimental investigation. The effects of these molecules were evaluated on both the thermal stability of HIV-1 CA by Differential Scanning Fluorimetry (DSF) and oligomerization rate of HIV-1 CA. With DSF method, the effect of protein-ligand interactions on the thermal stability of the protein was investigated. In the experiments, MD-MG-03 and MD-MG-04 compounds were observed to cause destabilization of CA monomer by -13°C and -12.4°C melting temperature shift, respectively.

Oligomerization experiments aimed to measure the effect of small molecules on the rate of capsid tube formation in vitro in high salt buffer conditions. In these experiments, ATB-01 and ATB-05 molecules were shown to increase the oligomerization rate of CA. In addition, ATB group molecules were subjected to further molecular docking against CA-CA interfaces in CA multimers. When docked to CA multimer form, ATB group molecules had better docking scores compared to monomer CA docking and formed more hydrogen bonds in LigPlot Analyses when bound to the protein multimer. The best docking result of all the molecules were at the tri-hexameric interface.

When all these promising results are evaluated together, the interaction of these molecules and HIV-1 CA needs further investigation. Since ATB group molecules accelerate oligomerization rate, they may cause aggregation rather than organized tube formation. HIV-1 CA oligomerization reaction product can be visualized with STEM or TEM instruments. We plan to study the binding of these molecules to HIV-1 CA with isothermal titration calorimetry (ITC).

In conclusion, the CA protein has emerged as an important therapeutic target in the ongoing need for new targets in the treatment of HIV-1. The studies conducted in this thesis provide valuable preliminary information by revealing the effects of 26 natural compounds out of 279 molecules on CA stability and oligomerization in detail. In future studies, binding affinity of the ATB and MD-MG group molecules to the capsid protein can be determined by isothermal titration calorimetry (ITC). Transmission electron microscopy (TEM) imaging of in vitro generated tubular structures in the presence of ATB or MD-MG group molecules will be a critical step to directly investigate the effects of these molecules on capsid assembly process. These experimental approaches will help us understand the interaction of these molecules with HIV-1 CA protein in more detail.

REFERENCES

Agu, Peter Chinedu, Celestine Azubike Afiukwa, Obasi Uche Orji, Ernest Mbamalu Ezeh, Ifeanyi Harrison Ofoke, Celestine O. Ogbu, Emmanuel Ike Ugwuja, and Patrick Maduabuchi Aja. 2023. "Molecular Docking as a Tool for the Discovery of Molecular Targets of Nutraceuticals in Diseases Management." *Scientific Reports* 13 (1): 13398. https://doi.org/10.1038/s41598-023-40160-2.

Aiken, Christopher, and Chin Ho Chen. 2005. "Betulinic Acid Derivatives as HIV-1 Antivirals." *Trends in Molecular Medicine* 11 (1): 31–36. https://doi.org/10.1016/j.molmed.2004.11.001.

Aiken, Christopher, and Itay Rousso. 2021. "The HIV-1 Capsid and Reverse Transcription." *Retrovirology* 18 (1): 1–9. https://doi.org/10.1186/s12977-021-00566-0.

Alakurtti, Sami, Taru Mäkelä, Salme Koskimies, and Jari Yli-Kauhaluoma. 2006. "Pharmacological Properties of the Ubiquitous Natural Product Betulin." *European Journal of Pharmaceutical Sciences* 29 (1): 1–13. https://doi.org/10.1016/j.ejps.2006.04.006.

Antonopoulou, Io, Eleftheria Sapountzaki, Ulrika Rova, and Paul Christakopoulos. 2022. "Ferulic Acid from Plant Biomass: A Phytochemical with Promising Antiviral Properties." *Frontiers in Nutrition* 8 (2): 1-21. https://doi.org/10.3389/fnut.2021.777576.

Aslanipour, Behnaz, Derya Gülcemal, Ayşe Nalbantsoy, Hasan Yusufoglu, and Erdal Bedir. 2017. "Secondary Metabolites from Astragalus Karjaginii BORISS and the Evaluation of Their Effects on Cytokine Release and Hemolysis." *Fitoterapia* 122 (10): 26–33. https://doi.org/10.1016/j.fitote.2017.08.008.

Atanasov, Atanas G., Sergey B. Zotchev, Verena M. Dirsch, Ilkay Erdogan Orhan, Maciej Banach, Judith M. Rollinger, Davide Barreca, et al. 2021. "Natural Products in Drug Discovery: Advances and Opportunities." *Nature Reviews Drug Discovery 2021 20:3* 20 (3): 200–216. https://doi.org/10.1038/s41573-020-00114-z.

Berman, Helen M., John Westbrook, Zukang Feng, Gary Gilliland, T. N. Bhat, Helge Weissig, Ilya N. Shindyalov, Philip E. Bourne. 2000. "The Protein Data Bank." Nucleic Acids Research 28 (1): 235–42. https://doi.org/10.1093/nar/28.1.235.

Bester, Stephanie M., Guochao Wei, Haiyan Zhao, Daniel Adu-Ampratwum, Naseer Iqbal, Valentine v. Courouble, Ashwanth C. Francis, et al. 2020. "Structural and Mechanistic Bases for a Potent HIV-1 Capsid Inhibitor." *Science* 370 (6514): 360–64. https://doi.org/10.1126/science.abb4808,.

Bhattacharya, Akash, Steven L. Alam, Thomas Fricke, Kaneil Zadrozny, Jaroslaw Sedzicki, Alexander B. Taylor, Borries Demeler, et al. 2014. "Structural Basis of HIV-1 Capsid Recognition by PF74 and CPSF6." *Proceedings of the National Academy of Sciences of the United States of America* 111 (52): 18625–30. https://doi.org/10.1073/pnas.1419945112,.

Blundell, Renald, Joseph Azzopardi, Jessica Briffa, Azhar Rasul, Celia Vargas-De La Cruz, and Muhammad Ajmal Shah. 2020. "Analysis of Pentaterpenoids." Recent Advances in Natural Products Analysis, 1 (1): 457–75. https://doi.org/10.1016/B978-0-12-816455-6.00013-5.

Bruce, Daniel, Emily Cardew, Stefanie Freitag-Pohl, and Ehmke Pohl. 2019. "How to Stabilize Protein: Stability Screens for Thermal Shift Assays and Nano Differential Scanning Fluorimetry in the Virus-X Project." *JoVE (Journal of Visualized Experiments)* 2019 (144): e58666. https://doi.org/10.3791/58666.

Burdick, Ryan C., Krista A. Delviks-Frankenberry, Jianbo Chen, Sanath K. Janaka, Jaya Sastri, Wei Shau Hu, and Vinay K. Pathak. 2017. "Dynamics and Regulation of Nuclear Import and Nuclear Movements of HIV-1 Complexes." *PLOS Pathogens* 13 (8): e1006570. https://doi.org/10.1371/journal.ppat.1006570.

Byeon, In Ja L., Xin Meng, Jinwon Jung, Gongpu Zhao, Ruifeng Yang, Jinwoo Ahn, Jiong Shi, et al. 2009. "Structural Convergence between Cryo-EM and NMR Reveals Intersubunit Interactions Critical for HIV-1 Capsid Function." *Cell* 139 (4): 780–90. https://doi.org/10.1016/j.cell.2009.10.010.

Campbell, Edward M., and Thomas J. Hope. 2015. "HIV-1 Capsid: The Multifaceted Key Player in HIV-1 Infection." *Nature Reviews Microbiology 2015 13:8* 13 (8): 471–83. https://doi.org/10.1038/nrmicro3503.

Curreli, Francesca, Hongtao Zhang, Xihui Zhang, Ilya Pyatkin, Zagorodnikov Victor, Andrea Altieri, and Asim K. Debnath. 2011. "Virtual Screening Based Identification of Novel Small-Molecule Inhibitors Targeted to the HIV-1 Capsid." *Bioorganic & Medicinal Chemistry* 19 (1): 77–90. https://doi.org/10.1016/j.bmc.2010.11.045.

Cushnie, T. P.Tim, and Andrew J. Lamb. 2005. “Antimicrobial Activity of Flavonoids.” *International Journal of Antimicrobial Agents* 26 (5): 343–56. https://doi.org/10.1016/j.ijantimicag.2005.09.002.

DIng, Yue, Zeyu Cao, Liang Cao, Gang DIng, Zhenzhong Wang, and Wei Xiao. 2017. “Antiviral Activity of Chlorogenic Acid against Influenza A (H1N1/H3N2) Virus and Its Inhibition of Neuraminidase.” *Scientific Reports* 7 (4): 45723. https://doi.org/10.1038/srep45723.

Dwivedi, Richa, Prem Prakash, Bajarang Vasant Kumbhar, Muthukumar Balasubramaniam, and Chandravanu Dash. 2024. “HIV-1 Capsid and Viral DNA Integration.” *MBio* 15 (1): e00212-22. https://doi.org/10.1128/mbio.00212-22.

“Endemism in Turkey.” n.d. İstanbul University the Herbarium of the Faculty of Pharmacy. Accessed March 27, 2025. https://iste.istanbul.edu.tr/en/content/flora-of-turkey-and-conservation/endemism-in-turkey.

Ganser-Pornillos, Barbie K., Mark Yeager, and Owen Pornillos. 2012. “Assembly and Architecture of HIV.” Advances in Experimental Medicine and Biology 726 (1): 441–65. https://doi.org/10.1007/978-1-4614-0980-9_20.

Ganser-Pornillos, Barbie K., Mark Yeager, and Wesley I. Sundquist. 2008. “The Structural Biology of HIV Assembly.” *Current Opinion in Structural Biology* 18 (2): 203. https://doi.org/10.1016/j.sbi.2008.02.001.

Gao, Kai, Rick Oerlemans, and Matthew R. Groves. 2020a. “Theory and Applications of Differential Scanning Fluorimetry in Early-Stage Drug Discovery.” *Biophysical Reviews* 12 (1): 85. https://doi.org/10.1007/s12551-020-00619-2.

Gezer, Emre, Göklem Üner, Melis Küçüksolak, Mustafa Ünver Kurt, Gamze Doğan, Petek Ballar Kırmızıbayrak, and Erdal Bedir. 2022. “Undescribed Polyether Ionophores from Streptomyces Cacaoi and Their Antibacterial and Antiproliferative Activities.” *Phytochemistry* 195 (3): 113038. https://doi.org/10.1016/j.phytochem.2021.113038.

Gifford, Levi B., and Gregory B. Melikyan. 2024. “HIV-1 Capsid Uncoating Is a Multistep Process That Proceeds through Defect Formation Followed by Disassembly of the Capsid Lattice.” *ACS Nano* 18 (4): 2928–47. https://doi.org/10.1021/acsnano.3c07678.

Gres, Anna T., Karen A. Kirby, Vineet N. KewalRamani, John J. Tanner, Owen Pornillos, and Stefan G. Sarafianos. 2015. "X-Ray Crystal Structures of Native HIV-1 Capsid Protein Reveal Conformational Variability." *Science* 349 (6243): 99–103. https://doi.org/10.1126/science.aaa5936.

"GS-6207, A Potent and Selective First-In-Class Long-Acting HIV-1 Capsid Inhibitor." n.d. Accessed March 22, 2025. https://www.natap.org/2019/croi/croi_172.htm.

Gülcemal, Derya, Behnaz Aslanipour, and Erdal Bedir. 2019. "Secondary Metabolites from Turkish Astragalus Species." *Plant and Human Health: Volume 2: Phytochemistry and Molecular Aspects* 2 (1): 43–97. https://doi.org/10.1007/978-3-030-03344-6_2.

Heydari, Hajar, Bülent Gözcelioğlu, and Belma Konuklugil. 2019. "Biodiversity and Secondary Metabolites of Marine Sponges from Turkey." *Records of Natural Products* 13 (5): 367–78. https://doi.org/10.25135/rnp.118.18.07.340.

Hulme, Amy E., Omar Perez, and Thomas J. Hope. 2011. "Complementary Assays Reveal a Relationship between HIV-1 Uncoating and Reverse Transcription." *Proceedings of the National Academy of Sciences of the United States of America* 108 (24): 9975–80. https://doi.org/10.1073/pnas.1014522108

Huynh, Kathy, and Carrie L. Partch. 2015. "Analysis of Protein Stability and Ligand Interactions by Thermal Shift Assay." Current Protocols in Protein Science 79 (2): 28.9.1-28.9.14. https://doi.org/10.1002/0471140864.PS2809S79.

Jacques, David A., William A. McEwan, Laura Hilditch, Amanda J. Price, Greg J. Towers, and Leo C. James. 2016. "HIV-1 Uses Dynamic Capsid Pores to Import Nucleotides and Fuel Encapsidated DNA Synthesis." *Nature 2016 536:7616* 536 (7616): 349–53. https://doi.org/10.1038/nature19098.

Jaisi, Amit, Prema, Siribhorn Madla, Yuan E. Lee, Abdi Septama, and Hiroyuki Morita. 2021. "Investigation of HIV-1 Viral Protein R Inhibitory Activities of Twelve Thai Medicinal Plants and Their Commercially Available Major Constituents." *Chemistry and Biodiversity* 18 (12): e2100540. https://doi.org/10.1002/cbdv.202100540.

Jassim, Sabah A.A., and Meena Akeel Naji. 2003. "Novel Antiviral Agents: A Medicinal Plant Perspective." *Journal of Applied Microbiology* 95 (3): 412–27. https://doi.org/10.1046/j.1365-2672.2003.02026.x.

Jogiraju, Vamshi, Elijah Weber, Jason Hindman, Steve West, John Ling, Martin Rhee, Sandhya Girish, Ramesh Palaparthy, and Renu Singh. 2024. “Pharmacokinetics of Long-Acting Lenacapavir in Participants with Hepatic or Renal Impairment.” *Antimicrobial Agents and Chemotherapy* 68 (4): e01344-23. https://doi.org/10.1128/aac.01344-23.

Keivan, Zandi, Teoh Boon-Teong, Sam Sing-Sin, Wong Pooi-Fong, Rais Mustafa Mohd, and Abubakar Sazaly. 2014. “In Vitro Antiviral Activity of Fisetin, Rutin and Naringenin against Dengue Virus Type-2.” *Journal of Medicinal Plants Research* 8 (6): 307–12. https://doi.org/10.5897/jmpr11.1046.

Kim, Hyun Woo, Mingxun Wang, Christopher A. Leber, Louis Félix Nothias, Raphael Reher, Kyo bin Kang, Justin J.J. van der Hooft, Pieter C. Dorrestein, William H. Gerwick, and Garrison W. Cottrell. 2021. “NPClassifier: A Deep Neural Network-Based Structural Classification Tool for Natural Products.” *Journal of Natural Products* 84 (11): 2795–2807. https://doi.org/10.1021/acs.jnatprod.1c00399.

Kobayakawa, Takuya, Masaru Yokoyama, Kohei Tsuji, Sayaka Boku, Masaki Kurakami, Masayuki Fujino, Takahiro Ishii, et al. 2024. “Development of Small-Molecule Anti-HIV-1 Agents Targeting HIV-1 Capsid Proteins.” *Chemical and Pharmaceutical Bulletin* 72 (1): 41–47. https://doi.org/10.1248/cpb.c23-00618.

Kobayakawa, Takuya, Masaru Yokoyama, Kohei Tsuji, Masayuki Fujino, Masaki Kurakami, Sayaka Boku, Miyuki Nakayama, et al. 2021. “Small-Molecule Anti-HIV-1 Agents Based on HIV-1 Capsid Proteins.” *Biomolecules* 11 (2): 208. https://doi.org/10.3390/biom11020208.

Lamorte, Louie, Steve Titolo, Christopher T. Lemke, Nathalie Goudreau, Jean François Mercier, Elizabeth Wardrop, Vaibhav B. Shah, et al. 2013. “Discovery of Novel Small-Molecule HIV-1 Replication Inhibitors That Stabilize Capsid Complexes.” *Antimicrobial Agents and Chemotherapy* 57 (10): 4622. https://doi.org/10.1128/aac.00985-13.

“Lenacapavir | C39H32ClF10N7O5S2 | CID 133082658 - PubChem.” n.d. Accessed March 27, 2025. https://pubchem.ncbi.nlm.nih.gov/compound/lenacapavir#section=2d-structure.

Li, Ranran, Chunduo Wang, Kexin Xu, Zongzhu Zhan, Siyi He, Jihua Ren, Fan Li, et al. 2024. “Asiatic Acid Inhibits HBV CccDNA Transcription by Promoting HBx Degradation.” *Virology Journal* 21 (1): 268. https://doi.org/10.1186/s12985-024-02535-3.

Li, Xiang, Yuanyuan Liu, Xueling Hou, Hongjun Peng, Li Zhang, Qingbo Jiang, Mei Shi, Yun Ji, Yuyue Wang, and Weifeng Shi. 2013. "Chlorogenic Acid Inhibits the Replication and Viability of Enterovirus 71 In Vitro." *PLoS ONE* 8 (9): e76007. https://doi.org/10.1371/journal.pone.0076007.

Link, John O., Martin S. Rhee, Winston C. Tse, Jim Zheng, John R. Somoza, William Rowe, Rebecca Begley, et al. 2020a. "Clinical Targeting of HIV Capsid Protein with a Long-Acting Small Molecule." *Nature 2020 584:7822* 584 (7822): 614–18. https://doi.org/10.1038/s41586-020-2443-1.

Lusvarghi, Sabrina, and Carole A. Bewley. 2016. "Griffithsin: An Antiviral Lectin with Outstanding Therapeutic Potential." *Viruses* 8 (10): 296. https://doi.org/10.3390/V8100296.

Mallery, Donna L., Chantal L. Márquez, William A. McEwan, Claire F. Dickson, David A. Jacques, Madhanagopal Anandapadamanaban, Katsiaryna Bichel, et al. 2018. "IP6 Is an HIV Pocket Factor That Prevents Capsid Collapse and Promotes DNA Synthesis." *ELife* 7 (5): 1-19. https://doi.org/10.7554/elife.35335.

Mancuso, Cesare, and Rosaria Santangelo. 2014. "Ferulic Acid: Pharmacological and Toxicological Aspects." *Food and Chemical Toxicology* 65 (3): 185–95. https://doi.org/10.1016/j.fct.2013.12.024.

Martins, Daniel Oliveira Silva, Igor De Andrade Santos, Débora Moraes de Oliveira, Victória Riquena Grosche, and Ana Carolina Gomes Jardim. 2020. "Antivirals Against Chikungunya Virus: Is the Solution in Nature?" *Viruses* 12 (3): 272. https://doi.org/10.3390/v12030272.

Matreyek, Kenneth A., and Alan Engelman. 2011. "The Requirement for Nucleoporin NUP153 during Human Immunodeficiency Virus Type 1 Infection Is Determined by the Viral Capsid." *Journal of Virology* 85 (15): 7818–27. https://doi.org/10.1128/jvi.00325-11.

Mattei, Simone, Florian Km Schur, and John Ag Briggs. 2016. "Retrovirus Maturation-an Extraordinary Structural Transformation." *Current Opinion in Virology* 18 (6): 27–35. https://doi.org/10.1016/j.coviro.2016.02.008.

McFadden, William M., Mary C. Casey-Moore, Grant A.L. Bare, Karen A. Kirby, Xin Wen, Gencheng Li, Hua Wang, et al. 2024. "Identification of Clickable HIV-1 Capsid-Targeting Probes for Viral Replication Inhibition." *Cell Chemical Biology* 31 (3): 477-486.e7. https://doi.org/10.1016/j.chembiol.2024.02.012.

McFadden, William M., Alexa A. Snyder, Karen A. Kirby, Philip R. Tedbury, Monika Raj, Zhengqiang Wang, and Stefan G. Sarafianos. 2021. “Rotten to the Core: Antivirals Targeting the HIV-1 Capsid Core.” *Retrovirology 2021 18:1* 18 (1): 1–24. https://doi.org/10.1186/s12977-021-00583-z.

McGraw, Aidan, Grace Hillmer, Stefania M. Medehincu, Yuta Hikichi, Sophia Gagliardi, Kedhar Narayan, Hasset Tibebe, et al. 2024. “Exploring HIV-1 Maturation: A New Frontier in Antiviral Development.” *Viruses* 16 (9): 1423. https://doi.org/10.3390/v16091423.

Miyazaki, Yasuyuki, Naoya Doi, Takaaki Koma, Akio Adachi, and Masako Nomaguchi. 2017. “Novel in Vitro Screening System Based on Differential Scanning Fluorimetry to Search for Small Molecules against the Disassembly or Assembly of HIV-1 Capsid Protein.” *Frontiers in Microbiology* 8 (7): 1–5. https://doi.org/10.3389/fmicb.2017.01413.

Nachega, Jean B., Kimberly K. Scarsi, Monica Gandhi, Rachel K. Scott, Lynne M. Mofenson, Moherndran Archary, Sharon Nachman, et al. 2023. “Long-Acting Antiretrovirals and HIV Treatment Adherence.” *The Lancet HIV* 10 (5): e332–42. https://doi.org/10.1016/s2352-3018(23)00051-6.

Nandu, Thrithamarassery Gangadharan, and Kottur Jithesh. 2024. “Natural Product-Based Anti-Viral Agents Against RNA Viruses: An Important Strategy for Pandemic Preparedness.” Drugs from Nature: Targets, Assay Systems and Leads 1 (1): 411–40. https://doi.org/10.1007/978-981-99-9183-9_15.

Newman, David J., and Gordon M. Cragg. 2020. “Natural Products as Sources of New Drugs over the Nearly Four Decades from 01/1981 to 09/2019.” *Journal of Natural Products* 83 (3): 770–803. https://doi.org/10.1021/acs.jnatprod.9b01285.

Niesen, Frank H., Helena Berglund, and Masoud Vedadi. 2007. “The Use of Differential Scanning Fluorimetry to Detect Ligand Interactions That Promote Protein Stability.” *Nature Protocols 2007 2:9* 2 (9): 2212–21. https://doi.org/10.1038/nprot.2007.321.

Noroozi, Jalil, Golshan Zare, Mahbubeh Sherafati, Mohammad Mahmoodi, Dietmar Moser, Zahra Asgarpour, and Gerald M. Schneeweiss. 2019. “Patterns of Endemism in Turkey, the Meeting Point of Three Global Biodiversity Hotspots, Based on Three Diverse Families of Vascular Plants.” *Frontiers in Ecology and Evolution* 7 (5): 444247. https://doi.org/10.3389/fevo.2019.00159/bibtex.

Nunzio, Francesca di. 2013. “New Insights in the Role of Nucleoporins: A Bridge Leading to Concerted Steps from HIV-1 Nuclear Entry until Integration.” *Virus Research* 178 (2): 187–96. https://doi.org/10.1016/j.virusres.2013.09.003.

Paik, Julia. 2022. “Lenacapavir: First Approval.” *Drugs* 82 (14): 1499–1504. https://doi.org/10.1007/S40265-022-01786-0.

Pantoliano, Michael W., Eugene C. Petrella, Joseph D. Kwasnoski, Victor S. Lobanov, James Myslik, Edward Graf, Ted Carver, et al. 2001. “High-Density Miniaturized Thermal Shift Assays as a General Strategy for Drug Discovery.” *Journal of Biomolecular Screening* 6 (6): 429–40. https://doi.org/10.1177/108705710100600609.

Petrillo, Amalia di, Germano Orrù, Antonella Fais, and Massimo C. Fantini. 2021. “Quercetin and Its Derivates as Antiviral Potentials: A Comprehensive Review.” *Phytotherapy Research* 36 (1): 266. https://doi.org/10.1002/ptr.7309.

Pornillos, Owen, Barbie K. Ganser-Pornillos, Sankaran Banumathi, Yuanzi Hua, and Mark Yeager. 2010. “Disulfide Bond Stabilization of the Hexameric Capsomer of Human Immunodeficiency Virus.” *Journal of Molecular Biology* 401 (5): 985–95. https://doi.org/10.1016/j.jmb.2010.06.042.

Pornillos, Owen, Barbie K. Ganser-Pornillos, Brian N. Kelly, Yuanzi Hua, Frank G. Whitby, C. David Stout, Wesley I. Sundquist, Christopher P. Hill, and Mark Yeager. 2009a. “X-Ray Structures of the Hexameric Building Block of the HIV Capsid.” *Cell* 137 (7): 1282–92. https://doi.org/10.1016/j.cell.2009.04.063.

Prassas, Ioannis, and Eleftherios P. Diamandis. 2008. “Novel Therapeutic Applications of Cardiac Glycosides.” *Nature Reviews Drug Discovery 2008 7:11* 7 (11): 926–35. https://doi.org/10.1038/nrd2682.

Price, Amanda J., David A. Jacques, William A. McEwan, Adam J. Fletcher, Sebastian Essig, Jason W. Chin, Upul D. Halambage, Christopher Aiken, and Leo C. James. 2014. “Host Cofactors and Pharmacologic Ligands Share an Essential Interface in HIV-1 Capsid That Is Lost upon Disassembly.” *PLOS Pathogens* 10 (10): e1004459. https://doi.org/10.1371/journal.ppat.1004459.

“Release v1.2.3 · Ccsb-Scripps/AutoDock-Vina · GitHub.” n.d. Accessed February 9, 2025. https://github.com/ccsb-scripps/AutoDock-Vina/releases/tag/v1.2.3.

Rossi, Eric, Megan E. Meuser, Camille J. Cunanan, and Simon Cocklin. 2021. “Structure, Function, and Interactions of the HIV-1 Capsid Protein.” *Life* 11 (2): 100. https://doi.org/10.3390/life11020100.

Şener, Bilge, and Ilkay Orhan. 2005. “Discovery of Drug Candidates from Some Turkish Plants and Conservation of Biodiversity.” *Pure and Applied Chemistry* 77 (1): 53–64. https://doi.org/10.1351/pac200577010053.

Sener, Bilge, and Ilkay Orhan. 2011. “Exploring Turkish Biodiversity: A Rich Source of Chemical Diversity for Drug Leads Discovery.” *Pure and Applied Chemistry* 83 (9): 1699–1707. https://doi.org/10.1351/pac-con-11-02-01.

Serna-Arbeláez, Maria S., Laura Florez-Sampedro, Lina P. Orozco, Katherin Ramírez, Elkin Galeano, and Wildeman Zapata. 2021. “Natural Products with Inhibitory Activity against Human Immunodeficiency Virus Type 1.” *Advances in Virology* 2021 (5): 5552088. https://doi.org/10.1155/2021/5552088.

Sharifi-Rad, Javad, Cristina Quispe, Carla Marina Salgado Castillo, Rodrigo Caroca, Marco A. Lazo-Vélez, Halyna Antonyak, Alexandr Polishchuk, et al. 2022. “Ellagic Acid: A Review on Its Natural Sources, Chemical Stability, and Therapeutic Potential.” *Oxidative Medicine and Cellular Longevity* 2022 (5): 3848084. https://doi.org/10.1155/2022/3848084.

Shen, Qi, Sushila Kumari, Chaoyi Xu, Sooin Jang, Jiong Shi, Ryan C. Burdick, Lev Levintov, et al. 2023a. “The Capsid Lattice Engages a Bipartite NUP153 Motif to Mediate Nuclear Entry of HIV-1 Cores.” *Proceedings of the National Academy of Sciences of the United States of America* 120 (13): e2202815120. https://doi.org/10.1073/pnas.2202815120

Shi, Jiong, Jing Zhou, Vaibhav B. Shah, Christopher Aiken, and Kevin Whitby. 2010. “Small-Molecule Inhibition of Human Immunodeficiency Virus Type 1 Infection by Virus Capsid Destabilization.” *Journal of Virology* 85 (1): 542. https://doi.org/10.1128/jvi.01406-10.

Srivastava, Rashmi, Neeraj Kumar Dubey, Megha Sharma, Harsha Kharkwal, Rajesh Bajpai, and Rakesh Srivastava. 2025. “Boosting the Human Antiviral Response in Conjunction with Natural Plant Products.” *Frontiers in Natural Products* 3 (1): 1470639. https://doi.org/10.3389/fntpr.2024.1470639.

Sun, Qinfang, Avik Biswas, R. S.K. Vijayan, Pierrick Craveur, Stefano Forli, Arthur J. Olson, Andres Emanuelli Castaner, et al. 2022. “Structure-Based Virtual Screening Workflow to Identify Antivirals Targeting HIV-1 Capsid.” *Journal of*

Computer-Aided Molecular Design 36 (3): 193–203. https://doi.org/10.1007/s10822-022-00446-5.

Tekman, Enes, Tugay Asgarlı, Hafize Yuca, Alptuğ Atila, Ömer Çeçen, and Songül Karakaya. 2024. "Exploring Quantitative Biological Major, Trace, and Ultratrace Elements Composition and Qualitative Primary-Secondary Metabolites in Lamiaceae Medicinal Plants from Turkey." *Biological Trace Element Research* 203 (2): 1188. https://doi.org/10.1007/s12011-024-04219-z.

Terefe, Ermias Mergia, and Arabinda Ghosh. 2022. "Molecular Docking, Validation, Dynamics Simulations, and Pharmacokinetic Prediction of Phytochemicals Isolated from Croton Dichogamus Against the HIV-1 Reverse Transcriptase." *Bioinformatics and Biology Insights* 16 (9): 1-20. https://doi.org/10.1177/11779322221125605

Thenin-Houssier, Suzie, and Susana T. Valente. 2016. "HIV-1 Capsid Inhibitors as Antiretroviral Agents." *Current HIV Research* 14 (3): 270–82. https://doi.org/10.2174/1570162x14999160224103555.

Trott, Oleg, and Arthur J. Olson. 2010. "AutoDock Vina: Improving the Speed and Accuracy of Docking with a New Scoring Function, Efficient Optimization, and Multithreading." *Journal of Computational Chemistry* 31 (2): 455–61. https://doi.org/10.1002/jcc.21334.

Tsiang, Manuel, Anita Niedziela-Majka, Magdeleine Hung, Debi Jin, Eric Hu, Stephen Yant, Dharmaraj Samuel, Xiaohong Liu, and Roman Sakowicz. 2012. "A Trimer of Dimers Is the Basic Building Block for Human Immunodeficiency Virus-1 Capsid Assembly." *Biochemistry* 51 (22): 4416–28. https://doi.org/10.1021/bi300052h.

Türe, Cengiz, and Harun Böcük. 2010. "Distribution Patterns of Threatened Endemic Plants in Turkey: A Quantitative Approach for Conservation." *Journal for Nature Conservation* 18 (4): 296–303. https://doi.org/10.1016/j.jnc.2010.01.002.

UNIAIDS. 2025. "Global HIV & AIDS Statistics — Fact Sheet | UNAIDS." 2025. https://www.unaids.org/en/resources/fact-sheet.

Vivoli, Mirella, Halina R. Novak, Jennifer A. Littlechild, and Nicholas J. Harmer. 2014. "Determination of Protein-Ligand Interactions Using Differential Scanning Fluorimetry." *Journal of Visualized Experiments: JoVE*, no. 91 (9): 51809. https://doi.org/10.3791/51809.

Wallace, Andrew C., Roman A. Laskowski, and Janet M. Thornton. 1995. “Ligplot: A Program to Generate Schematic Diagrams of Protein-Ligand Interactions.” *Protein Engineering, Design and Selection* 8 (2): 127–34. https://doi.org/10.1093/protein/8.2.127,.

Wang, Lei, Mary C. Casey, Sanjeev Kumar v. Vernekar, Rajkumar Lalji Sahani, Jayakanth Kankanala, Karen A. Kirby, Haijuan Du, et al. 2020. “Novel HIV-1 Capsid-Targeting Small Molecules of the PF74 Binding Site.” *European Journal of Medicinal Chemistry* 204 (10): 112626. https://doi.org/10.1016/j.ejmech.2020.112626.

Wang, Shuguang, Jiyang Li, Hai Huang, Wen Gao, Changlong Zhuang, Bo Li, Pei Zhou, and Deyun Kong. 2009. “Anti-Hepatitis B Virus Activities of Astragaloside IV Isolated from Radix Astragali.” *Biological and Pharmaceutical Bulletin* 32 (1): 132–35. https://doi.org/10.1248/bpb.32.132.

Wang, Weifeng, Jing Zhou, Upul D. Halambage, Kellie A. Jurado, Augusta v. Jamin, Yujie Wang, Alan N. Engelman, and Christopher Aiken. 2017. “Inhibition of HIV-1 Maturation via Small-Molecule Targeting of the Amino-Terminal Domain in the Viral Capsid Protein.” *Journal of Virology* 91 (9): e02155-16. https://doi.org/10.1128/jvi.02155-16.

World Health Organization. 2024. “HIV and AIDS.” 2024. https://www.who.int/news-room/fact-sheets/detail/hiv-aids.

Wu, Chung Yi, Jia Tsrong Jan, Shiou Hwa Ma, Chin Jung Kuo, Hsueh Fen Juan, Yih Shyun E. Cheng, Hsien Hua Hsu, et al. 2004. “Small Molecules Targeting Severe Acute Respiratory Syndrome Human Coronavirus.” *Proceedings of the National Academy of Sciences of the United States of America* 101 (27): 10012–17. https://doi.org/10.1073/pnas.0403596101.

Yamashita, Masahiro, and Alan N. Engelman. 2017. “Capsid-Dependent Host Factors in HIV-1 Infection.” *Trends in Microbiology* 25 (9): 741. https://doi.org/10.1016/j.tim.2017.04.004.

Yang, Xiu Wei, Jing Zhao, Yu Xin Cui, Xue Hui Liu, Chao Mei Ma, Masao Hattori, and Li He Zhang. 1999. “Anti-HIV-1 Protease Triterpenoid Saponins from the Seeds of Aesculus Chinensis.” *Journal of Natural Products* 62 (11): 1510–13. https://doi.org/10.1021/np990180u.

Yesilada, Erdem, Erdal Bedir, Ihsan Çaliş, Yoshihisa Takaishi, and Yasukazu Ohmoto. 2005. “Effects of Triterpene Saponins from Astragalus Species on in Vitro

Cytokine Release." *Journal of Ethnopharmacology* 96 (1–2): 71–77. https://doi.org/10.1016/j.jep.2004.08.036.

Yi, Bowen, Benjamin Xuan Zheng Chew, Huixin Chen, Regina Ching Hua Lee, Yuhui Deborah Fong, Wei Xin Chin, Chee Keng Mok, and Justin Jang Hann Chu. 2023. "Antiviral Activity of Catechin against Dengue Virus Infection." *Viruses* 15 (6): 1377. https://doi.org/10.3390/v15061377.

Yu, Alvin, Katarzyna A. Skorupka, Alexander J. Pak, Barbie K. Ganser-Pornillos, Owen Pornillos, and Gregory A. Voth. 2020. "TRIM5α Self-Assembly and Compartmentalization of the HIV-1 Viral Capsid." *Nature Communications 2020 11:1* 11 (1): 1–10. https://doi.org/10.1038/s41467-020-15106-1.

Zhang, Da Wei, Rong Hua Luo, Lei Xu, Liu Meng Yang, Xiao Shuang Xu, Yong Tang Zheng, and Heng Luo. 2020. "Natural-Product-Library-Based Screening for Discovery of Capsid C-Terminal Domain Targeted HIV-1 Inhibitors." *International Journal of Antimicrobial Agents* 55 (4): 1-8. https://doi.org/10.1016/j.ijantimicag.2020.105926.

Zhao, Gongpu, Juan R. Perilla, Ernest L. Yufenyuy, Xin Meng, Bo Chen, Jiying Ning, Jinwoo Ahn, et al. 2013. "Mature HIV-1 Capsid Structure by Cryo-Electron Microscopy and All-Atom Molecular Dynamics." *Nature* 497 (7451): 643–46. https://doi.org/10.1038/nature12162

Zhuang, Shentian, and Bruce E. Torbett. 2021. "Interactions of HIV-1 Capsid with Host Factors and Their Implications for Developing Novel Therapeutics." *Viruses* 13 (3): 417. https://doi.org/10.3390/v13030417.

Zubair, Muhammad Sulaiman, Saipul Maulana, Agustinus Widodo, Alwiyah Mukaddas, and Ramadanil Pitopang. 2020. "Docking Study on Anti-HIV-1 Activity of Secondary Metabolites from Zingiberaceae Plants." *Journal of Pharmacy and Bioallied Sciences* 12 (6): S763–67. https://doi.org/10.4103/jpbs.jpbs_261_19.

Zuo, Jiawei, Tao Meng, Yuanyuan Wang, and Wenjian Tang. 2023. "A Review of the Antiviral Activities of Glycyrrhizic Acid, Glycyrrhetinic Acid and Glycyrrhetinic Acid Monoglucuronide." *Pharmaceuticals* 16 (5): 641. https://doi.org/10.3390/ph16050641.

APPENDIX A

Table 9. Docking Results of 279 Molecules on HIV-1 CA Monomer Using AutoDock Vina

Molecule	2D Structure	AutoDock Vina Score kcal/mol	Molecule	2D Structure	AutoDock Vina Score kcal/mol
(D)-alpha-Tocopherol	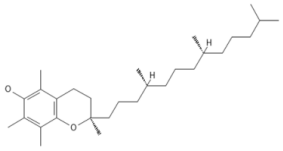	-5.67	**Gito-01**	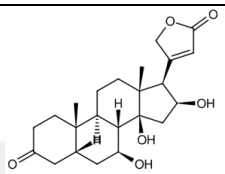	-6.84
1-(2-Hydroxyethyl)-2,2,6,6-tetramethyl-4-hydroxypiperidine	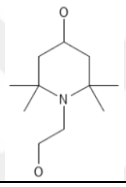	-4.74	**Gito-02**	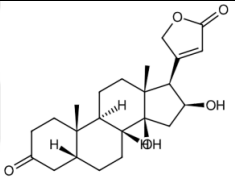	-7.17
10-Decarboxymethyl aclacinomycin T (12-dehydroxy iremycin)	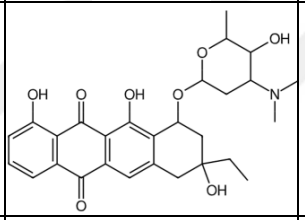	-7.86	**Gito-03**	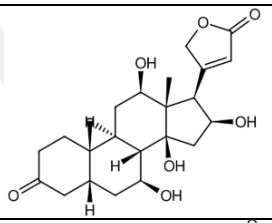	-6.68
2Z)-4,6-dihydroxy-2-[(3-hydroxy-4-methoxyphenyl)methylidene]-1-benzofuran-3-one	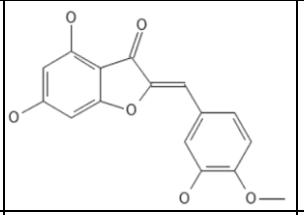	-7.06	**Gito-04**	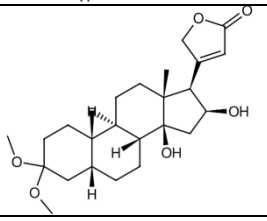	-6.34
3-Methyl-2-[[2,3,4-trihydroxy-5-(hydroxymethyl)oxolan-2-yl]methylamino]pentanoic acid	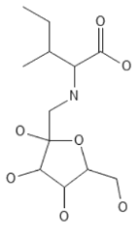	-5.41	**Gito-05**	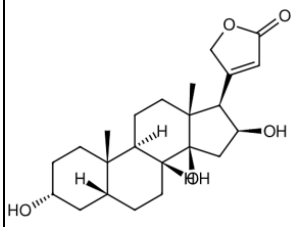	-7.19
4'-O-demethyl Anisomycin	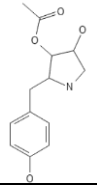	-5.83	**Gito-06**	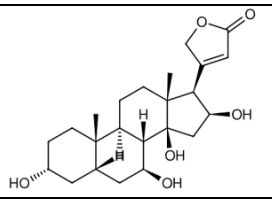	-7.01

(cont. on next page)

Table 9. (cont.)

5-hydroxyectoine	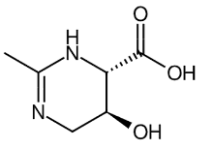	-4.67	**Gito-07**	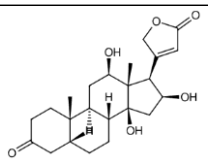	-6.57
ActD	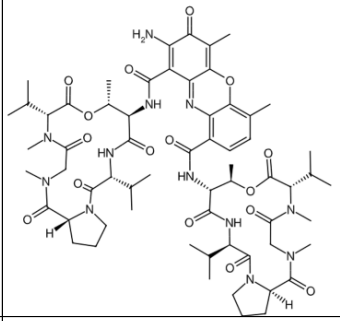	-10.13	**Gito-08**	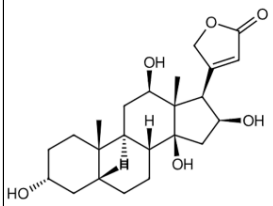	-6.31
Actinomycin D	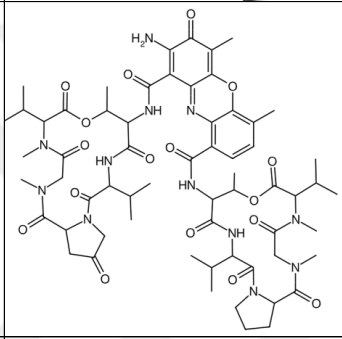	-7.76	**Gitoxigenin**	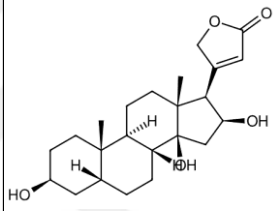	-6.56
Actinomycin X0(beta)	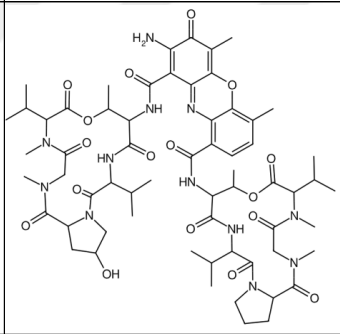	-9.44	**Iremycin**	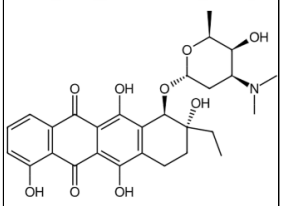	-7.85
Actinomycin X2	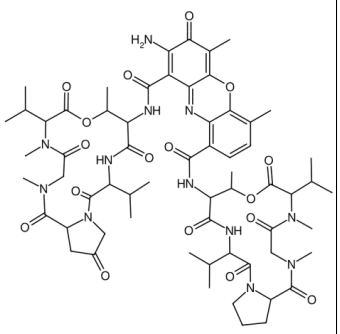	-9.85	**K-41A**	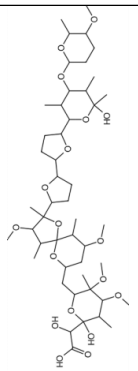	-7.7

(cont. on next page)

Table 9. (cont.)

ActX2	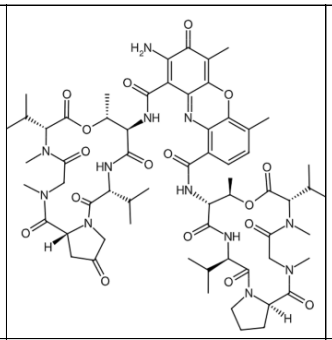	-7.95	**K-41AGm**	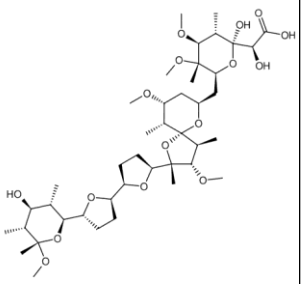	-6.55
ActXOB	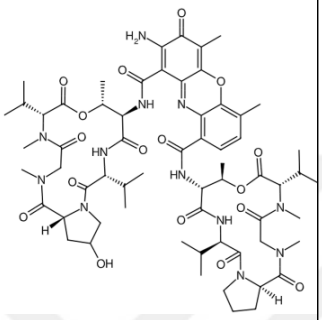	-8.15	**K-41Am**	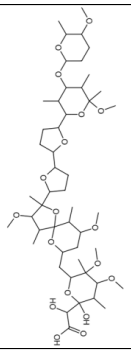	-6.92
Afrormosin	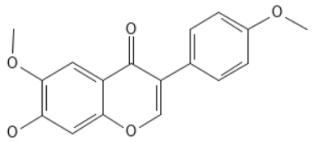	-5.3	**Kaempferol 3-O-(2,6-di-O-alpha-L-rhamnopyranosyl)-beta-D-galactopyranoside**	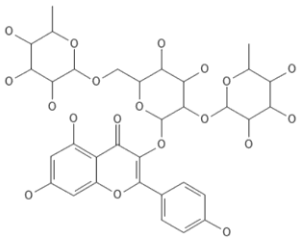	-8.39
Albocycline C	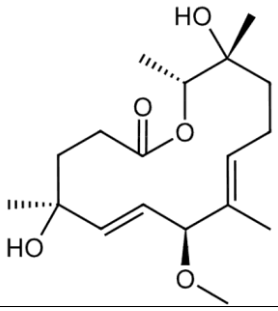	-5.92	**Kaempferol 3-O-(2,6-α-L-dirhamnopyranosyl-β-D-glucopyranoside)**	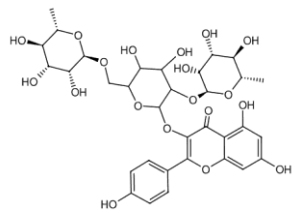	-7.63
Alismol	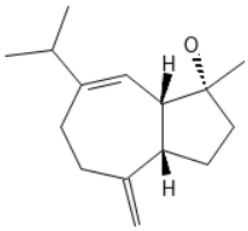	-6.57	**Kaempferol-3-O-rutinoside**	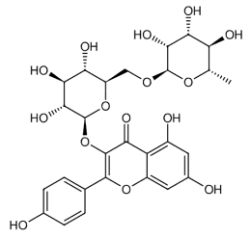	-7.17

(cont. on next page)

Table 9. (cont.)

Alt-Ole-01	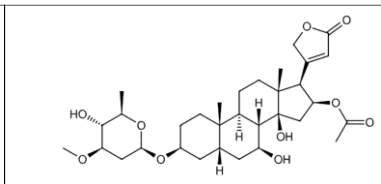	-6.81	**Kojic acid**	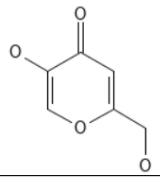	-4.82
Alt-Ole-02	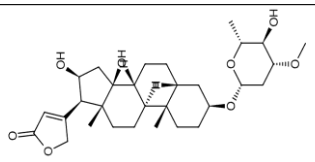	-7.59	**Licoagroside B**	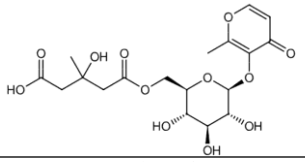	-6.02
Alt-Ole-03	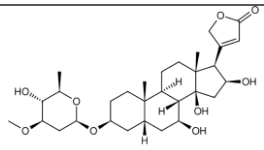	-7.08	**Loliolide**	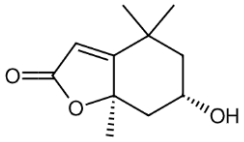	-5.44
Alt-Ole-04	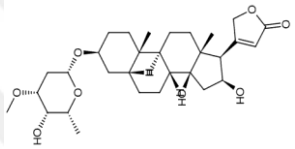	-7.93	**Maculosin**	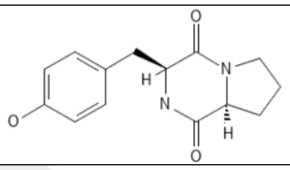	-6.62
Alt-Ole-05	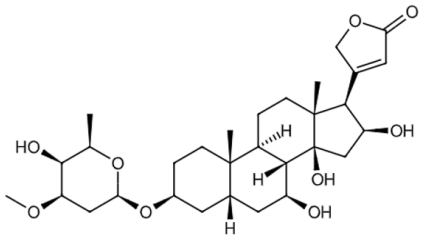	-6.9	**Methylamycin B**	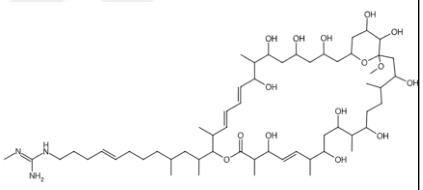	-7.57
Amycin B	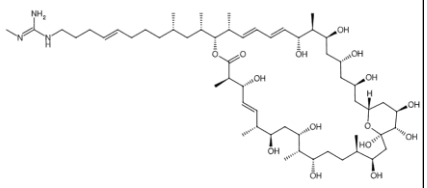	-8.6	**N-benzoyl-L-arginine**	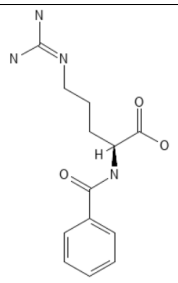	-6.72

(cont. on next page)

Table 9. (cont.)

Arenaric acid	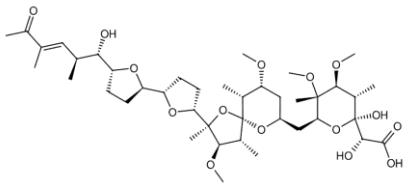	-6.87	**N-cis-p-coumaroyl tyrosine**	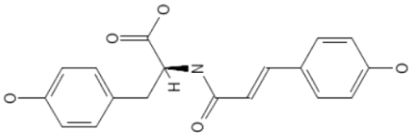	-6.84
B-SCG-06	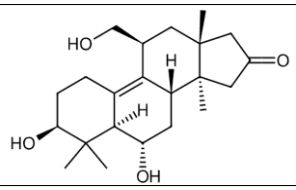	-6.03	**Neoruscogenin**	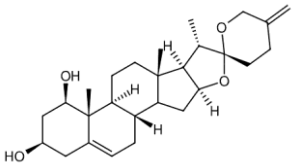	-9.06
B-SKG-07	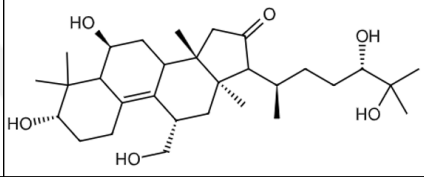	-7.03	**Oleandrin**	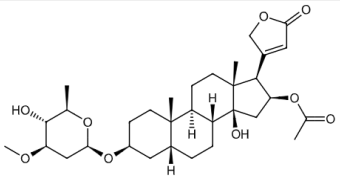	-7.37
C27-O-deglycosyl K-41A	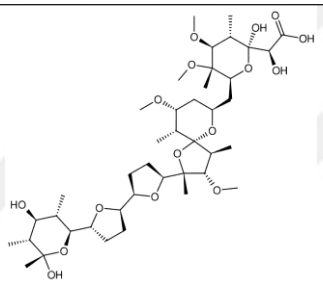	-7.24	**Pha-Ole-01**	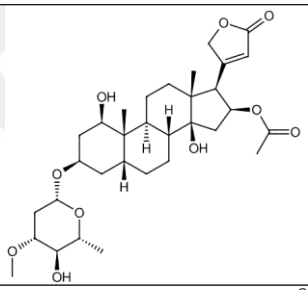	-7.75
Caffeine	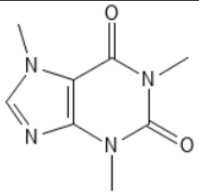	-4.85	**Pha-Ole-02**	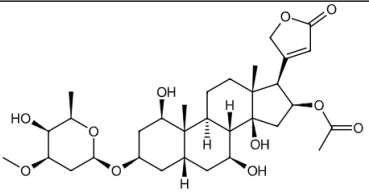	-7.02
Catechin	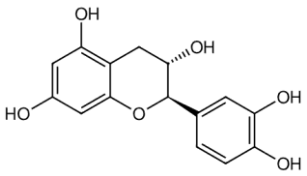	-7.2	**Prunetin**	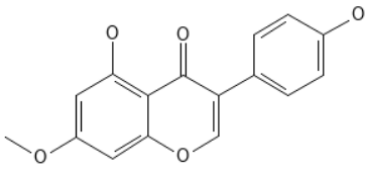	-7.12

(cont. on next page)

Table 9. (cont.)

Chloramphenicol	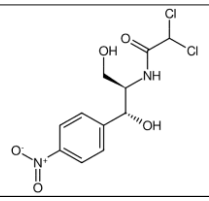	-5.71	**Putaminoxin B**	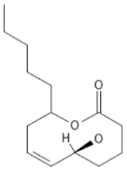	-5.96
Chlorogenic Acid	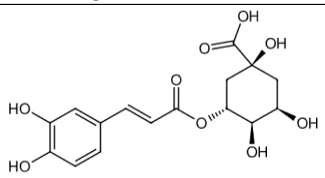	-6.57	**Quercetin**	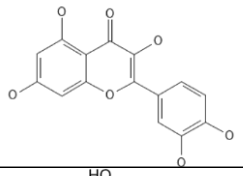	-7.40
Chromomycin A2	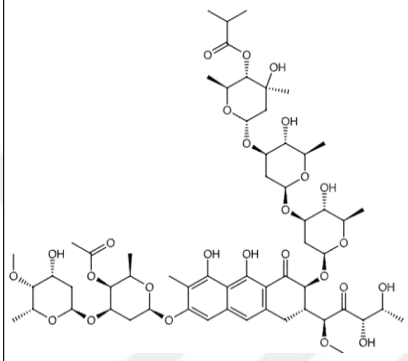	-8.08	**Quercetin 3-apiosyl-(1->2)-rhamnosyl-(1->6)-glucoside**	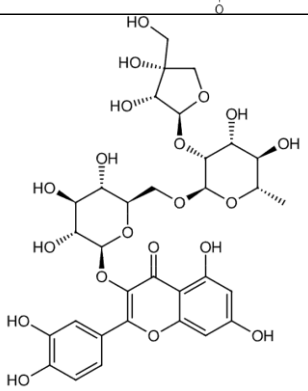	-7.89
Chromomycin A3	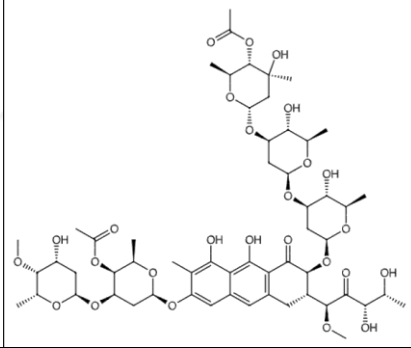	-7.69	**Rapamycin**	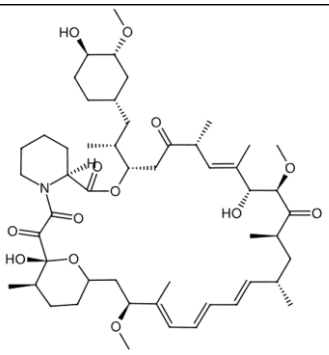	-7.83
Chromomycinone	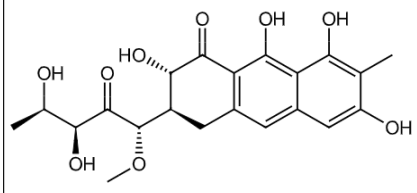	-6.75	**Rebaudioside A**	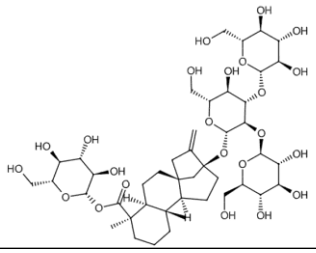	-6.24
Collismycin A	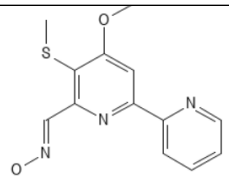	-5.93	**RES-01**	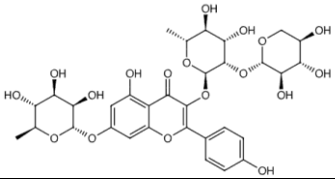	-8.61

(cont. on next page)

Table 9. (cont.)

Collismycin C	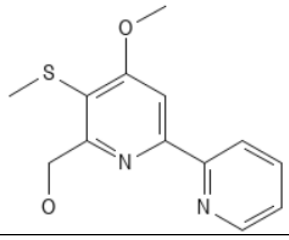	-5.49	**RES-04**	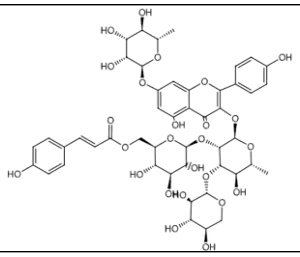	-8.07
Compound NP-002290	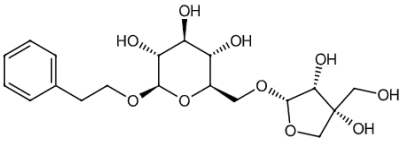	-6.36	**RES-05**	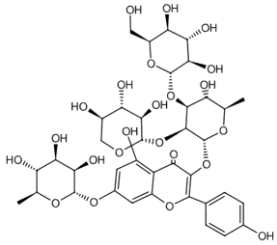	-6.99
Compound NP-004676	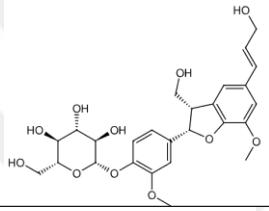	-6.91	**Rishitin**	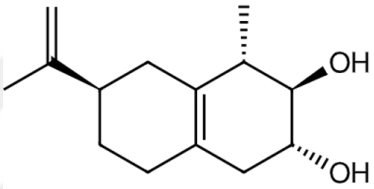	-5.98
Compound NP-005807	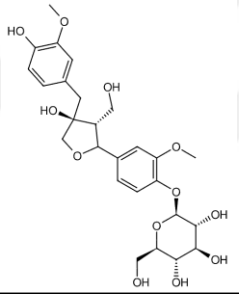	-7.31	**Rolloamide A**	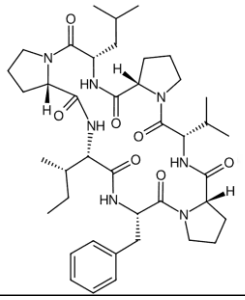	-7.69
Compound NP-016403	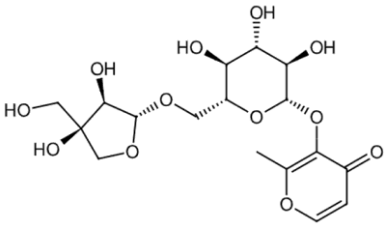	-6.45	**Rosmarinic acid**	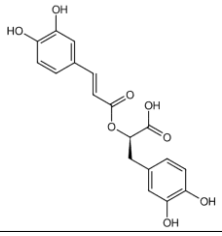	-6.50
Coproporphyrin III	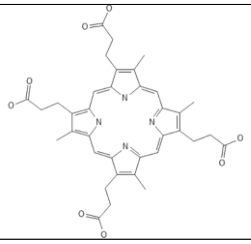	-7.29	**Ruscogenin**	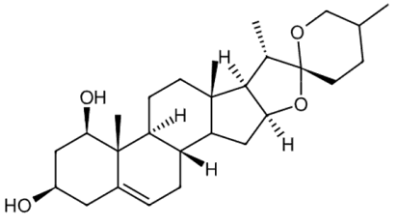	-9.11

(cont. on next page)

Table 9. (cont.)

Cyclo(-Leu-Pro)	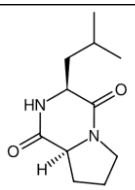	-5.68	**Rutin**	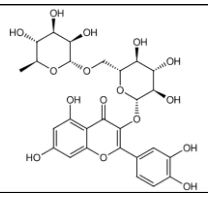	-6.65
cyclo(L-Phe-D-Pro)	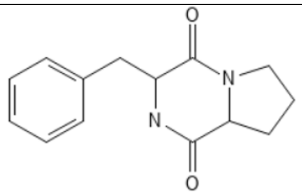	-6.16	**SC-EG-01**	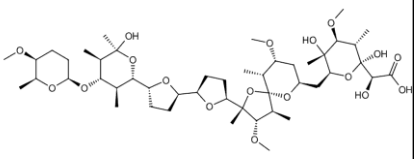	-7.47
Deacetyl Chromomycin A3	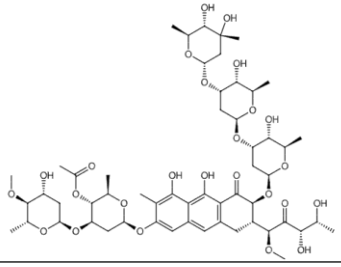	-7.25	**SC-EG-02**	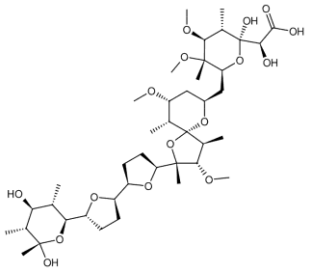	-7.48
Desferrioxamine E (Nocardamine)	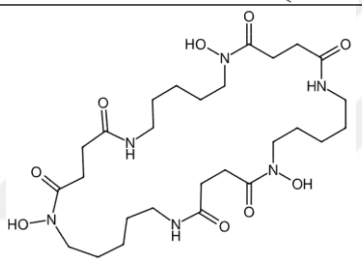	-9.1	**SC-EG-03**	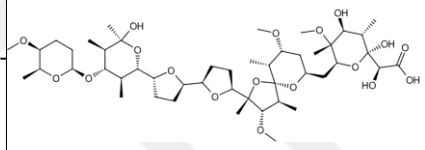	-8.09
Ditryptophenaline	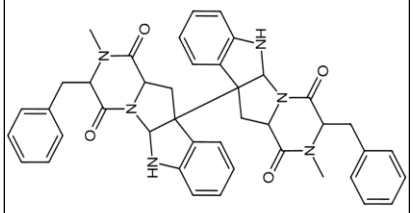	-9.84	**SC-EG-12**	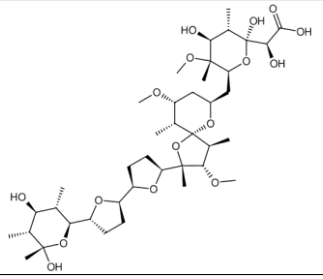	-7.09
Ellagic acid	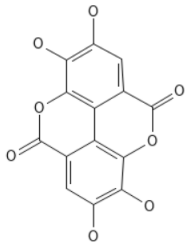	-6.63	**SC-EG-19**	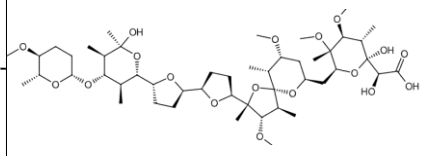	-6.09

(cont. on next page)

Table 9. (cont.)

Ferulic acid	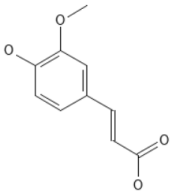	-5.2	**Speradine D**	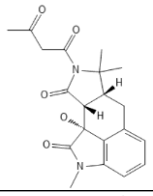	-7.34
Fisetin	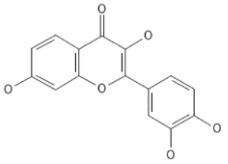	-7.48	**Butyrolactone I**	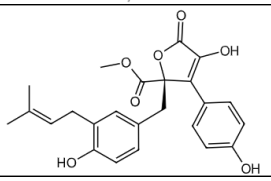	-7.36
Formononetin	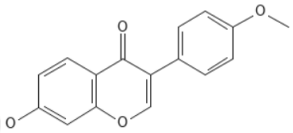	-7.02	**Tanzawaic acid O**	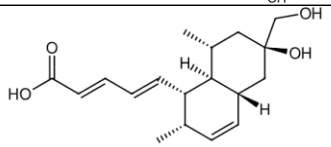	-6.49
Germicidin	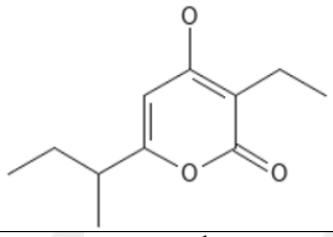	-5.83	**Tectorigenin, 7-O-[D-apiofuranosyl-(1-6)-D-glu**	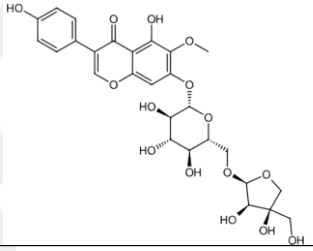	-7.88
Germicidin B	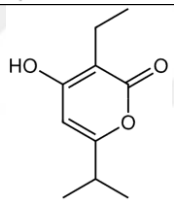	-5.68	**Tirandamycin A**	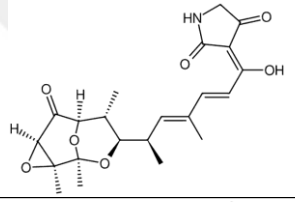	-7.32
AG08	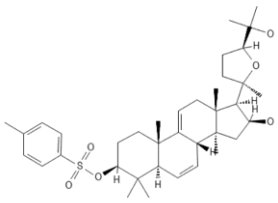	-6.83	**Tirandamycin B**	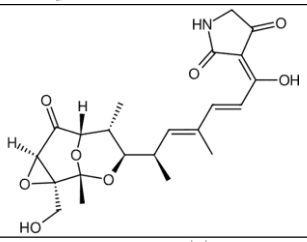	-7.44
Asiatic acid	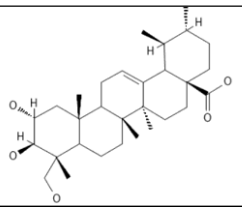	-7.15	**MD-MG-06**	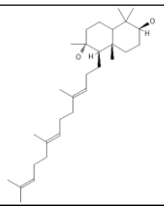	-6.96

(cont. on next page)

Table 9. (cont.)

Asiaticoside	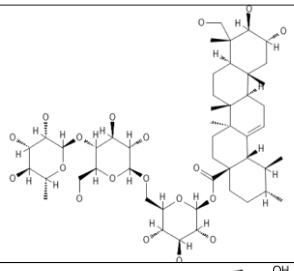	-7.75	**MD-MG-07**	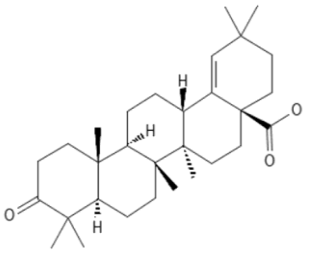	-6.13
AST IV	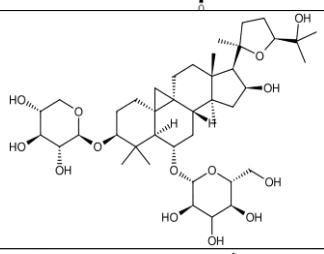	-7.69	**MD-MG-12**	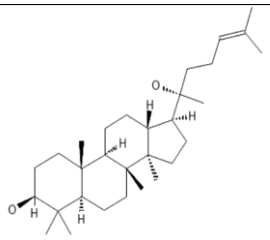	-7.11
AST VII	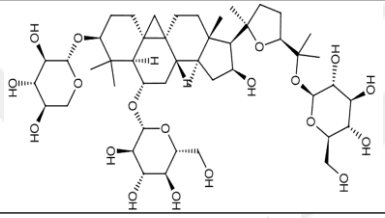	-6.97	**MD-MG-13**	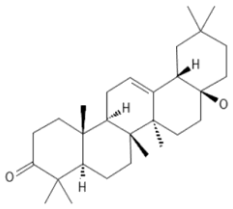	-7.18
Astragenol	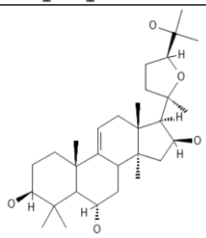	-7.63	**MD-MG-14**	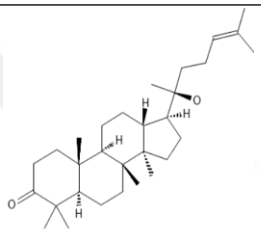	-6.36
ATB-01	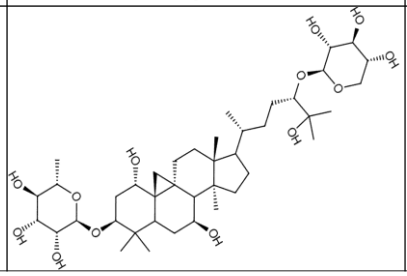	-6.96	**MD-MG-17**	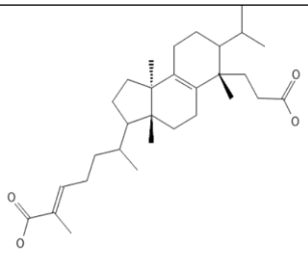	-6.52

(cont. on next page)

Table 9. (cont.)

ATB-03	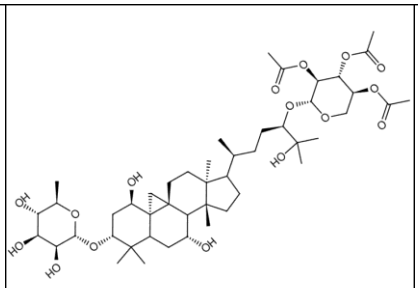	-6.43	**MD-MG-19**	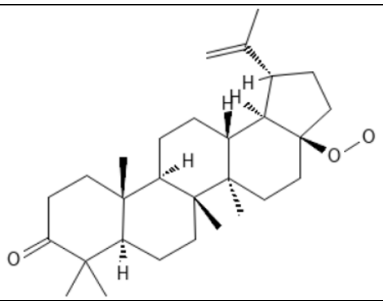	-6.62
ATB-05	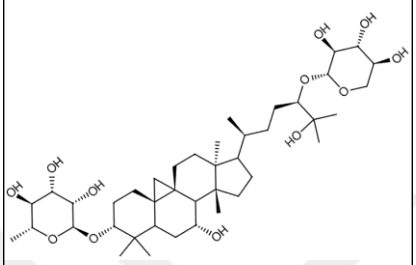	-7.41	**S-SCG-01**	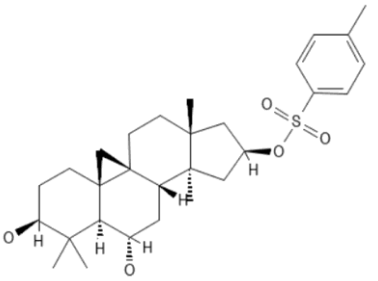	-8.26
B-AG-01	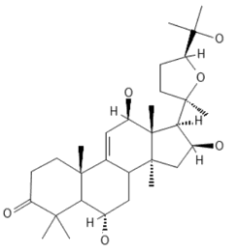	-7.17	**S-SCG-02**	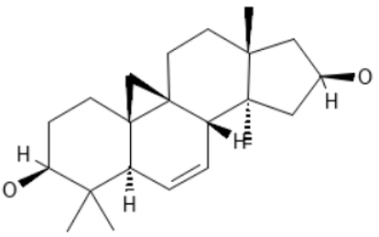	-5.95
B-AG-02	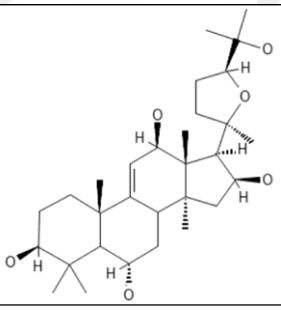	-7.5	**S-SCG-03**	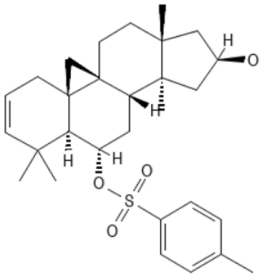	-7.35
B-AG-03	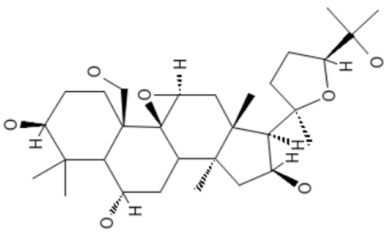	-7.85	**S-SCG-04**	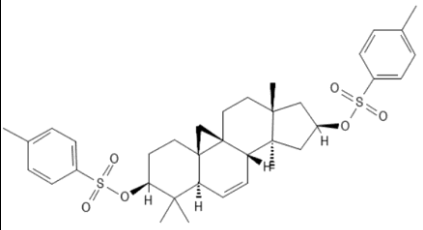	-8.32

(cont. on next page)

Table 9. (cont.)

B-AG-04	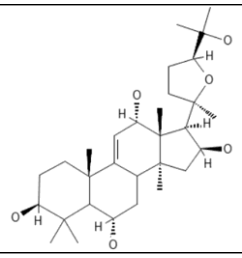	-7.08	**S-SCG-05**	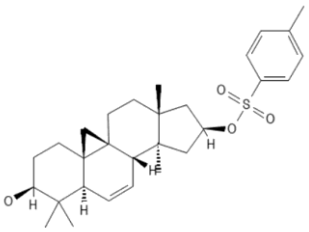	-7.88
B-AG-05	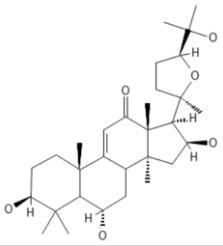	-6.6	**S-SCG-06**	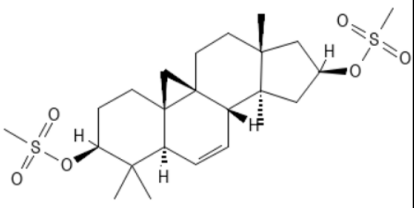	-6.91
B-AG-06	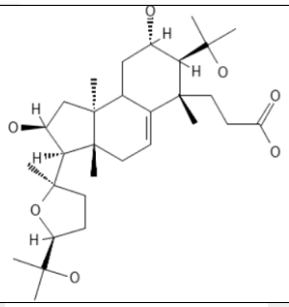	-7.72	**S-SCG-07**	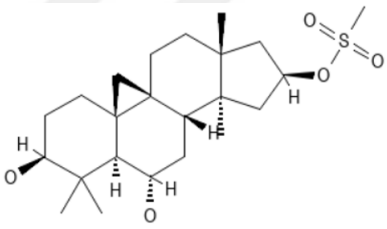	-7.06
B-AG-07	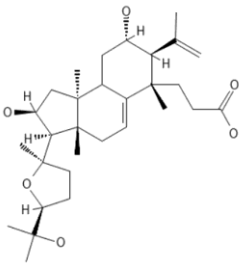	-7.31	**SCG**	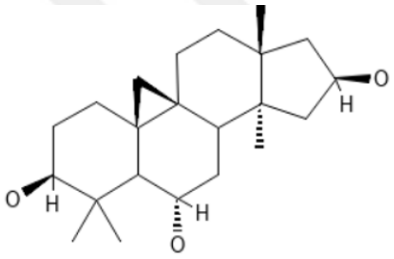	-6.61
B-AG-08	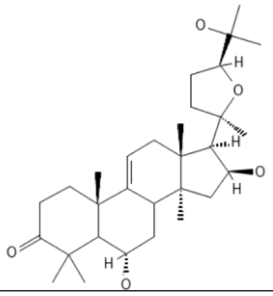		**SKG**	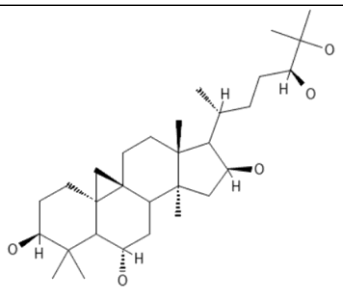	-6.84

(cont. on next page)

Table 9. (cont.)

B-CG-01	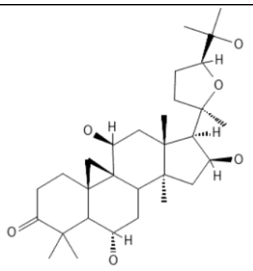	-7.83	**S-C2**	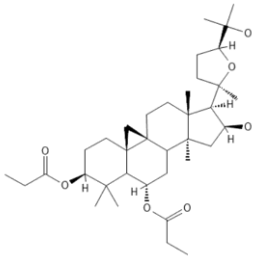	-7.06
B-CG-02	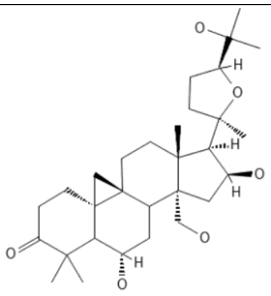	-6.58	**S-C3**	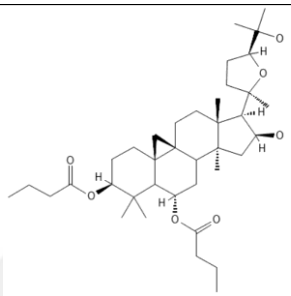	-7.78
B-CG-03	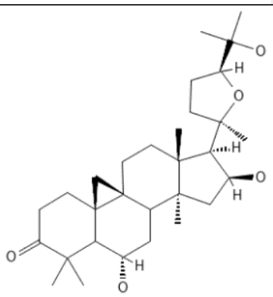	-6.91	**S-C4**	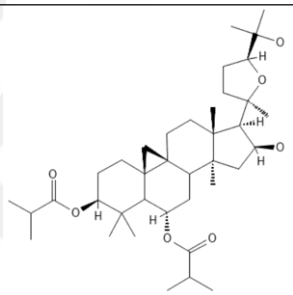	-7.54
B-CG-04	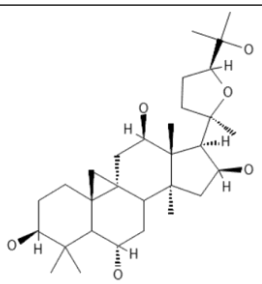	-6.94	**S-C5**	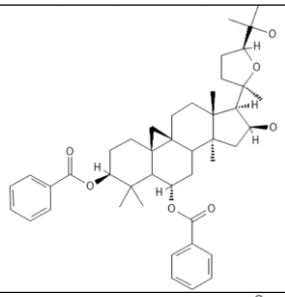	-9.11
B-CG-05	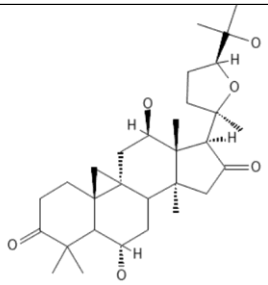	-7.15	**S-C6**	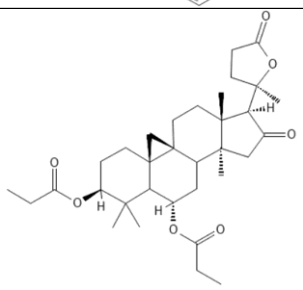	-7.35

(cont. on next page)

Table 9. (cont.)

B-CG-06	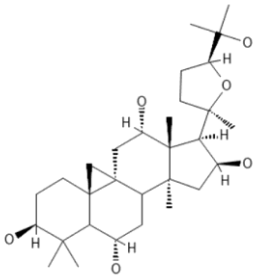	-6.58	**S-C7**	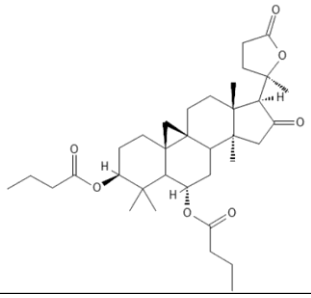	-6.95
B-CG-07	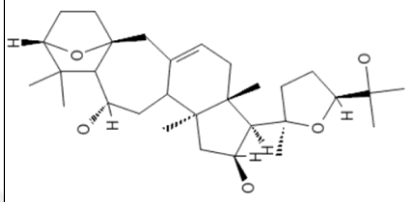	-7.1	**S-C8**	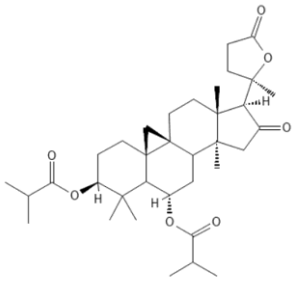	-7.80
B-CG-08	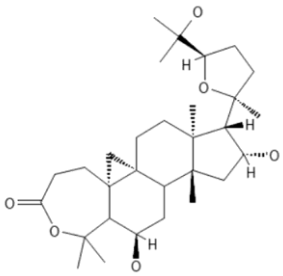	-7.93	**S-C9**	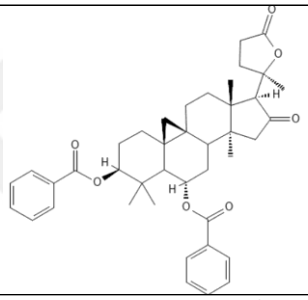	-9.34
B-CG-09	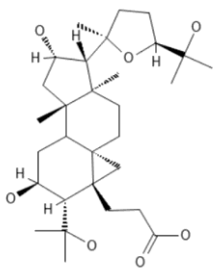	-6.66	**S-C10**	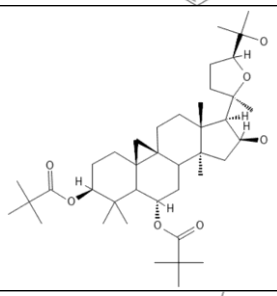	-7.53
B-CG-10	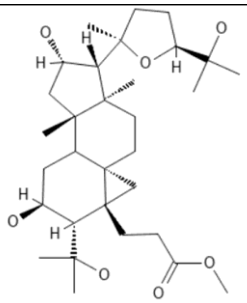	-6.58	**S-C11**	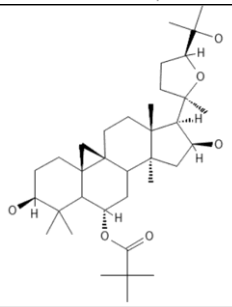	-7.58

(cont. on next page)

Table 9. (cont.)

B-SCG-05	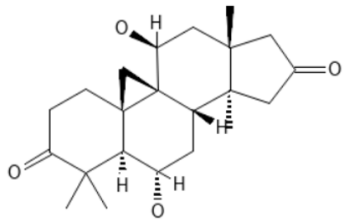	-7.29	**S-C12**	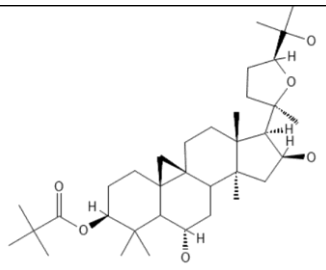	-7.19
B-SCG-07	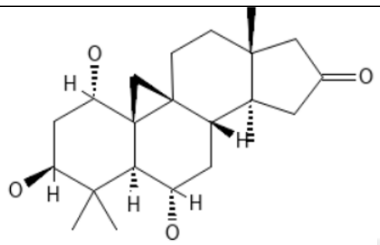	-6.55	**S-C13**	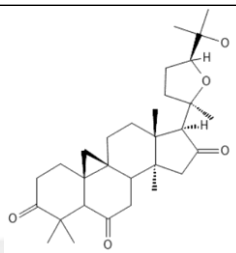	-7.93
B-SCG-08	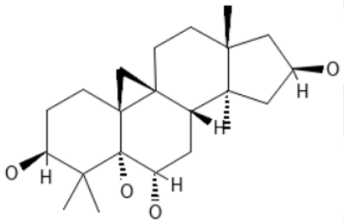	-5.7	**S-C14**	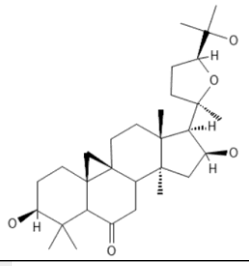	-7.52
B-SCG-09	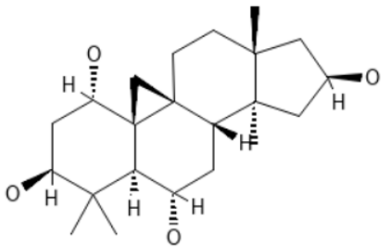	-6.02	**S-C15**	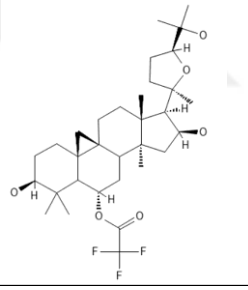	-7.61
B-SCG-10	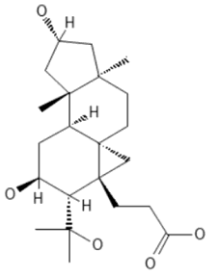	-5.69	**S-C16**	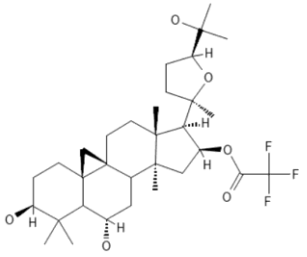	-7.96

(cont. on next page)

Table 9. (cont.)

B-SCG-11	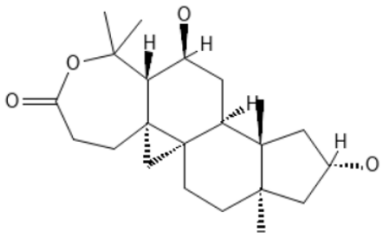	-5.49	**S-C17**	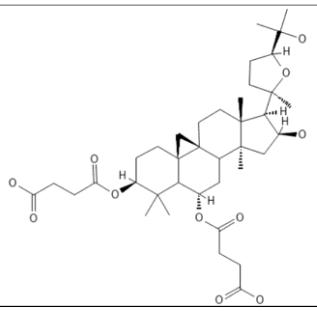	-7.23
B-SCG-12	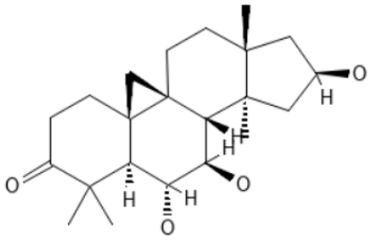	-6.66	**S-C18**	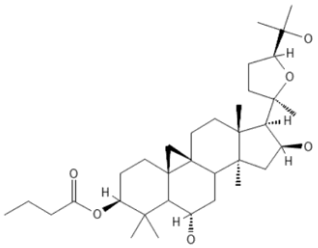	-7.26
B-SCG-13	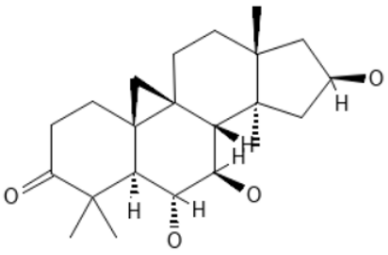	-7.07	**S-C19**	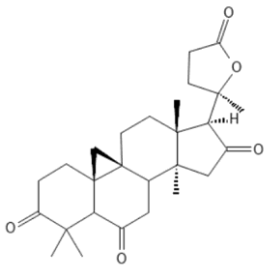	-8.06
B-SCG-14	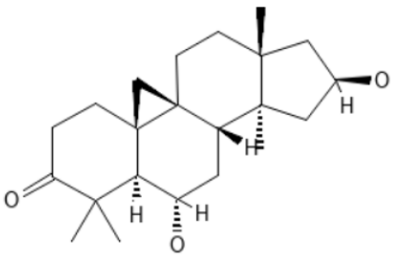	-6.27	**S-C20**	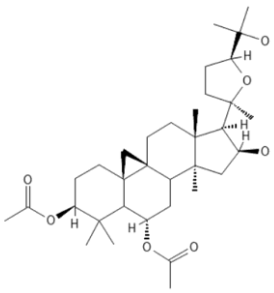	-7.18
B-SCG-15	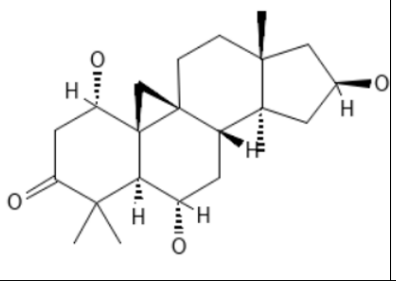	-6.3	**S-C21**	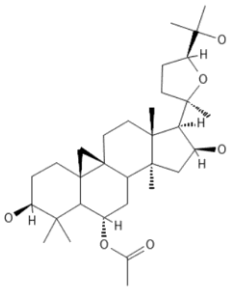	-7.20

(cont. on next page)

Table 9. (cont.)

B-SCG-16	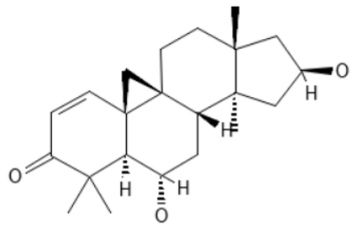	-6.131	**S-C22**	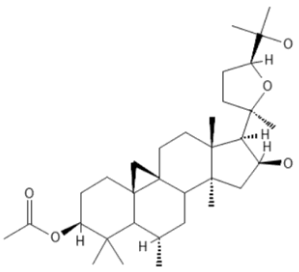	-7.32
B-SKG-01	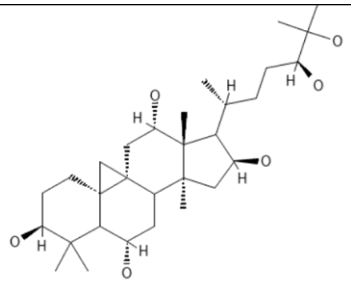	-6.26	**S-C23**	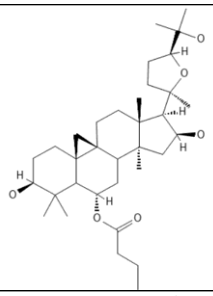	-7.71
B-SKG-02	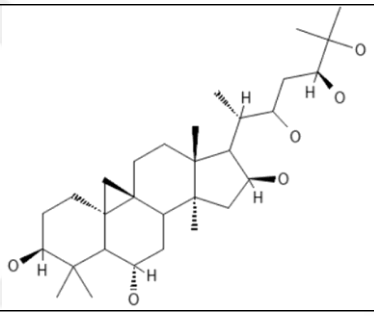	-6.9	**S-C24**	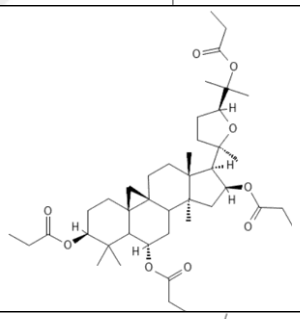	-6.88
B-SKG-03	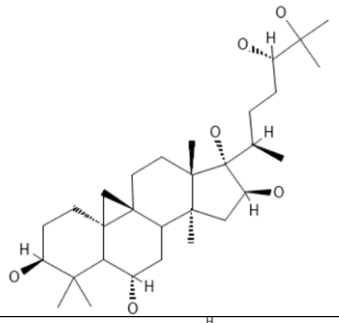	-7.43	**S-C25**	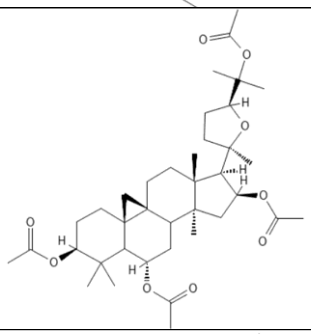	-7.29
B-SKG-04	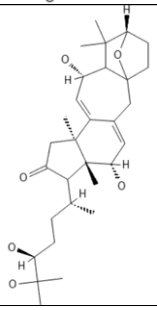	-7.58	**S-C26**	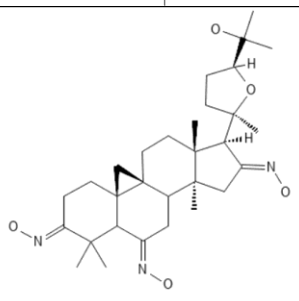	-8.56

(cont. on next page)

Table 9. (cont.)

B-SKG-05	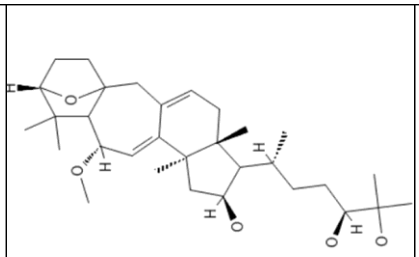	-6.8	**S-C27**	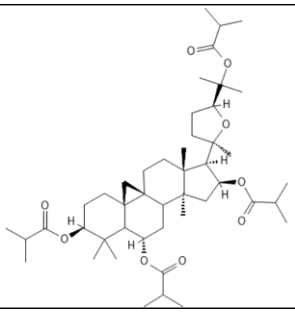	-7.62
B-SKG-06	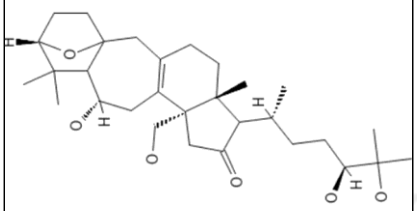	-6.9	**S-C28**	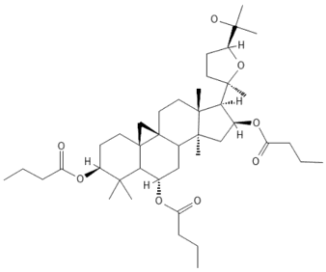	-6.98
B-SKG-07	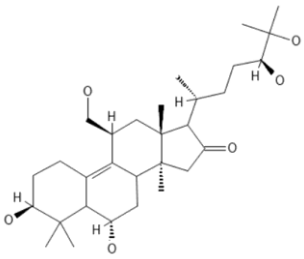	-7.03	**S-C29**	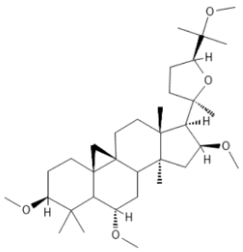	-7.12
B-SKG-08	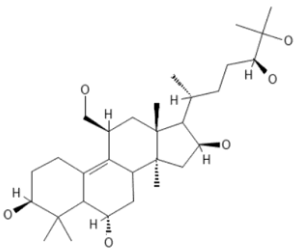	-6.26	**S-C30**	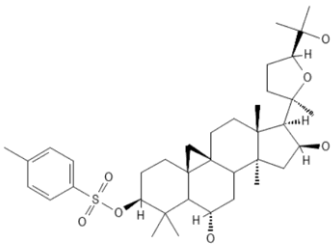	-8.40
Betulin	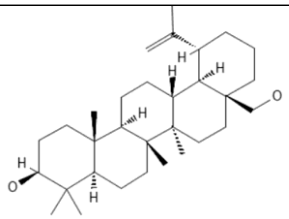	-6.52	**S-C31**	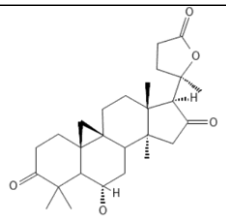	-7.95
CCPG	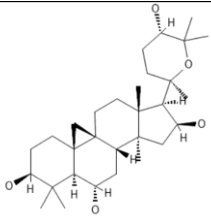	-6.92	**S-C32**	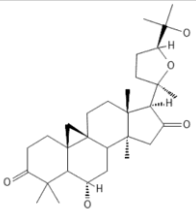	-8.07

(cont. on next page)

Table 9. (cont.)

CCPG-02	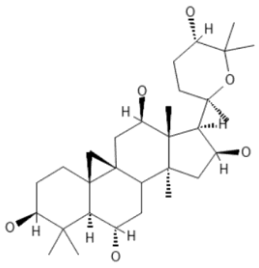	-7.45	**S-C33**	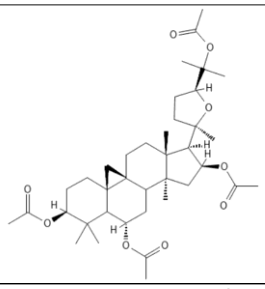	-7.10
CCPG-03	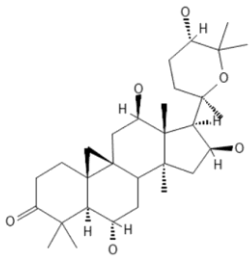	-7.09	**S-C34**	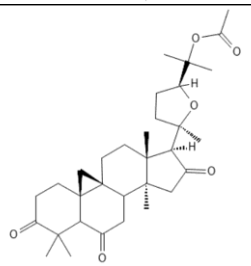	-7.80
CCPG-04	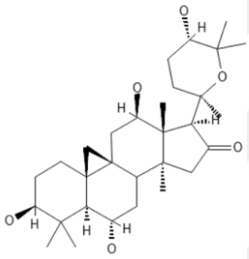	-7.45	**S-C35**	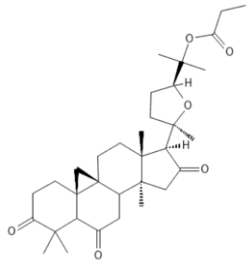	-7.99
CCPG-05	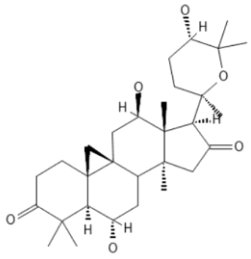	-7.42	**S-C36**	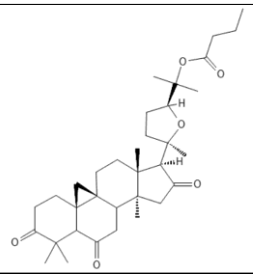	-8.23
CCPG-06	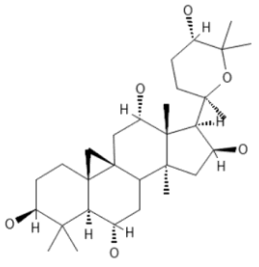	-7.36	**S-A2**	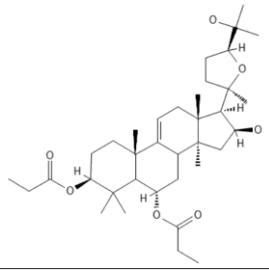	-7.48

(cont. on next page)

Table 9. (cont.)

CCPG-07	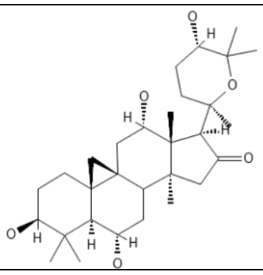	-7.05	**S-A3**	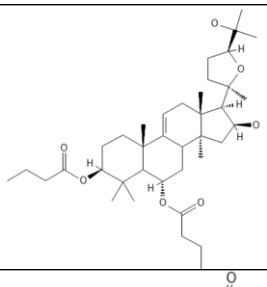	-7.54
CCPG-08	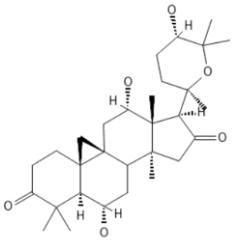	-7.07	**S-A4**	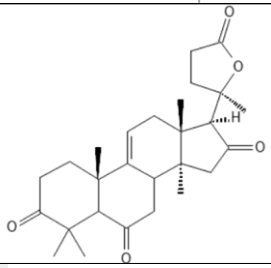	-8.36
CCPG-09	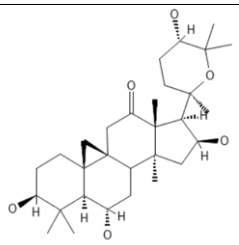	-7.38	**S-A5**	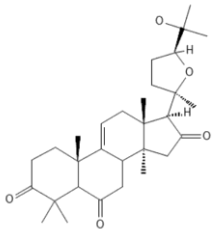	-8.28
CCPG-10	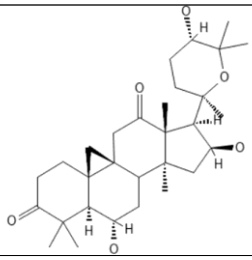	-7.69	**S-A6**	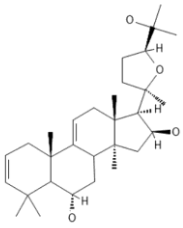	-7.92
CCPG-11	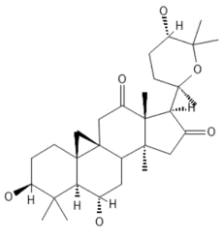	-8.17	**S-A7**	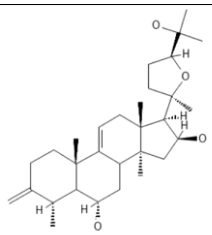	-8.70
CCPG-12	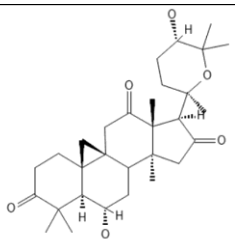	-7.84	**S-A8**	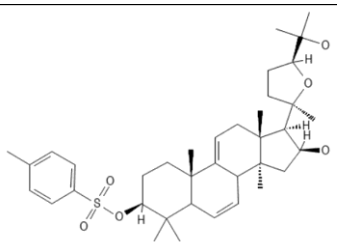	-8.77

(cont. on next page)

Table 9. (cont.)

CCPG-13	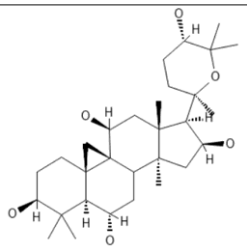	-6.91	**S-A9**	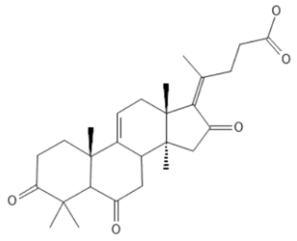	-8.09
CCPG-14	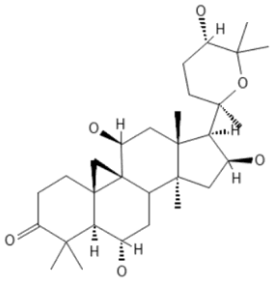	-6.55	**S-A10**	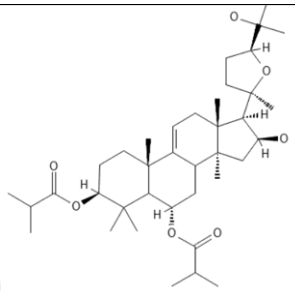	-8.16
CCPG-15	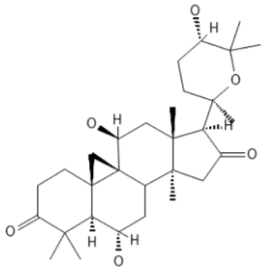	-7.63	**S-A11**	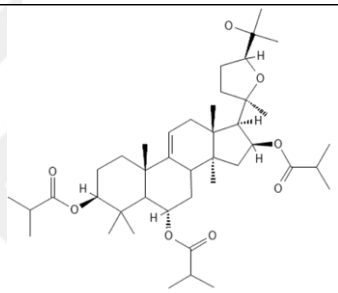	-7.84
CCPG-16	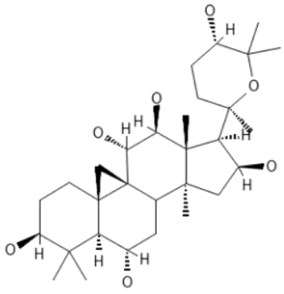	-7.28	**S-A12**	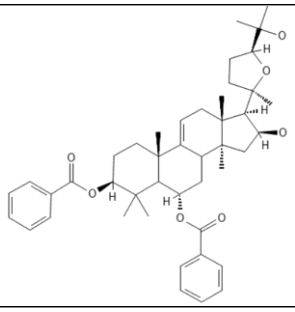	-9.39
CCPG-17	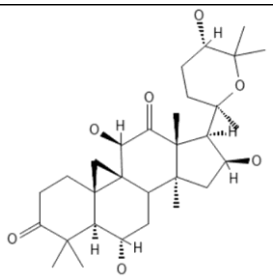	-7.5	**S-A13**	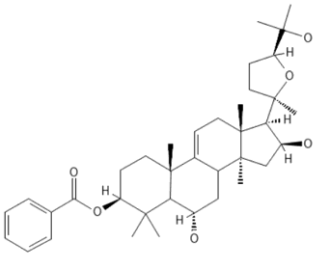	-8.72

(cont. on next page)

Table 9. (cont.)

CCPG-18	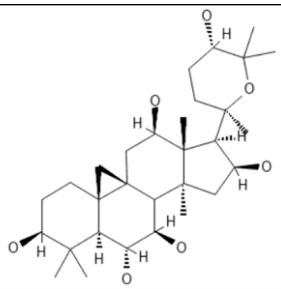	-7.62	**S-A14**	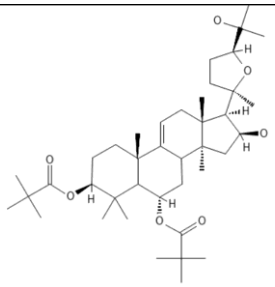	-7.57
CCPG-19	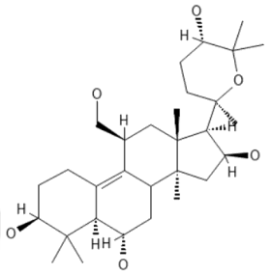	-6.37	**S-A15**	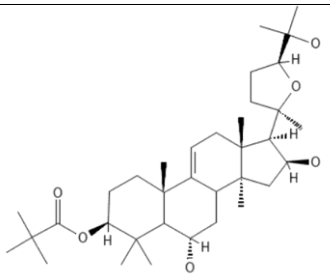	-7.85
CCPG-20	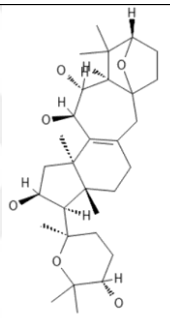	-6.62	**S-A16**	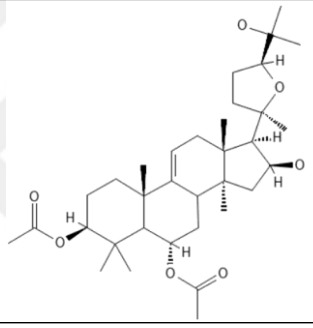	-7.67
CCPG-21	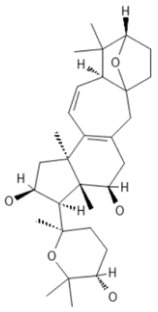	-6.91	**S-A17**	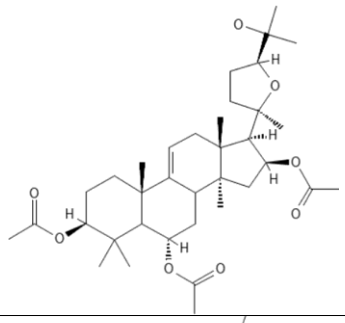	-7.48
CCPG-22	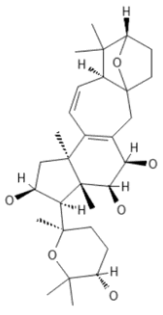	-7.03	**S-A18**	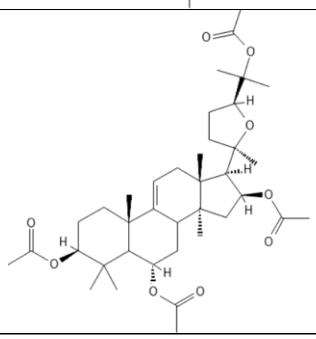	-7.22

(cont. on next page)

Table 9. (cont.)

CCPG-23	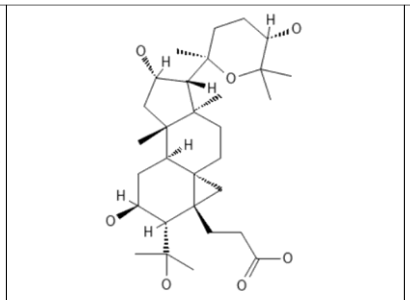	-6.96	**S-A19**	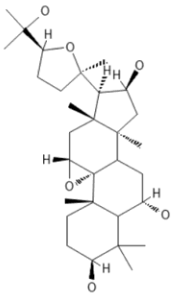	-7.83
CCPG-24	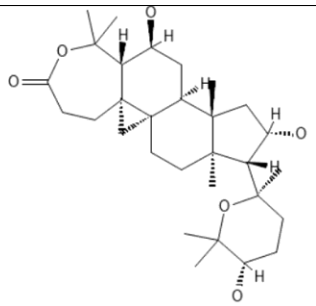	-8.27	**S-A20**	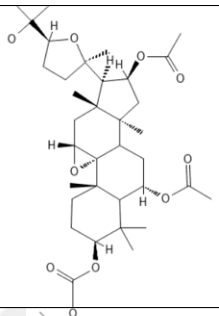	-7.02
CCPG-25	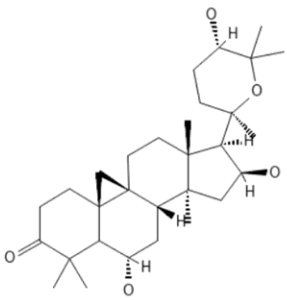	-7.54	**S-A21**	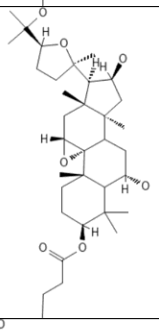	-7.46
CCPG-26	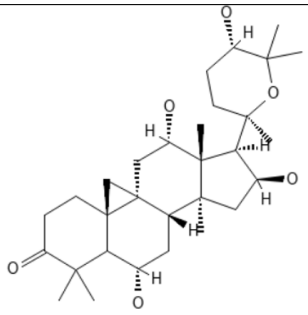	-6.66	**S-A22**	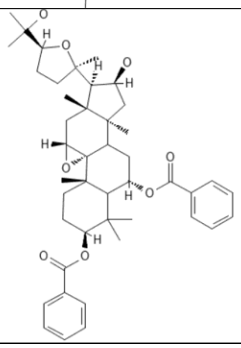	-8.51
CCPG-27	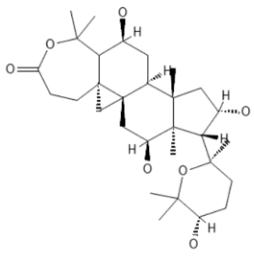	-7.86	**S-A23**	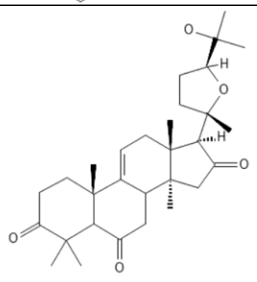	-8.24

(cont. on next page)

Table 9. (cont.)

CCPG-23	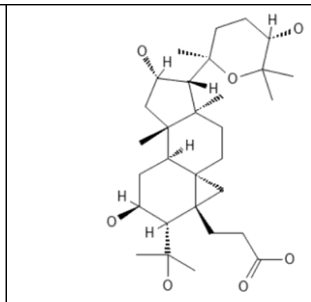	-6.96	**S-A19**	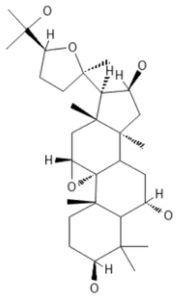	-7.83
CCPG-24	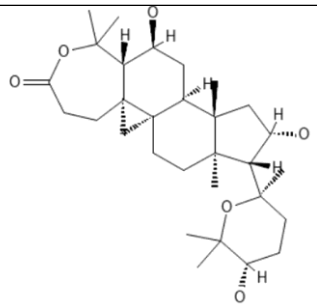	-8.27	**S-A20**	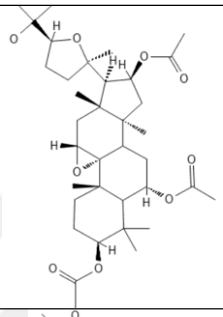	-7.02
CCPG-25	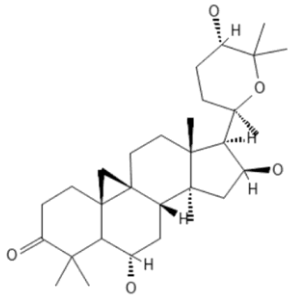	-7.54	**S-A21**	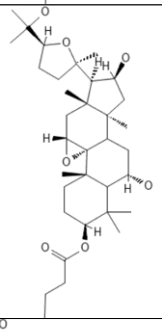	-7.46
CCPG-26	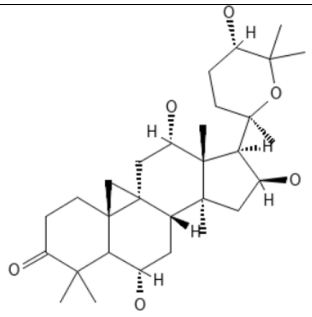	-6.66	**S-A22**	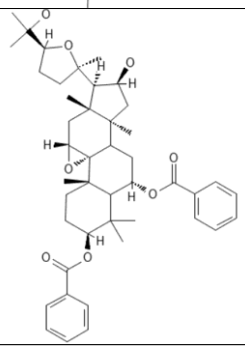	-8.51
CCPG-27	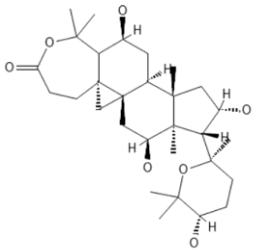	-7.86	**S-A23**	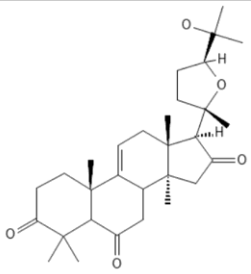	-8.24

(cont. on next page)

Table 9. (cont.)

CCPG-28	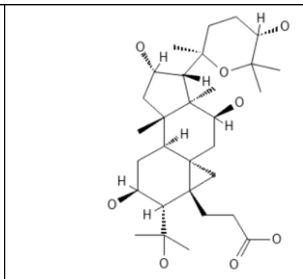	-6.9	**S-A24**	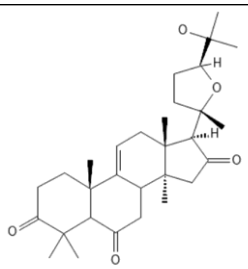	-8.26
CCPG-29	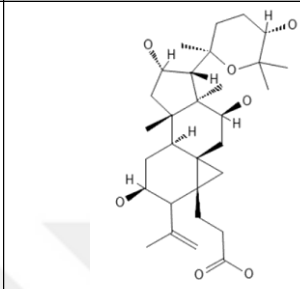	-6.48	**S-A25**	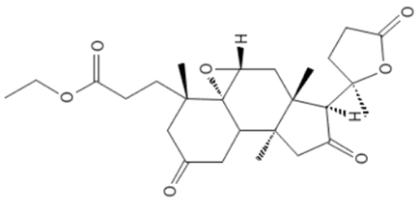	-7.29
CG	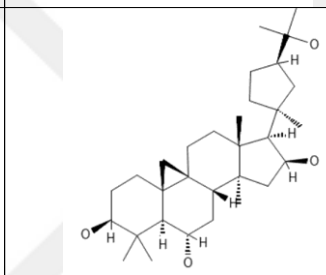	-6.89	**S-A26**	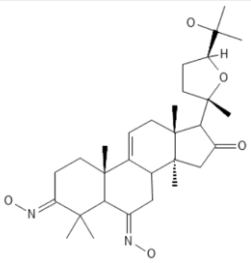	-8.42
Cycloasgenin C	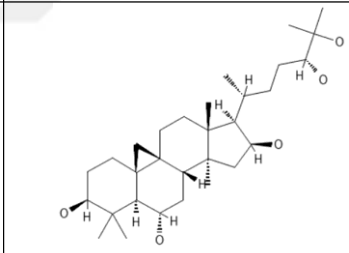	-6.92	**S-A27**	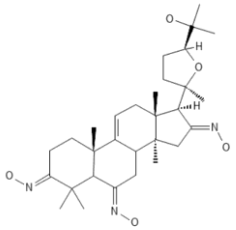	-8.59
Escin	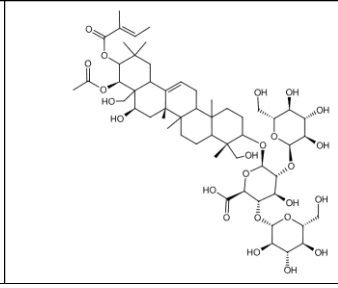	-5.96	**S-A28**	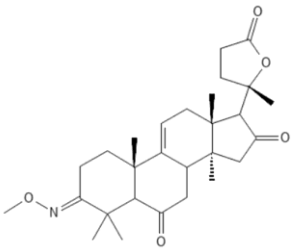	-8.26

(cont. on next page)

Table 9. (cont.)

Glycyrrhetinic Acid	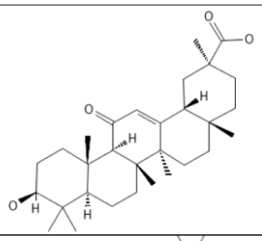	-6.93	**S-A29**	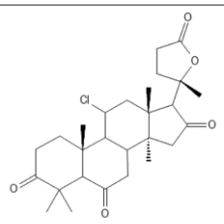	-8.99
Hederagenin	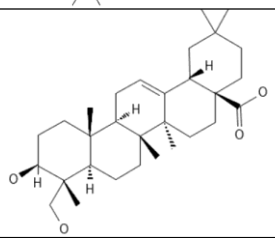	-6.27	**S-A30**	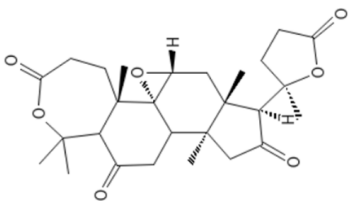	-8.43
Madecassic acid	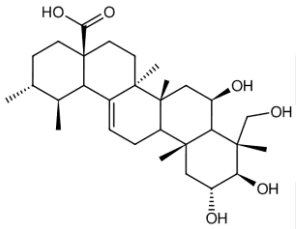	-7.01	**S-A31**	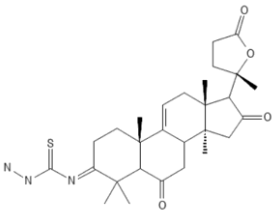	-8.48
Madecassoside	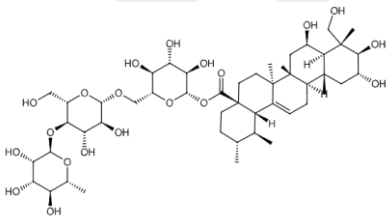	-8	**S-A32**	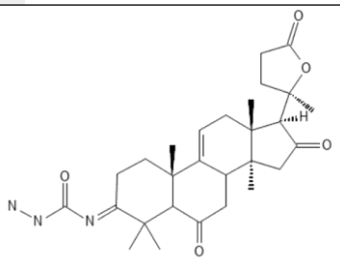	-8.85
MD-MG-01	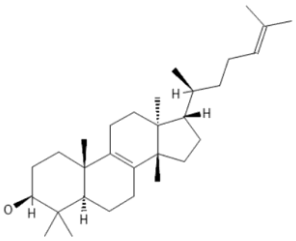	-7.2	**S-A33**	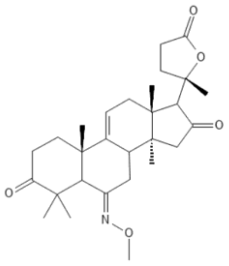	-8.85

(cont. on next page)

Table 9. (cont.)

MD-MG-02	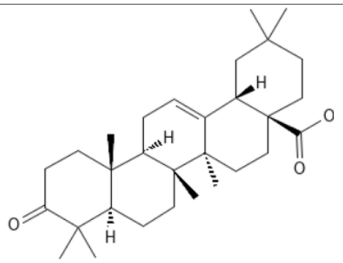	-7.03	**S-A34**	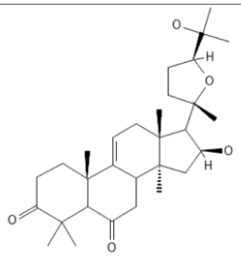	-8.46
MD-MG-03	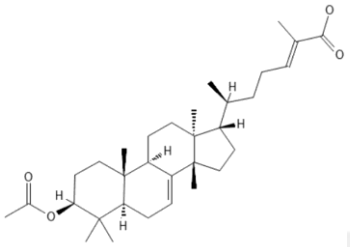	-8.58	**S-A35**	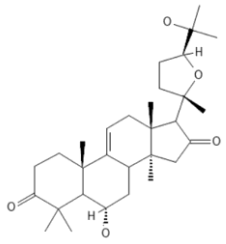	-8.14
MD-MG-04	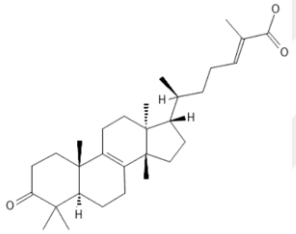	-7.83	**S-A36**	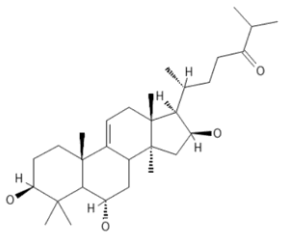	-6.84
MD-MG-05	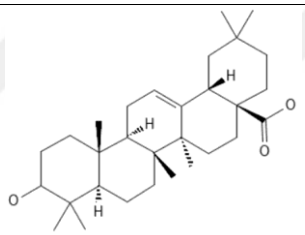	-6.54	**S-A37**	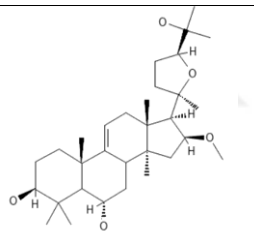	-7.69